An Investigation of Heterogeneity and the Impact of Acidic Regions on Bulk Effluent from a Deconstructed Low Sulfide Waste-Rock Pile

by

Colleen Atherton

A thesis
presented to the University of Waterloo
in fulfillment of the
thesis requirement for a degree of
Master of Science
in
Earth Sciences

Waterloo, Ontario, Canada, 2017

Author's Declaration

This thesis consists of material all of which I authored or co-authored: see Statement of Contributions included in the thesis. This is a true copy of the thesis, including any required final revisions, as accepted by my examiners.

I understand that my thesis may be made electronically available to the public.

Statement of Contributions

I would like to acknowledge the names of my co-authors who contributed to the research described in this thesis, these include:

- Steven Holland (Section 1.1.1.2.3.2.1.1 Most probable number enumeration and 1.1.1.2.3.2.1.2 DNA isolation), and
- David Barsi (Section 2.3.2.7 Particle-size distribution).

Abstract

Waste rock is a potential source of low quality drainage resulting from oxidation of naturally occurring sulfide minerals. Sulfide oxidation may result in the generation of effluent with elevated concentrations of SO_4 and dissolved metals and low pH. The sulfide content of waste rock is typically much lower than that of tailings; however, the large volumes of waste rock produced during mining may create a large environmental liability. Improving the understanding of the processes affecting the generation of acid mine drainage (AMD) from waste rock will facilitate improved prediction, mitigation, and remediation strategies.

Three waste-rock test piles were constructed at the Diavik Diamond Mine, Northwest Territories to investigate the potential for AMD generation in a permafrost environment. The test piles were constructed in 2006 and consisted of low sulfide (0.035 wt. % S), high sulfide (0.53 wt. % S), and covered test piles. The covered test pile was constructed to model the mine closure plan and consisted of a high sulfide (0.082 wt. %) core, covered by a low-permeability layer, and a low-sulfide thermal insulation layer. In 2014, the low-sulfide Type I test pile was systematically deconstructed to investigate the geochemical, hydrogeological, and geotechnical evolution of the waste rock. Samples were collected for microbial community analysis, mineralogical characterization, pore-water extraction, ice distribution, volumetric moisture content, and particle-size distribution.

The geochemical evolution of the test pile was investigated using mineral saturation index calculations, neutralization potential ratios, aqueous geochemistry, most probable number enumeration, adsorption isotherm modeling within the test pile, and mass loading calculations at the basal drain. Regions of low pH with elevated dissolved metal and SO_4 concentration developed within the test pile as a result of the heterogeneity inherent in the waste rock.

Sulfide oxidation rates were depressed in regions that remained frozen for a larger part of the year. Depression of sulfide oxidation rates allowed neutralization reactions within the waste

rock to maintain circumneutral pH in these regions. Saturation index calculations indicate circumneutral pH regions were conducive to precipitation of Fe (oxy)hydroxides which have a large capacity to adsorb cations. Adsorption isotherm modeling indicates that adsorption of Cu, Zn, Co, and Ni on ferrihydrite can account for the observed attenuation of these metals with increasing pH. Attenuation reactions resulted in reduced mass loading of metals and SO_4 in effluent compared to the higher sulfide waste-rock pile.

Acknowledgements

This project was made possible by funding contributions from the National Science and Engineering Council – Collaborative Research Development program, the Canadian Innovation Fund, the International Network for Acid Prevention, Mine Environment Neutral Drainage, the Northern Scientific Training Program, and the Diavik Diamond Mine. The Diavik Diamond Mine is owned by a joint venture between Rio Tinto (60%) and Dominion Diamond Corporation (40%), and is operated by Diavik Diamond Mines (2012) Inc., a subsidiary of Rio Tinto plc.

I would like to thank Dr. Carol Ptacek for seeing my potential as a graduate student and for bringing me into the Groundwater Geochemistry and Remediation (GGR) research group, and for her invaluable guidance along the way. Following my initiation into the GGR group I owe Dr. David Blowes for entrusting me with the deconstruction project, for pushing me to obtain more data than I thought possible, and for his expansive knowledge and experience. This project was a mammoth undertaking which I never would have been able to accomplish without the guidance and support of Dr. Rich Amos, Dr. Jeff Langman, Dr. Dogan Paktunc, Dr. Leslie Smith, and Dr. Dave Sego.

I am deeply indebted to the technicians, Julia Jamieson-Hanes, Laura Groza, and especially Joy Hu, who work tirelessly behind the scenes to complete the analyses and possess an immense wealth of knowledge of all things laboratory. Jack of all trades Jeff Bain was indispensable for determining the best way to implement new techniques and troubleshoot old equipment. Without the help of generations of coops students who lugged and spun rock for hours on end, I would never have been able to analyze the hundreds of samples that the deconstruction project produced. This project is a legacy of all the graduate students who came before me and all the others that will come after. Individually we are weak, but together we moved a mountain.

The Diavik Environment team has always been a strong supporter of the Test Piles research and the project never would have succeeded without them.

To Steve Holland and David Wilson: thank you for the commiseration and the lunch dates. You have been instrumental for bouncing ideas off of and for memorable Diavik meetings.

To Mum and Dad: thank you for your lifelong support of all my pursuits. You have been there when I needed you and provided me with the independence to find my own path.

Finally to Russ. My best friend and confidant. We embarked on this journey together and without your encouragement and support I would never have pursued graduate work. Come what may, it is to you above all others that I owe this thesis.

Table of Contents

List of Figures....x
List of Tables....xiv
Chapter 1. Introduction....1
1.1. Research objectives and organization of thesis....2
1.2. Background on acid mine drainage....3
Chapter 2. Deconstruction of a low sulfide waste rock test pile: design and preliminary results....4
2.1. Introduction....6
2.2. Site description....8
2.3. Methodology....9
2.3.1. Deconstruction design....9
2.3.2. Sample collection and analysis....10
2.4. Results....17
2.4.1. Pore water....17
2.4.2. Paste pH....19
2.4.3. Microbiology....19
2.4.4. Solid-phase geochemistry....20
2.5. Discussion....24
2.5.1. Pore water composition....24
2.5.2. Mineralogical evolution....24
2.5.3. Change in carbon and sulfur content....26
2.5.4. Neutralization potential ratios....27
2.5.5. Microbiology....28
2.6. Conclusions....29
2.7. Figures....30
2.8. Tables....40
Chapter 3. The Impact of heterogeneity on the generation of acidic regions and bulk effluent in a low sulfide waste rock test pile....41
3.1. Introduction....43
3.1.1. Site description....46
3.2. Methodology....48

3.2.1. Deconstruction and sample collection 48
3.2.2. Temperature data 48
3.2.3. Water sample collection 49
3.2.4. Water sample analysis 50
3.2.5. Geochemical modeling 51
3.2.6. Mineralogy samples 51
3.2.7. Most probable number enumeration 52
3.3. Results 53
3.3.1. In situ samples 53
3.3.2. Pore-water samples 55
3.3.3. Geochemical modeling 57
3.3.4. Temperature distribution 59
3.3.5. Basal drain 60
3.3.6. Adsorption isotherms 62
3.3.7. Mineralogy investigation 64
3.3.8. Most probable number analysis 66
3.4. Discussion 68
3.4.1. Effect of heterogeneity on geochemical evolution 68
3.4.2. Comparison of in situ and pore-water samples 69
3.4.3. Dissolved Metal Attenuation 72
3.4.4. Microbial communities 75
3.5. Conclusions 77
3.6. Figures 79
3.7. Tables 96
Chapter 4. Conclusions 100
4.1. Summary of findings 101
4.2. Recommendations 103
References 104

LIST OF FIGURES

Figure 2-1: A) Location of Diavik Diamond Mine, Northwest Territories, Canada (Smith et al., 2013c) and B) location of the 15 m and 35 m cross sections and (□) TW115B, (o) TW115C, and (Δ) TE135C profiles. Image shows the Type I test pile following excavation of the third level of sampling trenches. 30

Figure 2-2: Deconstruction design indicating location of trenches (dashed lines), sample locations (yellow triangles), bench surfaces (solid grey lines), and basal collection lysimeters (red). View looking down the long axis of the test pile. 31

Figure 2-3: Aqueous geochemistry results for selected parameters including duplicate sample at 447 masl. Low pH duplicate sample associated with elevated concentrations of sulfide oxidation products. 32

Figure 2-4: Calculated saturation index normalized by number of ions present in the mineral. 33

Figure 2-5: Paste pH of the 15 m cross section. (▪) indicates sample location. (◇) indicates location of TW115C priority profile 34

Figure 2-6: MPN enumeration by sample elevation 35

Figure 2-7: Whole rock analyses of selected oxides and metals. 36

Figure 2-8: Carbon verses sulfur (A-H), pore-water pH (I), and NPR (J-P) results from particle size fraction samples from construction (black) and deconstruction (white) samples. Error bars on C/S construction samples are one standard deviation. On the 15 m cross section, the profile from 5 m west of the center line is represented by □ and the profile from 8 m west of the center line is represented by Δ. The profile 7 m east of the center line on the 35 m cross section is represented by o. On figures I – P, closed circles represent μ(NP:AP) whereas closed squares represent μNP:μAP (Smith et al., 2013b). 37

Figure 2-9: NPR results for the 15 m cross section, (▪) indicates sample location. 38

Figure 2-10: Dashed lines represent NPR of 1 and 2, dotted line represents pH of 5.6 (rain water). 39

Figure 3-1: Instrumentation distribution for the Type I test pile adapted from Smith et al. (2013c). 79

Figure 3-2: A) Location of Diavik Diamond Mine, Northwest Territories, Canada (Smith et al., 2013c) and B) approximate location of the 15 m (solid), 25 m (dotted), 35 m (dash-dot), and transverse (dashed) cross sections. Red boxes indicate approximate location of 1BWBlys4S, 1BWClys4S, and 1BCElys4S. Image shows the Type I test pile following excavation of the third level of sampling trenches. 80

Figure 3-3: SWSS and BCL data. Each point represents the average concentration of sample collection points at the depth specified and error bars represent the 95% confidence interval. The average Fe concentration was >1.5 mg L^{-1} and Co, Cu, and Zn distribution was similar to Ni. 81

Figure 3-4: Carbonate and aluminium mineral saturation index calculations for SWSS and BCL samples. Each point represents the average concentration of several sample collection points at the depth specified and error bars are the 95% confidence interval. 82

Figure 3-5: Iron and sulfate saturation index calculations for SWSS and BCL samples. Each point represents the average concentration of several sample collection points at the depth specified and error bars are the 95% confidence interval. 83

Figure 3-6: Distribution of pore-water concentrations in the 15 m cross section. (▪) indicates sample location and black outline indicates test pile boundary. A) pH, B) Fe (mg L^{-1}), C) Ni (mg L^{-1}), D) Co (mg L^{-1}), E) Ni:Co ratio, F) alkalinity (as mg L^{-1} $CaCO_3$), G) SO_4 (g L^{-1}), H) Ca (mg L^{-1}), I) Cu (mg L^{-1}), J) Zn (mg L^{-1})..... 84

Figure 3-7: Distribution of pore-water concentrations in the 25 m cross section. (▪) indicates sample location and black outline indicates test pile boundary. A) pH, B) alkalinity (as mg L^{-1} CaCO3), C) SO_4 (g L^{-1})..... 85

Figure 3-8: Distribution of pore-water concentrations in the 35 m cross section. (▪) indicates sample location and black outline indicates test pile boundary. A) pH, B) Fe (mg L^{-1}), C) Ni (mg L^{-1}), D) Co (mg L^{-1}), E) Ni:Co ratio, F) alkalinity (as mg L^{-1} CaCO3), G) SO_4 (g L^{-1}), H) Ca (mg L^{-1}), I) Cu (mg L^{-1}), J) Zn (mg L^{-1}). Note similarity of the Ni, Co, Cu, and Zn distributions. In addition, Ca and SO_4 distributions are remarkably similar. 86

Figure 3-9: Distribution of pore-water concentrations in the transverse cross section. (▪) indicates sample location, black outline indicates test pile boundary, and grey lines indicate position of construction faces. Sulfur content (in wt. %) of construction faces was Face 1: 0.018, Face 2: 0.022, Face 3: 0.033, Face 4: 0.021, Face 5: 0.041 (from left to right). A) pH, B) Fe (mg L^{-1}), C) Ni (mg L^{-1}), D) Co (mg L^{-1}), E) Ni:Co ratio, F) alkalinity (as mg L^{-1} CaCO3), G) SO_4 (g L^{-1}), H) Ca (mg L^{-1}), I) Cu (mg L^{-1}), J) Zn (mg L^{-1}). 87

Figure 3-10: Normalized pore-water saturation index calculations for the 15 m cross section. (▪) indicates sample location..... 88

Figure 3-11: Normalized pore-water saturation index calculations for the 35 m cross section. (▪) indicates sample location..... 89

Figure 3-12: Temperature distribution for the transverse (A, B, and C) and 15 m (D, E, and F) cross sections for June (A and D), August (B and E), and October (C and F). (▪) indicates in situ measurement location, (Δ) indicates inferred temperature based on average of adjacent samples, and the white line indicates region where pH≤7. 90

Figure 3-13: Mass loading of selected constituents at the basal drain by year including daily outflow volume (grey bars), cumulative outflow volume (black line) and individual pH measurements (black circle). Cl and NO_3 concentration peaked in 2010 and 2011 respectively. 91

Figure 3-14: Adsorption isotherms. (●) represents pore-water sample, solid lines represent model results at 0.09 (upper) and 0.4 (lower) g L^{-1} total Fe, red dashed line represents 0.2 g L^{-1} total Fe. 92

Figure 3-15: Photomicrographs and µ-XRF maps of individual pyrrhotite grains from a vertically aligned profile from the core of the test pile. From left to right: reflected light photomicrograph, S distribution (grey), Fe distribution (red), Ni distribution (blue), and Cu distribution (green). From a depth of A) 2.4 m and pH 4.4, B) 5.6 m and pH 8.3, and C) 11.7 m and pH 5.0. Scale bar on each image represents 100 µm. The sample from the top of the profile (A) indicates limited metal accumulation. The sample from the middle elevation (B) indicates secondary accumulation of Fe and Ni adjacent to the pyrrhotite grain, identified by circle. The sample from the bottom of the profile (C) indicates limited accumulation of secondary Fe but not Ni, identified by circle; arrow indicates residual sulfide grain responsible for strong Cu signal. 93

Figure 3-16: SEM and EDX image of grain (B) in Figure 3-15 with EDX spectra. Top - SEM image showing bright, unaltered sulfide core and grey reaction rim. Letters indicate location of EDX analysis. a) EDX within the unaltered sulfide core indicating a dominantly Fe sulfide mineralogy. b) EDX from the reaction rim indicating a mixed Fe oxide and Fe sulfide composition. c) EDX from a grain located adjacent to the sulfide grain having a Na-Ca aluminosilicate composition (plagioclase). d) EDX from the secondary coating on grain (c) indicating a Mn oxide composition. 94

Figure 3-17: MPN enumeration from the 15 m and 35 m cross sections..... 95

LIST OF TABLES

Table 2-1 - Comparison of carbon and sulfur analyses from particle size fractions collected from unweathered (n = 5) and weathered (n = 22) waste rock. Statistical analysis was conducted using a two-tailed t-Test (normal data and normal log transformed data) and/or rank sum analysis (non-normal data). a) Unweathered data from Smith et al. (2013a) 40

Table 3-1 - Annual Type I basal drain mass loading (a) Type III data from Sinclair (2014) with exception of Zn and Cu which are from personal communication (2016) (b) data from Krentz (2014) 96

Table 3-2 - Adsorption constants, (a) inferred based on linear free energy relationships (Balistrieri et al., 2003) 97

Table 3-3 - Anomalous pore-water samples excluded from adsorption isotherm fitting. N/A - values not considered anomalous and therefore included in the analysis. 98

Table 3-4 - Summary of two-sided t-test results (A) All SWSS and all pore-water data included in analysis, (B) 2013 SWSS and all pore-water data, and (C) 2013 SWSS and pore-water data from the 15 m cross section. 99

“There are strange things done in the midnight sun by the men who moil for gold”

- Robert Service

CHAPTER 1. INTRODUCTION

1.1. Research objectives and organization of thesis

This thesis is the first in a decade long research project at the Diavik Diamond Mine to focus on results from the low-sulfide Type I waste-rock test pile. Previous work has focused equally on the Type I and Type III test piles or exclusively on the Type III test pile. The focus of this study is to investigate the evolution of the pore-water geochemistry through the deconstruction of a 40,000 m^3 waste-rock test pile. During deconstruction, samples were collected from over 600 locations within the test pile.

A large number of samples was collected to facilitate characterization of the heterogenous media. The heterogeneity inherent in waste rock makes prediction of effluent quality a challenge. The partitioning of flow through matrix or macropores, gravity sorting, the presence of low permeability compaction surfaces, seasonal temperature changes, and flushing of dissolved constituents during precipitation or snowmelt are difficult to quantify (Amos *et al.*, 2015). An improved understanding of the role heterogeneity plays in the evolution of AMD will allow for improved prediction, prevention, and remediation techniques.

This thesis is divided into four chapters. Chapter 1 is a global introduction. Chapter 2 and 3 are written as articles for submission to refereed journals. Chapter 2 describes the deconstruction process and includes preliminary aqueous geochemistry and microbiology results from a high-priority vertical profile. Chapter 2 also includes a more detailed discussion of mineralogical results including X-ray fluorescence analysis and acid base accounting results. Chapter 3 describes the factors affecting the geochemical evolution of the pore water including the temperature dependence of sulfide oxidation and the attenuation of cations via adsorption onto Fe (oxy)hydroxides. Chapter 4 is a global conclusion tying findings from Chapter 2 and 3 together and providing recommendations.

1.2. Background on acid mine drainage

Sulfide minerals, such as pyrrhotite, are commonly associated with ore deposits. Pyrrhotite has low economic value and is typically deposited in waste rock dumps and tailings impoundments. Sulfide minerals oxidize when they are exposed to O_2, microbes, and water through particle-size reduction and excavation inherent to the mining process. The resulting effluent can contain high concentrations of SO_4 and dissolved metals with acidic pH, referred to as acid mine drainage (AMD), or neutral pH, referred to as neutral mine drainage (NMD) (Nordstrom, 2011). In waste rock deposits with low neutralization potential, oxidation of sulfide minerals has the potential to produce acidic drainage through sulfide mineral oxidation with O_2 or Fe^{3+} as the primary oxidant. Pyrrhotite is oxidized according to the following reactions (Belzile *et al.*, 2004):

$$Fe_{(1-x)}S + \left(2 - \frac{1}{2}x\right)O_2 + xH_2O \rightarrow (1-x)Fe^{2+} + SO_4^{2-} + 2xH^+ \quad (1)$$

$$Fe_{(1-x)}S + (8-2x)Fe^{3+} + 4H_2O \rightarrow (9-3x)Fe^{2+} + SO_4^{2-} + 8H^+ \quad (2)$$

The regeneration of Fe^{3+} through oxidation of ferrous iron is required to maintain reaction (2); however, the solubility of Fe is low at pH>4 and Fe will precipitate in (oxy)hydroxides. The oxidation of Fe^{2+} consumes H^+, whereas the precipitation of Fe (oxy)hydroxides generates H^+:

$$4Fe^{2+} + O_2 + 4H^+ \rightarrow 4Fe^{3+} + 2H_2O \quad (3)$$

$$Fe^{3+} + 3H_2O \rightarrow Fe(OH)_{3(s)} + 3H^+ \quad (4)$$

Reaction (3) occurs abiotically but the rate of reaction is accelerated by orders of magnitude in the presence of bacteria capable of oxidizing Fe^{2+} (Johnson & Hallberg, 2003). As a result of the above reactions, a positive feedback loop forms as pH decreases and the solubility of Fe^{3+} increases, resulting in greater oxidation rates at lower pH.

CHAPTER 2. DECONSTRUCTION OF A LOW SULFIDE WASTE ROCK TEST PILE: DESIGN AND PRELIMINARY RESULTS

Summary

Three test piles were constructed at the Diavik Waste Rock Research Facility from 2005-2007. In 2014, the low sulfide test pile (0.035 wt. % S) was deconstructed to obtain samples from over 600 locations. Samples were collected for characterization of multiple parameters including geochemical evolution of the solid-phase, microbiological community development, pore-water composition, particle-size distribution, volumetric moisture content, ice composition, and ice distribution. This paper explores the geochemical evolution of the waste rock and presents preliminary mineralogy and microbiology results.

The mineralogical evolution was examined through comparison of the C and S content of unweathered and weathered samples and comparison of oxide and metal content with pore-water pH. This analysis indicates that the C content of the particle-size fractions <4.00 mm has been depleted by 29-55%, and the C content of the bulk-matrix waste rock has been depleted by 40%. No statistically significant change in the total S content of the waste rock was observed in the bulk matrix or particle-size fractions. These analyses do not distinguish sulfide-sulfur from sulfate-sulfur. No correlation between oxide content and pH was observed.

Neutralization potential ratios calculated using C and total S indicate that regions of low paste pH are typically well predicted by the presence of potentially acid generating material or material with uncertain acid generating potential. Pore water with low pH was associated with elevated concentrations of SO_4 and dissolved metals.

2.1. Introduction

Mineral resource extraction requires the excavation of large volumes of sub-economic grades of ore and waste rock to gain access to valuable ore bodies. It is estimated that one million tonnes of waste rock is generated daily in Canada (Government of Canada, 1991). Waste rock typically has a lower sulfide content than mill tailings (Moncur *et al.*, 2009, Lindsay *et al.*, 2015, Jurjovec *et al.*, 2002, Parviainen *et al.*, 2012); however, because of the large volumes, waste-rock stockpiles may contain large reservoirs of sulfide minerals with the potential to impact drainage quality (Dockrey *et al.*, 2014, Sinclair, 2014, Stockwell *et al.*, 2006).

The oxidation of sulfide minerals exposed by mineral resource extraction may result in the release of acidic and metal- and sulfate-laden effluent to surface water and groundwater. The generation of acid mine drainage (AMD) results from a complex series of microbiological, geochemical, and hydrological processes. Understanding the interactions among these processes is complicated by the physical, mineralogical, and geochemical heterogeneity inherent in waste rock.

Construction of the Diavik Waste Rock Research Facility (DWRRF) was completed in 2007 to investigate hydrology, microbiology, geochemistry, thermal regime, and gas transport mechanisms in waste rock (Smith *et al.*, 2013c). At the DWRRF, three waste-rock test piles were constructed composed of (1) Type I waste rock containing 0.035 wt. % S; (2) Type III waste rock containing 0.053 wt. % S; and (3) a covered pile, consisting of a high sulfide core (0.082 wt. % S), a low permeability till layer, and a low sulfide thermal insulation layer, to model the mine closure plan for mitigation of AMD. All three test piles were constructed using standard mining equipment and the push- and end-dumping techniques employed on the full-scale waste-rock dump. The Type I and Type III test piles had base dimensions of 50 x 60 m and heights of 15 m, whereas the covered pile dimensions were 125 x 80 m with a height of 15 m.

The low-sulfide Type I test pile was deconstructed in 2014 to obtain a high-resolution data set to investigate the geochemical, hydrological, and geotechnical characteristics or the waste rock after exposure to almost a decade of natural weathering conditions in an arctic environment. Previous studies conducted at the DWRRF focused primarily on the Type III test pile and included initial characterization of the test piles (Smith *et al.*, 2013a, Smith *et al.*, 2013b, Smith *et al.*, 2013c), and investigation of gas-transport (Amos *et al.*, 2009, Chi *et al.*, 2013); temperature (Pham *et al.*, 2013); hydrology (Neuner *et al.*, 2013); and microbiology, geochemistry, and mineralogy (Bailey *et al.*, 2015, Bailey *et al.*, 2016, Smith *et al.*, 2013a, Bailey *et al.*, 2013, Langman *et al.*, 2015b, Langman *et al.*, 2015a, Sinclair *et al.*, 2015). This research builds on those previous studies and previous studies at other sites that utilized a similar data collection technique, but occurred in different climates and analyzed fewer samples (Stockwell *et al.*, 2006, Azam *et al.*, 2007). This chapter focuses on the solid-phase composition and preliminary geochemical and microbial data from the deconstruction of the Type I test pile.

2.2. Site description

Diavik Diamond Mine is located approximately 300 km NE of Yellowknife, NT, on a 20 km^2 island in Lac de Gras (Figure 2-1A). The mine is located in a region of continuous permafrost with an active zone 1.5-5 m thick (Smith *et al.*, 2013c). The average ambient air temperature at Diavik is -9.0 °C (1998-2007), with the maximum temperature of 27 °C recorded in July and the minimum temperature of -44 °C recorded in January/February. Diavik receives 280 mm of precipitation on average, 65% of which typically falls as snow (Environment Canada, 2010).

Diamonds are hosted within kimberlite pipes emplaced into granite and granite-pegmatite country rocks. The granite and granite pegmatite are composed of 30-70% K-feldspar [$KAlSi_3O_8$], 15-46% quartz [SiO_2], 0-35% albite [$NaAlSi_3O_8$], 0-5% biotite [$KMg_3AlSi_3O_{10}(OH)_2$], 1-4% muscovite [$KAl_2(Si_3AlO_{10})(OH)_2$], and 2% other minerals including trace amounts of pyrite [FeS_2], chalcopyrite [$CuFeS_2$], sphalerite [(Zn,Fe)S], and galena [PbS] (Jambor, 1997).

The granite and granite pegmatite contain biotite schist xenoliths composed of 20-50% quartz, 10-25% biotite, and 35-55% albite. The biotite schist contains 0.02-0.42 wt. % sulfide, with an average of 0.14 wt. %, present dominantly as pyrrhotite [$Fe_{0.85}S$] (Diavik Diamond Mines Inc., 1998). The biotite schist contains lesser masses of pyrite and traces of chalcopyrite and sphalerite (Jambor, 1997). Diavik segregates and disposes waste rock on the basis of sulfide content using three categories: Type I (<0.04 wt. % S), Type II (0.04<wt. % S<0.08), and Type III (>0.08 wt. % S).

The Type I waste rock, composed principally of granite and granite-pegmatite, is considered to be non-acid generating (Smith *et al.*, 2013b) due to the net acid consuming mineralogy and the low sulfide content. Although the Type III waste rock contains a greater proportion of biotite schist, the sulfide content is low relative to many waste rock and mine tailings deposits (Jurjovec *et al.*, 2002, Lindsay *et al.*, 2015, Elberling, 1993, Moncur *et al.*, 2009).

2.3. Methodology

2.3.1. Deconstruction design

Deconstruction was conducted using Hitachi EX1200 and Hitachi EX1900 excavators and Komatsu 789 rock trucks from July 1 to September 6, 2014, after eight years of weathering under natural conditions. The deconstruction proceeded in layers, through excavation of a series of six benches, each comprised of two trenches excavated parallel to the long axis of the test pile (Figure 2-2). A final layer was comprised of two trenches perpendicular to the long axis of the test pile excavated in high priority locations. The trench sides were sloped to 18° (3H:1V) to maintain slope stability and to provide safe working surfaces for sampling. Samples were collected at 5 m intervals along each trench. Samples were collected at 1 m vertical spacing on both sides of the trench at each sample interval. Consistency in sample location between benches was maintained using a Real Time Kinetic Global Positioning System (RTK GPS) with +/- 2 cm accuracy. This allowed the generation of vertically aligned cross sections at each sample interval.

The depth of the first trench was limited to 1.2 m to accommodate the limited space available at the crest of the test pile. Trenches 2, 3, and 4 were excavated to depths of 2.5-3 m (Figure 2-2). No trenches were excavated on bench 5 (elev. 441 masl) due to the presence of ice. Two final trenches oriented perpendicular to the long axis of the test pile were excavated on bench 6 after a period of thawing. The bench 6 trenches were excavated to a depth of 1.2 m at the 15 m and 35 m cross section locations. Samples were collected at the base of the bench 6 trenches.

Most samples were collected from within the core of the test pile. Where space was available, which occurred on bench 3 and below, test pits were excavated to facilitate collection of samples from the batters of the test pile. Where insufficient space was available for test pits, samples were occasionally collected from the bench surface adjacent to the trench in the batter portion of the pile.

Sample locations were selected prior to deconstruction to maintain lateral sample position between benches. Sample locations were adjusted during deconstruction to obtain an adequate volume of matrix material. For the purpose of deconstruction, matrix material is defined as the particle-size fraction <10 mm. In locations where matrix material was unavailable due to the presence of cobbles or boulders, the location was shifted up to 1 m laterally and 0.5 m vertically to obtain the sample and the adjusted sample location was surveyed.

Samples were unable to be collected in some planned locations and additional samples were collected in others. Additional samples were collected from the eastern half of the surface of the test pile and the entire surface of bench 2 prior to excavation of trenches. This occurred because additional time was available due to scheduling delays. Safety berms were constructed at the edge of the test pile, and slopes steeper than 18° were created during the excavation of large boulders. These conditions prevented sample collection at a number of planned locations. The inability to collect samples typically occurred in the batter areas of the test pile and near the access ramp at the southeast end.

2.3.2. Sample collection and analysis

Samples were collected for DNA isolation, MPN enumeration, mineralogical study, and pore-water extraction at each of the sample locations. Microbiology samples were collected first as they are the most susceptible to cross contamination. Samples were subsequently collected for mineralogical study due to the small volume required. Mineralogy samples were followed by larger samples for pore-water characterization. Samples were also collected for particle-size distribution, volumetric moisture content (VMC), ice composition and ice distribution. These results are described by Barsi (2017) and Zak (2017).

Samples were collected from 622 discrete locations within the test pile with pore-water samples collected at 568 locations (54 duplicates), mineralogy samples at 562 locations (52

duplicates), and DNA/MPN samples at 591 locations (53 duplicates). Duplicate samples were collected at pre-identified, randomly selected locations at an approximate frequency of 10%.

2.3.2.1 Microbiology

Samples for microbiological characterization were collected using aseptic techniques. Nitrile gloves were sterilized between samples using 70% (v/v) ethanol. A sterile scoopula was used to remove surficial sediment at the sampling location. A second sterile scoopula was used to collect and deposit waste-rock samples (<10 mm fraction) into manufacturer-sterilized 50 mL Falcon™ tubes. One Falcon™ tube was collected for MPN enumeration and a separate Falcon™ tube was collected for DNA isolation at each location.

Samples for MPN enumeration were stored at 4 °C to preserve sample integrity. Samples for DNA isolation were frozen immediately at -20 °C to minimize community shifts and to prevent sustained bacterial growth prior to isolation. All samples for microbiological characterization were shipped to the University of Waterloo for analysis.

2.3.2.1.1. Most probable number enumeration

Most probable number enumeration (Cochran, 1950) of acidophilic iron oxidizing (aIOB), acidophilic sulfur oxidizing (aSOB), and neutrophilic sulfur oxidizing (nSOB) bacteria were conducted on field-collected waste-rock samples using selective culture media described by Benner *et al.* (2000). This technique produces ten dilution steps to theoretical extinction with five replicates per step. These enumerations were conducted to provide a comparison to enumerations conducted on the test-pile effluent since 2006.

Media solutions were sterilized via autoclaving or filtration (0.2 µm) prior to use. Inoculations were conducted within a HEPA-filtered Forma Laminar Airflow Workstation. Work surfaces were sterilized using 70% (v/v) ethanol prior to use. In each of five replicate culture tubes 9 mL of selective growth media were inoculated with 1 g of waste rock and vortexed. The inoculated growth media was diluted in a ten-step series by transferring 1 mL inoculated media

into 9 mL fresh culture media. Once inoculated, culture tubes were incubated at 22 °C +/- 3 °C in the dark for four weeks. Following the incubation period, positive growth in each tube was determined via the appearance of an ochre precipitate in the case of the acidophilic iron oxidizing media or via a decrease in pH in the acidophilic and neutrophilic sulfur oxidizing media relative to negative controls (i.e., uninoculated growth media).

2.3.2.1.2. DNA Isolation

DNA isolations were performed on field-collected samples using the Mo Bio PowerSoil® DNA Isolation Kit within an AirClean® Systems 600 Workstation vertical laminar flow hood with HEPA filter to minimize airborne/dust-borne sample contamination. All materials entering the Workstation were sterilized with 70% (v/v) ethanol. Pipette tips were autoclaved and the working surface in the flow hood and all materials required for the isolation process were UV sterilized prior to use.

The isolation procedure followed the manufacturer's protocols with manufacturer-recommended modifications to adapt for low-biomass (Mo Bio, personal communication). Deviations to the manufacturer's protocols are as follows: (1) after adding 150 µL of Solution C2, samples were vortexed; (2) 150 µL of C3 was added, and the samples were vortexed and incubated at 4 °C for 5 minutes; and (3) in the elution step, Solution C6 was added to the centre of the spin filter membrane and allowed to incubate at room temperature for 1 minute prior to centrifuging. DNA isolates were stored at -20 °C until sequencing.

2.3.2.2 Mineralogy

Samples for mineralogical study were collected using a clean stainless-steel trowel and stored in manufacturer-sterilized pre-labeled 24 oz Whirlpak® bags. The <10 mm particle-size fraction was collected for mineralogical study. Samples were stored frozen and shipped to the University of Waterloo. The sample was thawed for processing and a 400-500 g subsample was collected using the ASTM Quartering method (ASTM C702/C702M-11 Standard Practice, 2011),

and the remaining sample was refrozen. The subsample was freeze dried for a minimum of 48 hours using a Labconco FreeZone 1 Liter Benchtop Freeze Dry System with a 12-Port Drying Chamber and sealed following complete drying. From the dried sample, a 10 g subsample was split using the ASTM Quartering method for creation of grain mount thin sections. Thin sections were mounted on quartz glass slides.

A 50-100 g subsample, split from the dried sample using the ASTM Quartering method, was pulverized for carbon and sulfur analysis (C/S), X-Ray Fluorescence (XRF), and X-Ray Diffraction (XRD). The C/S analysis was conducted using an ELTRA CS-2000 Carbon/Sulfur analyzer, XRF analysis using a PANalytical MiniPal 4 - Benchtop EDXRF Spectrometer and MiniMate Software (version 6.0.E), and XRD analysis using a Bruker D8-Focus at the University of Waterloo. Bulk matrix samples were pulverized using a low chrome steel mill by the minerals division of ALS Global in Sudbury, Ontario to 85% passing a 75 micron sieve.

A selection of samples from the 15 m and 35 m cross sections, representing three complete vertical profiles, were selected for C/S analysis of particle-size fractions to determine the C and S content of the most reactive particle-size fractions. The bulk freeze-dried sample was split and sieved to pan, 0.15, 0.30, 0.60, 1.18, 2.36, 4.00, 9.50, 16.00, and 19.00 mm particle-size fractions. Particle-size fraction samples were milled at the University of Waterloo using a Fritsch Pulverisette 5 Laboratory Planetary Mill to <80 microns and analyzed using the ELTRA 2000 C/S analyzer.

2.3.2.3 Pore water

A two to three kg sample was collected in manufacturer-sterilized pre-labeled 69 oz Whirlpak® bags for pore-water extraction using the same collection and preservation methodology as mineralogy samples. Pore water was extracted via centrifugation in modified Falcon™ tubes using a Thermo Scientific Sorvall™ Legend™ XT Centrifuge. An 80-90 g aliquot of thawed sample was placed in the modified Falcon™ tubes and centrifuged for 30 minutes at

8500 RPM. Pore water was extracted from 6-12 aliquots for each sample to produce sufficient sample volume for the required analyses. The water extracted from all aliquots was combined prior to further analysis and laboratory duplicates were collected from approximately 10% of samples, where sufficient sample volume was available.

The pH was determined on 2-3 mL, 0.45 µm filtered sample aliquots using an Orion 3 Star Plus meter with an Orion Ross Ultra pH probe calibrated using pH 4, 7, and 10 buffers (traceable to NIST) each day prior to use and checked throughout the day. The solution Eh was determined using an Orion Combination Redox/ORP Pt electrode verified with Zobell's (Nordstrom, 1977) and Light's solutions (Light, 1972) and also checked throughout the day. Following pH and Eh analysis, the same aliquot was weighed and titrated using 0.0016 N sulfuric acid and a bromocresol green/methyl red indicator solution to determine alkalinity.

The remaining sample was 0.45 µm filtered and divided between dissolved cation and anion sample aliquots. The dissolved cation sample was preserved using HNO_3 to lower the pH to <2. Samples were analysed at the University of Waterloo by Inductively Coupled Plasma Optical Emission Spectrometry (ICP-OES; Thermo iCAP 6500 Duo) and Inductively Coupled Plasma Mass Spectrometry (ICP-MS; Thermo XSeries 2) for determination of dissolved cation concentrations and by Ion Chromatography (IC; Dionex ICS-3000) for determination of anion concentrations.

2.3.2.3.1. Geochemical modeling

Geochemical species calculations were conducted for each of the pore-water samples using PHREEQCi (Parkhurst & Appelo, 1999) and a modified WATEQ4F database including aqueous and solid Co species and the mineral phases lepidocrocite, siderite, and schwertmannite (Langman *et al.*, 2015b). The results were normalized according to the following equation (Jurjovec *et al.*, 2002):

$$SI_N = \frac{\left(\log \frac{IAP}{K}\right)}{N}$$

where N is the number of ions in the solid phase, K is the equilibrium constant, and IAP is the ion activity product. Normalization of saturation indices simplifies comparison of minerals with many components, and correspondingly large absolute saturation index (SI) values, to those with relatively simple structures and SI values near zero.

2.3.2.4 Paste pH

Paste pH measurements were conducted using air-dried subsamples from pore-water samples using the method of Hageman *et al.* (2015). The solid phase was sieved to <2 mm and mixed in a 1:1 (solid:water) ratio. The paste pH of each sample was measured using both distilled water and a 0.01 M $CaCl_2$ saturated solution. The solid-water solution was allowed to equilibrate for a period of one hour prior to measurement of pH. Prior to pH measurement, the pH probe was calibrated using pH 4, 7, and 10 buffers (traceable to NIST).

2.3.2.5 Volumetric moisture content

Samples for VMC were collected using a metal cup with a known volume. The cup was pressed into intact matrix material to collect a sample of known volume. The sample was placed in a metal container of known mass and sealed with plastic to retain moisture until weighing and drying. The sample was weighed immediately after sampling of a trench was completed and dried in an oven at 105 °C for 24 hours. Following drying, the sample was weighed again and the difference in mass was used to calculate VMC. Drying samples for longer than 24 hrs did not have an impact on the results obtained.

2.3.2.6 Ice

The distributions of matrix ice and ice lenses were mapped throughout the pile by visual observation and located using GPS. Matrix ice is defined as granular ice crystals filling the pore

space of matrix. Ice lenses are defined as discrete blocks of ice filling large void spaces between boulder and cobble sized material. Ice lenses contain minimal entrained sand- or gravel-sized waste rock. Samples of matrix and ice lenses were collected in re-sealable polypropylene bags using a hammer and clean chisels. The ice was allowed to thaw before water was collected for pH, Eh, electrical conductivity, alkalinity, deuterium, dissolved cations, and anions. Samples of melted ice were processed using the same methods as pore-water samples.

2.3.2.7 Particle-size distribution

Recovery of material for particle-size analysis was the final step of sample collection at each sample location. Collection and testing procedures were modified from ASTM D6913, C136, and C702. The testing program aimed to collect material with a nominal maximum particle size of <75.0 mm. This required that 70 kg specimens be collected at each sample location for a representative sample (ASTM D6913, 2009). Two 35 kg sample aliquots were collected from each location to facilitate handling of the large amount of material. Material that was larger than 75.0 mm was discarded. The samples were shipped to the University of Alberta for particle-size analysis.

Samples were dried at 110±5°C for 24 hours prior to sieve analysis. Dry samples were sieved using 19.0, 25.0, 37.5, 50.0, and 75.0 mm sieves using a TS-2 Gilson Testing Screen. The fine fraction was split using a universal-chute style mechanical splitter. A sample of 5 kg or less was then sieved through 0.075, 0.106, 0.15, 0.25, 0.425, 0.85, 2.0, 4.75, and 9.5 mm sieves using a motorized Economy sieve shaker.

2.4. Results

2.4.1. Pore water

Concentrations of cations, anions, and alkalinity and pH were determined for seven samples including one duplicate sample from the TW115C profile from the 15 m cross section. These seven samples are from a vertically aligned profile from the core of the test pile. The TW115C profile crosses regions of high and low pH. The pH values obtained from the profile ranged from 4.1 to 8.3 with the lowest value observed in the duplicate sample (Figure 2-3).

The maximum concentrations of the sulfide oxidation products Fe (2.36 mg L^{-1}) and SO_4 (2894 mg L^{-1}); aluminosilicate dissolution products Al (57.9 mg L^{-1}) and Si (61.6 mg L^{-1}); and dissolved metals Ni (14.2 mg L^{-1}), Co (3.2 mg L^{-1}), Cu (8.1 mg L^{-1}), and Zn (22.1 mg L^{-1}) correspond with the minimum pH value of the profile (Figure 2-3). The maximum alkalinity as $CaCO_3$ (64.3 mg L^{-1}) was observed in the sample with the maximum pH (8.3). Where pH was low, the capacity of the pore water to neutralize acid generated through sulfide oxidation has been depleted as indicated by the low alkalinity in samples with low pH.

2.4.1.1 Geochemical modeling

Geochemical model calculations indicate that pore water was undersaturated with respect to calcite [$CaCO_3$] and dolomite [$CaMg(CO_3)_2$] in the upper portion and at the base of the profile (Figure 2-4). Pore water in the middle portion of the profile, where pH >7, was near equilibrium with respect to these carbonate minerals. These observations indicate that the acid neutralization capacity of the rock has not yet been exhausted in the circumneutral regions of the profile.

Dissolved Al was present in the pore water at concentrations of up to 57.9 mg L^{-1}. Pore water within the profile approached equilibrium with respect to gibbsite [$Al(OH)_3$], but was at equilibrium or slightly undersaturated with respect to amorphous $Al(OH)_3$. Because the Al:Si ratio is approximately 1:1 in the sample with low pore-water pH, it is more likely that the elevated

concentration of dissolved Al in the sample was a result of dissolution of aluminosilicate minerals rather than the dissolution of amorphous $Al(OH)_3$. This elevated dissolved Al concentration that resulted from aluminosilicate dissolution caused the porewater to approach equilibrium with respect to gibbsite. If dissolution of amorphous $Al(OH)_3$ was the source of the elevated concentration of Al, a higher Al:Si ratio would be expected. Although secondary amorphous $Al(OH)_3$ has seldom been observed in AMD systems, it is frequently inferred that precipitation of Al-bearing (oxy)hydroxide phases limits the concentrations of dissolved Al and that subsequent dissolution of Al oxyhydroxides contributes to acid consumption (Blowes *et al.*, 2014). Alunite $[KAl_3(SO_4)_2(OH)_6]$ is a secondary mineral that forms in water concentrated through evaporation (Lapakko, 2015). Geochemical modeling indicated that alunite formation was possible throughout the profile presented, but evaporative fluxes were likely insufficient to form alunite in this system due to the low temperatures and low precipitation received at the site.

Pore water in the profile was generally slightly oversaturated with respect to ferrihydrite $[Fe_2O_3{\cdot}0.5H_2O]$ and oversaturated with respect to goethite [α-FeOOH]. This observation indicates an Fe-bearing mineral, likely pyrrhotite, was dissolving and oxidizing to Fe(III). Following oxidation, conditions were favourable for Fe(III) (oxy)hydroxide precipitation and this mechanism was likely controlling the concentration of Fe in solution.

Sulfate minerals barite $[BaSO_4]$, gypsum $[CaSO_4]$, and potassium jarosite $[KFe_3(SO)_4)_2(OH)_6]$ were investigated as potential controls on SO_4 concentration within the profile. The pore water was generally near saturation with respect to both barite and gypsum, but based on the higher solid phase concentration of Ca (μ = 6099 ppm, σ = 1303) than Ba (μ = 385 ppm, σ = 145) it is likely that gypsum exerted a stronger control on SO_4 concentration. Saturation with respect to jarosite was more variable than the other SO_4-bearing minerals. Undersaturation with respect to jarosite was observed at the top and bottom of the profile where SO_4 concentrations were <1250 mg L^{-1}. Oversaturation with respect to jarosite was observed at the

central portion of the profile where SO_4 concentrations were >2350 mg L^{-1}. Although jarosite has not been observed in waste rock at Diavik, it is a potential sink for both Fe(III) and SO_4 within the test pile.

2.4.2. Paste pH

Paste pH analysis was conducted on samples from the 15 m cross section. The location of the TW115C profile is indicated by open diamonds (Figure 2-5). The paste-pH data indicate several regions of low pH developed within the test pile. The low pH regions are indicated consistently using the measurements conducted using distilled water and a $CaCl_2$ saturated supernatant solution. The pH determined via $CaCl_2$ saturated solution was, on average, 0.5 units lower than the pH determined via distilled water.

The most prominent low pH region is located in the upper west (left) region of the 15 m cross section. Two less prominent low pH regions are located near the base of the test pile and in the upper east (right) region. The aqueous pH data from the TW115C profile is consistent with the results determined via paste pH analysis. The region of low paste pH in the upper portion of the test pile was captured by the TW115C profile. The $CaCl_2$-saturated paste pH results were on average 0.1 (σ = 0.2) pH units higher than the aqueous pH measurements whereas the distilled-water paste pH measurements were on average 0.6 (σ = 0.2) pH units higher.

2.4.3. Microbiology

Six samples from the TW115C profile were enumerated for MPN (Figure 2-6). Measurable counts of aSOB, aIOB, and nSOB were detected at each location. Acidophilic SOB were the least prolific bacteria with counts ranging from 5 to 350 g^{-1} and a median count of 23 g^{-1}. The maximum count was recorded at a location with a pore-water pH of 4.7 (elev. 447.5 masl). Acidophilic IOB counts ranging from 4 to $5.3x10^5$ g^{-1} were recorded with a median count of 170 g^{-1}. The maximum aIOB count was recorded at a location with pH 6.5 (elev. 44o.0 masl). The highest counts of any

group were of nSOB (elev. 440.0 masl). Neutrophilic SOB counts ranged from 240 to $5.3x10^6$ g^{-1} with a median count of $5.4x10^3$ g^{-1}. The maximum nSOB count was recorded at the same location as the maximum aIOB count. A large population of nSOB, $2.8x10^4$ g^{-1}, was recorded at the same location as the maximum aSOB count.

2.4.4. Solid-phase geochemistry

2.4.4.1 Whole rock analyses

XRF analysis of the samples (Figure 2-7) indicates that SiO_2 was the main oxide component in the weathered waste rock at 70.2-72.3 wt. % ($\mu = 71.3$, $\sigma = 0.4$). This observation is consistent with the predominant granite and granitic-pegmatite lithology of the unweathered Type I waste rock. Al_2O_3 was the next most prominent component at 17.9-18.7 wt. % ($\mu = 18.3$, $\sigma = 0.2$).

K_2O, associated with feldspar minerals, was present in the weathered waste rock at 4.5-6.0 wt. % ($\mu = 5.2$, $\sigma = 0.3$), while MgO and CaO were present in small quantities at 0.6-0.9 wt. % ($\mu = 0.7$, $\sigma = 0.1$) and 0.6-1.1 wt. % ($\mu = 0.8$, $\sigma = 0.1$), respectively. Iron, represented as Fe_2O_3, a component of pyrrhotite and potential secondary Fe(oxy)hydroxides, was present in the waste rock at 1.6-3.1 wt. % ($\mu = 2.2$, $\sigma = 0.4$).

Zinc and Ni were the most abundant trace metals in the waste rock at 33.9-124.3 ppm ($\mu = 46.4$, $\sigma = 12.6$) and 0-121.1 ppm ($\mu = 17.6$, $\sigma = 18.9$), respectively. The Cu content of the waste rock was 5.3-29.3 ppm ($\mu = 11.7$, $\sigma = 5.3$) and Co content was 3.9-10.2 ppm ($\mu = 6.7$, $\sigma = 1.6$).

2.4.4.2 Carbon and sulfur analysis

2.4.4.2.1. Bulk samples

Approximately 60% of the sample locations from the 15 m cross section were analyzed for C and S concentration. The bulk C concentration of the unweathered waste rock in the region of the 15 m cross section (Table 2-1) was 0.033 wt. % ($\sigma = 0.009$ wt. %, $n = 5$) whereas the bulk S

concentration was 0.020 wt. % (σ = 0.017 wt. %, n = 74) (Smith *et al.*, 2013b). The average C concentration of the bulk weathered waste rock from the 15 m cross section was 0.020 wt. % (σ = 0.006, n = 50) whereas the average S concentration was 0.019 wt. % (σ = 0.011, n = 50). Carbon and S concentrations in bulk matrix samples are presented in Figure 2-8A.

2.4.4.2.2. Particle size fractions

Particle-size fractions were analyzed to determine in which particle size the greatest loss or gain of C and S occurred. The particle-size fractions used for unweathered samples were slightly different from those used for weathered samples. Unweathered particle-size fractions were pan, 0.106, 0.315, 0.625, 1.25, 2.5, and 5 mm (Smith *et al.*, 2013b). Weathered particle-size fractions were pan, 0.15, 0.30, 0.60, 1.18, 2.36, and 4 mm. The variation arising from the slight differences in particle-size fractions are assumed to be negligible and the fractions used for the weathered samples are used as identifiers going forward.

Analysis of weathered waste rock indicates that the pan-size fraction had the greatest proportion of C and S with an average C concentration of 0.049 wt. % (σ = 0.004) and S concentration of 0.048 wt. % (σ = 0.011). The lowest S content was present in the largest particle-size fraction with an average of 0.006 wt. % (σ = 0.006). The 1.18-2.36 mm particle-size fraction had the lowest C content at 0.016 wt. % (σ = 0.004). A summary of the mean values and standard deviations for each particle-size fraction is provided in Table 2-1. Results of C and S analysis for particle-size fractions are presented in Figure 2-8B to H.

2.4.4.3 Acid base accounting

Neutralization potential (NP) and acid-generating potential (AP) are commonly used to determine the AMD generating capacity of tailings and waste rock. NP:AP ratios (NPR) are used to predict drainage quality with NPR <1 indicating potentially acid generating (PAG), 1<NPR<2 uncertain acid generation potential, and NPR>2 non-potentially acid generating (non-PAG) (Price, 2009). NP was calculated using the analytically determined C content of the bulk matrix

and particle-size fraction samples of the waste rock. These calculations assume that the C content is contained entirely within $CaCO_3$. This assumption is considered reasonable on the basis of previous mineralogical investigations (Jambor, 1997). The neutralization of acid by the dissolution of $CaCO_3$ proceeds as:

$$CaCO_3 + 2H^+ \rightarrow Ca^{2+} + H_2O + CO_2$$

Similarly, the AP was calculated using the analytically determined S content. AP calculations assume that all S is present as sulfide and the calculation is based on the sulfide oxidation reaction:

$$Fe_{(1-x)}S_{(s)} + \frac{(9-3x)}{4}O_{2(aq)} + \frac{(5-3x)}{2}H_2O_{(aq)} \rightarrow (1-x)Fe(OH)_{3(s)} + SO_4^{2-} + 2H^+$$

This reaction for the specific sulfide mineralogy of the Diavik country rock, pyrrhotite [$Fe_{17}S_{20}$], is (Smith *et al.*, 2013b):

$$Fe_{(0.85)}S_{(s)} + 2.1375O_{2(aq)} + 2.275H_2O_{(aq)} \rightarrow 0.85Fe(OH)_{3(s)} + SO_4^{2-} + 2H^+$$

Therefore, one mole of $CaCO_3$ is required to neutralize the acid generated from one mole of pyrrhotite. The assumption concerning the occurrence of S in the weathered samples only as sulfide is somewhat uncertain because of the possible presence of sulfate-bearing secondary minerals.

2.4.4.3.1. Bulk samples

Carbon and sulfur analyses were used to conduct NPR calculations on bulk matrix samples from the 15 m cross section. Of the 50 samples used in bulk matrix NPR calculations, 31 were non-PAG and three were PAG (Figure 2-9). The three PAG samples were associated with $CaCl_2$ paste pH of 4.0, 4.7, and 5.9 and distilled-water paste pH of 4.3, 5.1, and 5.9. The low paste pH regions in the upper west and basal portions of the 15 m cross section were accurately indicated by PAG or uncertain PAG. Only one of the two samples that defined the low paste pH region in the upper

east portion of the cross section was analyzed for C and S. The NPR of this sample indicated it was non-PAG (distilled-water paste pH = 6.0, $CaCl_2$ paste pH = 5.5, NPR = 5.0).

2.4.4.3.2. Particle size fractions

NPR analysis was conducted on weathered particle-size fractions from the three vertically aligned sample profiles. All three profiles were selected because they crossed regions of low and high pH. The pH at the surface of the test pile at all three profile locations was circumneutral. The pH declined to 4.1-4.6 at elevations below 449.6 masl in all profiles. At an elevation of 447.3 masl the pH of all three profiles rose to >7. Conditions at the base of the test pile were variable for the profiles. The TE135C and TW115B profiles remained circumneutral to the base of the test pile. The TW115C profile declined to a pH value of 5.0 at the base of the test pile (Figure 2-8).

NPR calculations for the deconstruction particle-size fraction data neglected samples where the S concentration was undetectable. Only particle-size fractions >1.18 mm of the weathered samples had undetectable S concentrations. The general trend of NPR values mimics the trend in pH values for particle-size fractions <1.18 mm. Regions of low pH were commonly PAG or uncertain PAG and regions of circumneutral pH were typically non-PAG. An exception to the association of low pH with PAG or uncertain PAG material was a cluster of samples at 446 masl. At 446 masl, samples from all three profiles had pH >7.2. Samples from two of the profiles indicated uncertain PAG in the <0.30 mm particle-size fractions and non-PAG in the >0.30 mm particle-size fraction. The third profile was non-PAG for all particle-size fractions at 446 masl.

Approximately 35% of samples in the pan, 0.075-0.15 mm, and 0.15-0.30 mm particle-size fractions were uncertain PAG or PAG. The proportion of PAG or uncertain PAG samples decreased with increasing grain size. In the 0.30-0.60, 0.60-1.18, 1.18-2.36 and 2.36-4.00 mm particle-size fractions the majority of samples were non-PAG (86, 90, 94 and 100%, respectively, Figure 2-8).

2.5. Discussion

Previous studies using deconstruction of waste rock test piles have analyzed a limited number of samples (Stockwell *et al.*, 2006) or had lower sample density (Azam *et al.*, 2007). These studies investigated waste rock in sub-arctic and continental climates, respectively. The deconstruction of the Type I test pile at Diavik is the first to collect samples for a broad range of parameters including microbiology, pore water chemistry, mineralogy, ice distribution and characterization, volumetric moisture content, and particle size distribution in an arctic climate. This comprehensive data set will facilitate elucidation of the relationships between the parameters and their contribution to the evolution of the waste rock. The deconstruction project at Diavik also collected the largest number of samples with the greatest density, providing a high-resolution data set to investigate the manner in which heterogeneity affects waste rock evolution.

2.5.1. Pore water composition

Preliminary results indicate that low-pH pore water is associated with elevated concentrations of SO_4 and dissolved metals. Comparison of paste pH and pore-water pH results indicate that both distilled water and $CaCl_2$ saturated paste pH measurements provide an over-estimate of the pore-water pH within the test pile. The measurements of paste pH from the 15 m cross section show low-pH regions with lateral extent have developed within the test pile, and the pH in the test pile changes sharply from low to circumneutral over short distances. Pore-water results from both the 15 and 35 m cross sections indicate that regions of low pH, and likely elevated SO_4 and dissolved metal concentrations, are present in the upper elevations of the test pile.

2.5.2. Mineralogical evolution

Locally, circumneutral paste pH was observed to occur where CaO content was slightly elevated. Individual low-pH samples were associated with slightly elevated Al_2O_3 content and

slightly depleted SiO_2 content. A slightly elevated Fe_2O_3 content was observed in the low paste pH region at the base of the 15 m cross section. When considering the full data set, statistical analysis using regression indicated that the correlation between pH and oxide content was weak with R^2 values of 0.11 for CaO, 0.04 for Al_2O_3, 0.14 for SiO, and 0.04 for Fe_2O_3. The observation that the oxide content of individual samples had little association with pH may be a consequence of natural variation in the waste rock rather than the geochemical evolution of the composition.

Metal leaching and mobility can be enhanced under low pH conditions (Amos *et al.*, 2015). As a result, it may be expected that the metal content of the waste rock would be lower in locations with low paste pH but in the Type I test pile this was not observed in the bulk composition. Statistical analysis of metal content verses pH resulted in no significant correlation, with R^2 values for Ni of 0.07, Zn of 0, Cu of 0.01, and Co of 0.02.

Correlation between solid element content of the bulk matrix and pH was poor. It is possible that a greater correlation between solid element content and pH would be observed if XRF analysis was conducted on the <0.075 mm particle-size fraction. Insufficient sample volumes precluded the completion of XRF analysis on the <0.075 mm fraction during this study. Analysis of the solid element content of particle-size fractions is required to further elucidate the relationship between oxide content and pore-water pH due to the higher reactivity of small particle sizes.

Although there is no correlation between metal content and pH, the relationship between metals provides insight into the geochemical evolution of the waste rock. The heavy metals in the waste rock are primarily contained in sulfide minerals with Zn present in sphalerite, Cu present in chalcopyrite, and Ni and Co within pyrrhotite. Nickel and Co are present in unweathered pyrrhotite at a ratio of 4:1 (Jambor, 1997). The Ni:Co of the weathered waste rock was 0-14.0 (μ = 2.5, σ = 2.2) indicating that more Ni than Co has been released from the waste rock, or that an additional source of Co is present, resulting in an apparent depletion of Ni throughout the cross section.

2.5.3. Change in carbon and sulfur content

A comparison between weathered (n = 22) and unweathered (n = 5) samples was conducted to determine the significance of the differences between the data sets. Data were first analyzed using a two-tailed t-test. For sample sets that lacked normal distribution due to the small number of unweathered particle-size fraction samples available, a Mann-Whitney Rank Sum test was conducted. The log of non-normally distributed data was also analyzed for normal distribution. A two-tailed t-test was used to analyze normally-distributed log-transformed data.

Comparison of construction and deconstruction samples indicated that there is a statistically significant difference between the C concentration of the unweathered and weathered bulk matrix samples (P-values: rank sum = 0.005, t-Test (log C) = <0.001). There is no statistically significant difference between the S concentration of the unweathered and weathered bulk matrix samples (P-values: rank sum = 0.425, t-Test (log S) = 0.493).

The majority of the particle-size fractions followed the trend observed in the bulk matrix C and S data: the weathered C data set was significantly different from the unweathered data set, but the weathered S data set was not significantly different from the unweathered data set. The exception to the trend was the pan-size fraction where the decrease in C content was not statistically significant. The C content of the waste rock decreased by 29-55% relative to unweathered samples for all particle-size fractions and, with the exception of the <0.075mm fraction, this reduction was statistically significant.

The S content of the weathered waste rock was typically the same or greater than the S content of the unweathered waste rock. The ELTRA CS2000 measurements do not differentiate between sulfate-S and sulfide-S. The similarity between the S content of the unweathered and weathered samples may be the result of formation of secondary S-bearing minerals within the test pile resulting in S retention. Sinclair (2014) determined that the release of S from the Type III test

pile was lower than expected based on the mass loading of Ni. The retention of S within the Type I test pile is consistent with these findings from the Type III test pile.

2.5.4. Neutralization potential ratios

Smaller particles have greater surface area to volume ratios and are typically more reactive as a result. Analysis of unweathered samples indicated that the smallest particle-size fraction of the Type I waste rock had the greatest acid generation potential. Acid generating potential decreased with increasing particle size up to 0.63 mm. Analysis of particle-size fractions from unweathered samples >0.63 mm indicated that NPR were generally >12 or that the material was non-PAG (Smith *et al.*, 2013b).

Low pore-water pH was often indicated by material classified as PAG or uncertain PAG at particle-size fractions <0.60 mm in the weathered samples. The majority of particle-size fractions >0.60 mm were non-PAG regardless of pore-water pH. Regression analysis of particle-size fraction NPRs of the weathered samples and pore-water pH was conducted to determine the strength of the association of NPR with pH. Regression analysis indicated poor correlation between NPR and pore-water pH (Figure 2-10), but the correlation was strongest when the smallest particle-size fraction was considered (R^2 value of 0.33 for <0.75 mm).

Because S content is used to calculate acid generating potential and all S was assumed to be present as sulfide, it is possible that these NPRs overestimate the remaining acid-generation potential of the waste rock at the time of deconstruction. Further analysis is required to determine the relative abundance of the SO_4^{2-} and S^{2-} bearing mineral content of the weathered waste rock to provide a more accurate estimate of the change in acid generating potential of the waste rock.

Although NPR calculations using total S are imperfect, the regions of low paste-pH are typically indicated by low NPR calculations conducted using bulk-matrix waste rock. An exception is a region in the middle elevations of the 15 m cross section where uncertain PAG material is associated with circumneutral paste pH. This region is also associated with low microbial

densities indicating that other processes are likely contributing to decrease acid generation or enhance acid neutralization.

2.5.5. Microbiology

The observation of matrix filling ice at an elevation of approximately 441 masl corresponds with circumneutral pH and lower concentrations of sulfide oxidation products and metals. Although the presence of ice throughout the year indicates limited availability of free water and temperatures that are not conducive to the growth of microbial communities capable of catalyzing sulfide oxidation, the maximum MPN counts of nSOB and aIOB were observed in the frozen region at the base of the profile.

2.6. Conclusions

Deconstruction of the Type I test pile facilitated the collection of a much larger number of samples, with greater sample density, and from more precise locations than would be possible by other means. Using this technique, it was also possible to collect samples for multiple parameters from each location so that relationships between parameters can be evaluated. The deconstruction of the Type I test pile facilitated (1) the visual observation and mapping of spatial distribution of features indicative of oxidative dissolution of sulfide minerals in 3-D and (2) collection of intact and undisturbed samples for mineralogical, geochemical, and microbiological characterization.

The data presented here illustrates that variable conditions exist within the test pile with sharp changes from neutral to acidic pH present over a few meters. This observation suggests that heterogeneity inherent in the waste rock has influenced the geochemical evolution of the pore water within the test pile.

The C content of the waste rock has been reduced by approximately 29-55% because of acid neutralization within the test pile. The S content of the weathered waste rock is unchanged compared to the unweathered waste rock. This is likely due to S retention within the test pile as a result of formation of secondary S-bearing minerals. Estimates of remaining acid generating potential are likely overestimated as a result of inclusion of oxidized S species in NPR calculations. Although acid generating potential is likely over-estimated, PAG and uncertain PAG results correspond to regions with low paste pH.

Due to the greater reactivity of smaller particle-size fractions, it is important to use smaller particle-size fractions when looking for connections between solid-phase composition and other parameters in heterogeneous waste rock. The NPR of small particle-size fractions were a better predictor of pore-water pH than large particle-size fractions. Use of particle-size fractions for XRF analysis would also likely result in stronger correlation between aqueous geochemical conditions and alteration mineralogy.

2.7. Figures

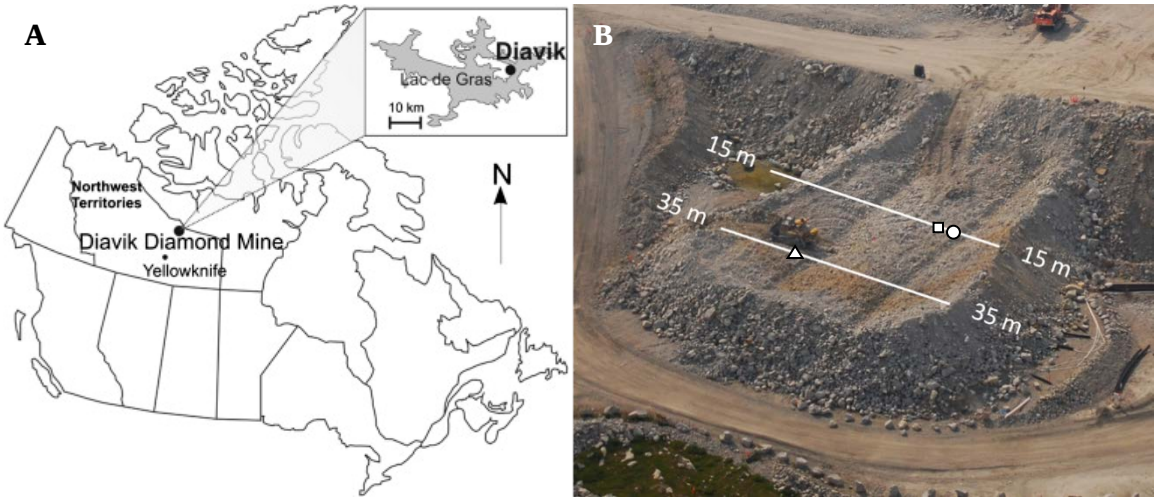

Figure 2-1: A) Location of Diavik Diamond Mine, Northwest Territories, Canada (Smith et al., 2013c) and B) location of the 15 m and 35 m cross sections and (□) TW115B, (o) TW115C, and (Δ) TE135C profiles. Image shows the Type I test pile following excavation of the third level of sampling trenches.

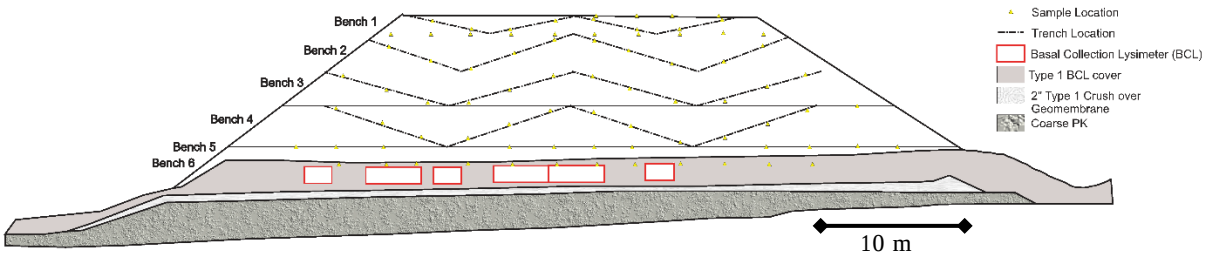

Figure 2-2: Deconstruction design indicating location of trenches (dashed lines), sample locations (yellow triangles), bench surfaces (solid grey lines), and basal collection lysimeters (red). View looking down the long axis of the test pile.

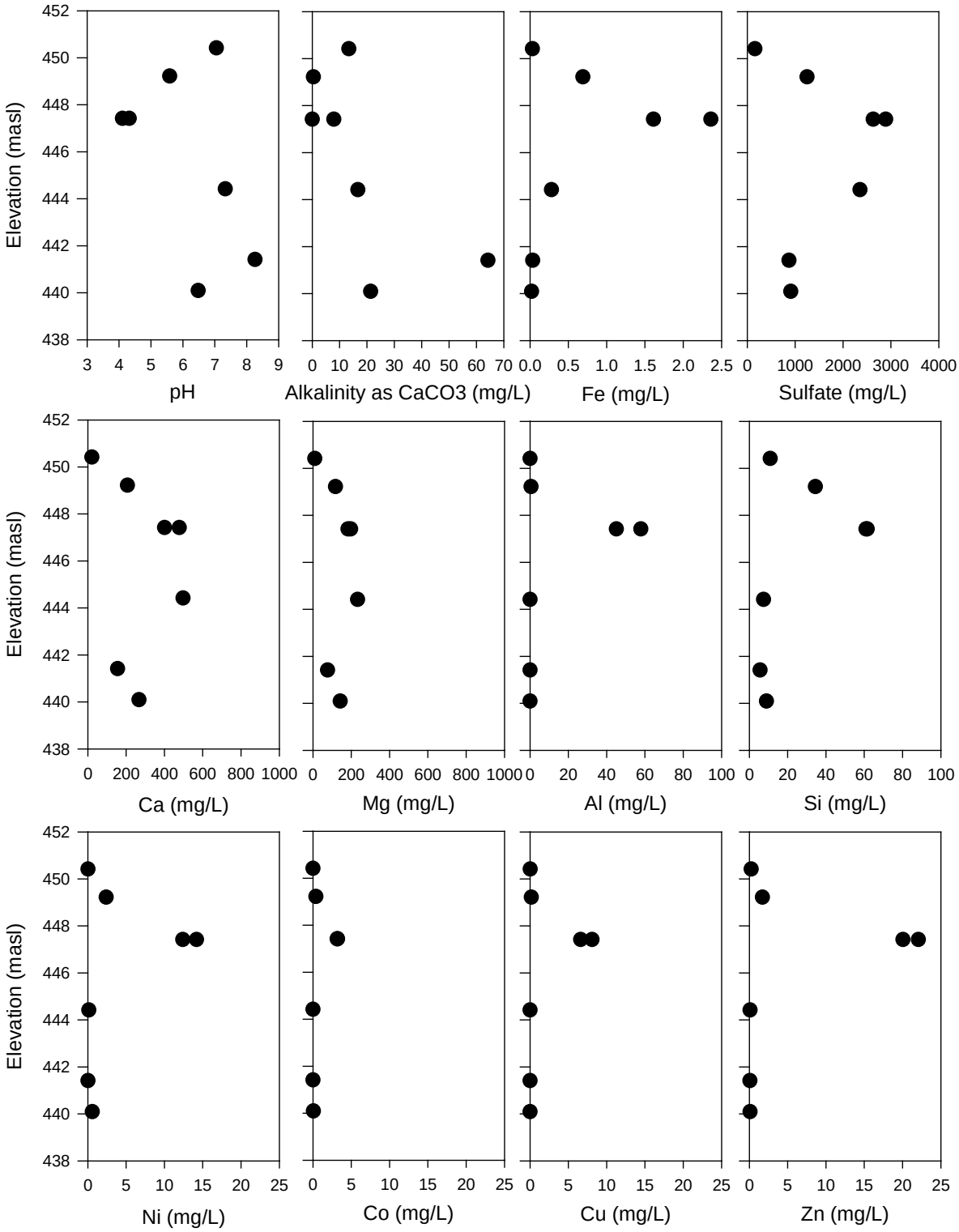

Figure 2-3: Aqueous geochemistry results for selected parameters including duplicate sample at 447 masl. Low pH duplicate sample associated with elevated concentrations of sulfide oxidation products.

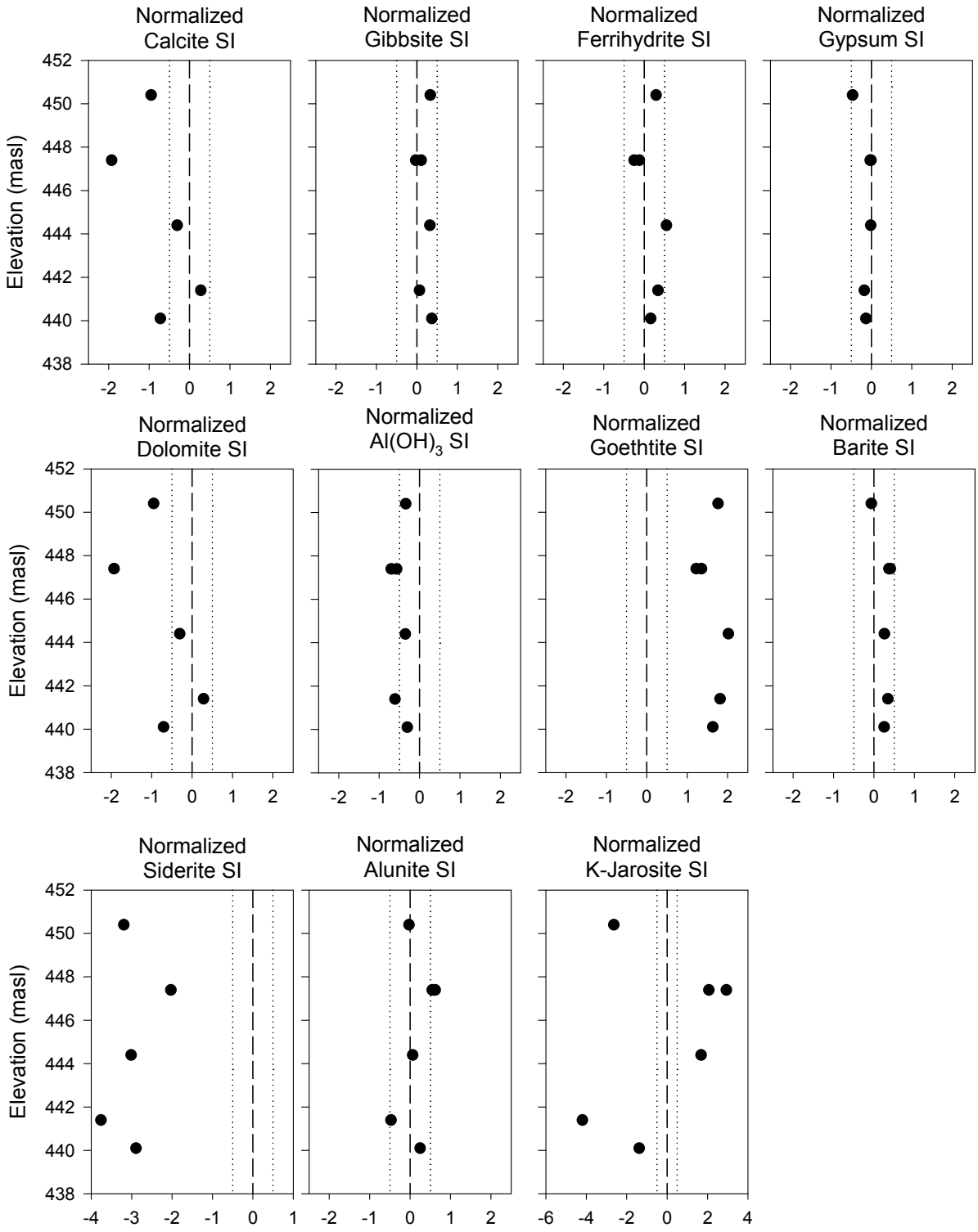

Figure 2-4: Calculated saturation index normalized by number of ions present in the mineral.

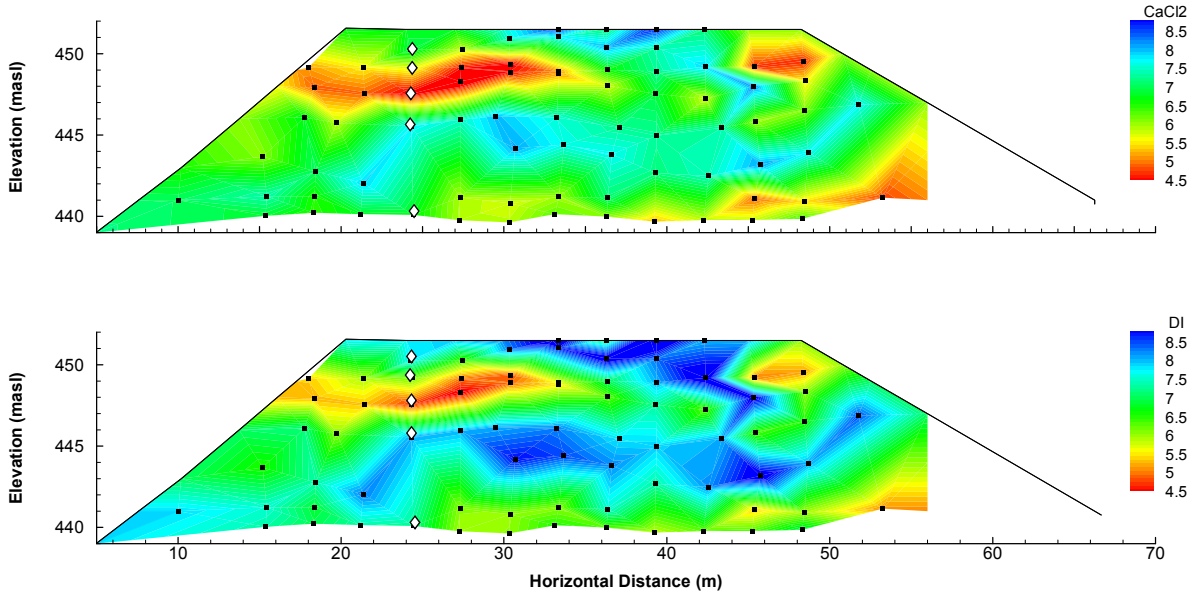

Figure 2-5: Paste pH of the 15 m cross section. (▪) indicates sample location. (◇) indicates location of TW115C priority profile

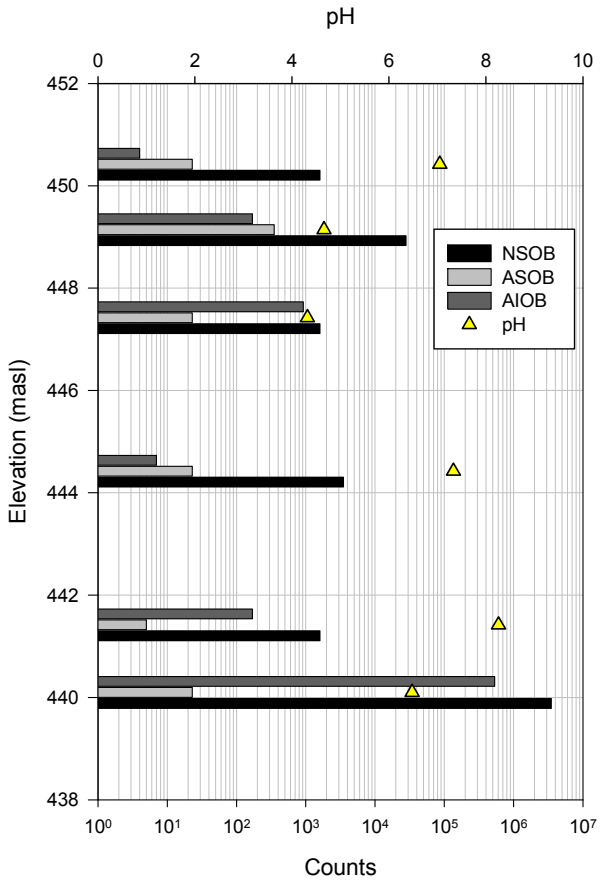

Figure 2-6: MPN enumeration by sample elevation.

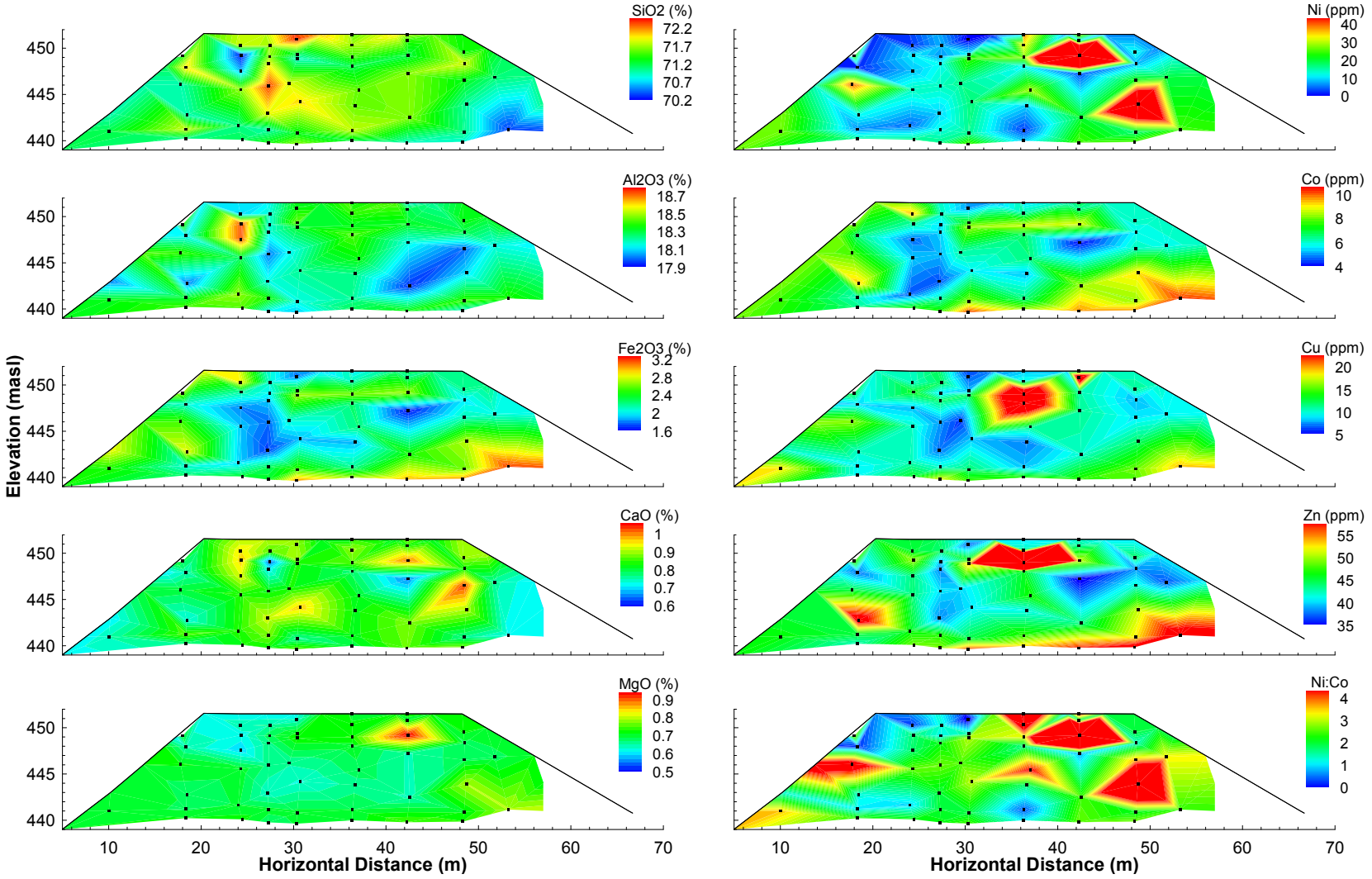

Figure 2-7: Whole rock analyses of selected oxides and metals.

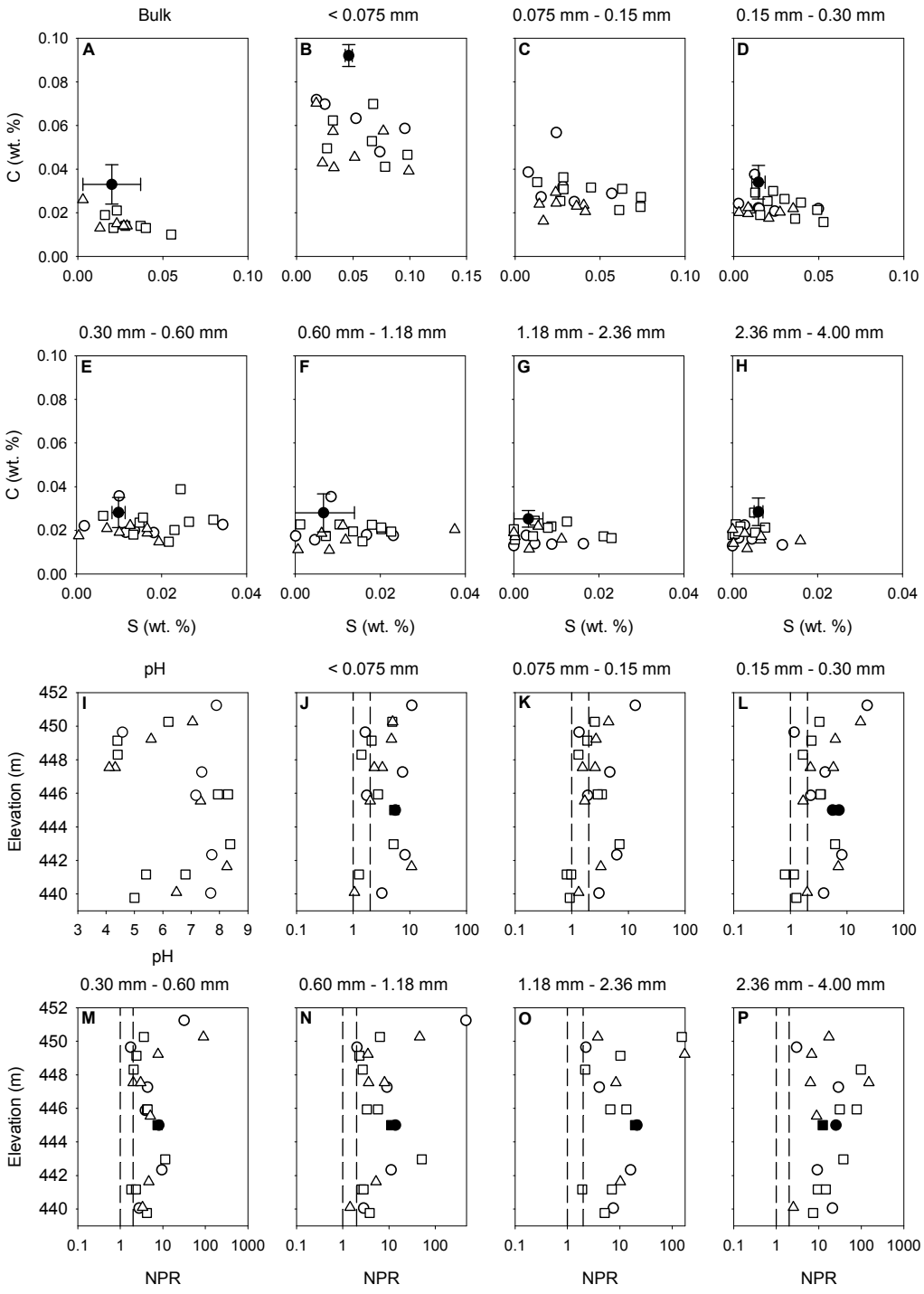

Figure 2-8: Carbon verses sulfur (A-H), pore-water pH (I), and NPR (J-P) results from particle size fraction samples from construction (black) and deconstruction (white) samples. Error bars on C/S construction samples are one standard deviation. On the 15 m cross section, the profile from 5 m west of the center line is represented by □ and the profile from 8 m west of the center line is represented by Δ. The profile 7 m east of the center line on the 35 m cross section is represented by o. On figures I – P, closed circles represent μ(NP:AP) whereas closed squares represent μNP:μAP (Smith et al., 2013b).

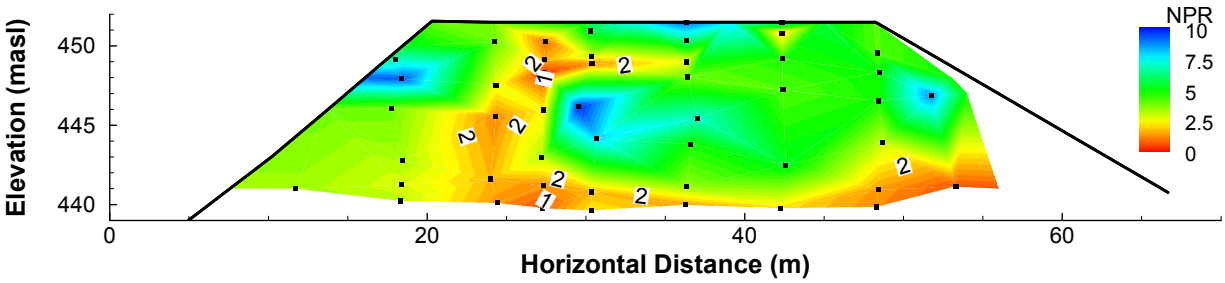

Figure 2-9: NPR results for the 15 m cross section, (▪) indicates sample location.

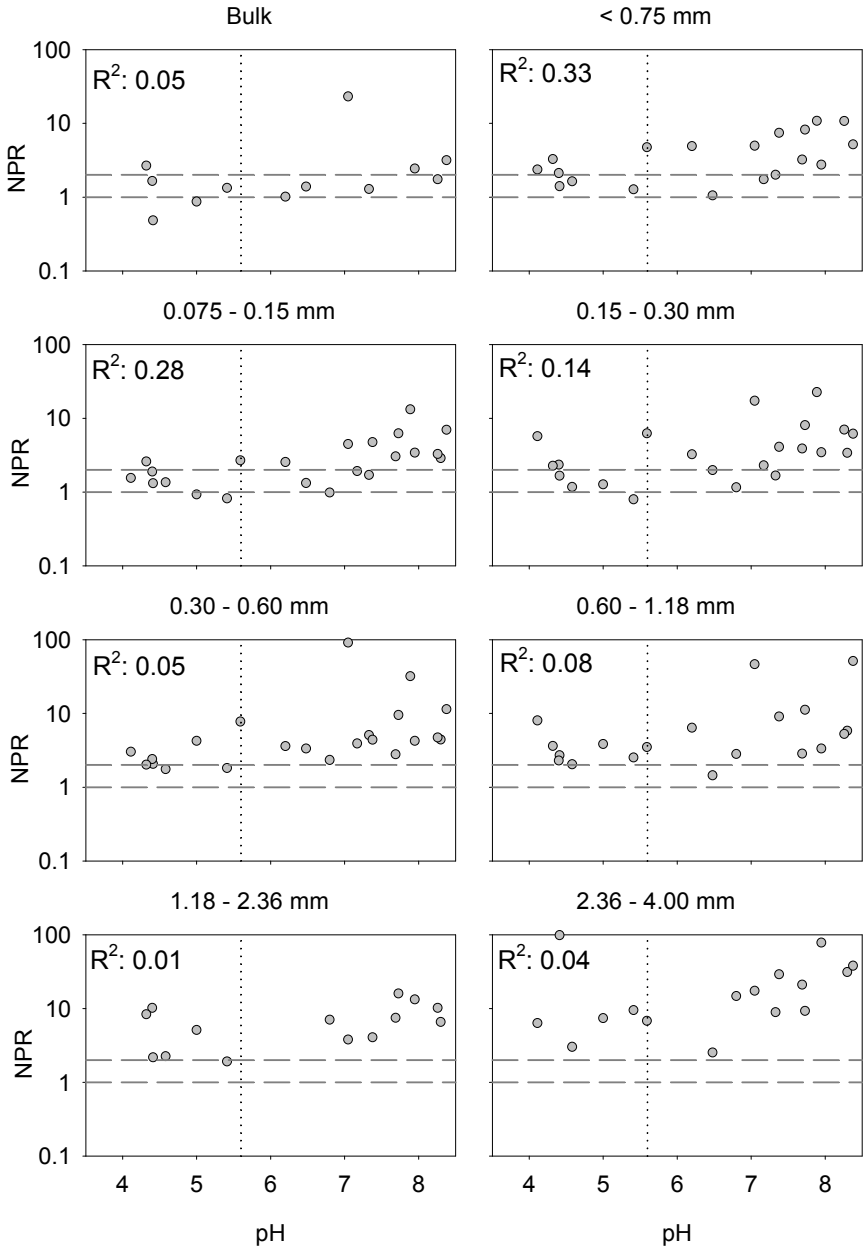

Figure 2-10: Dashed lines represent NPR of 1 and 2, dotted line represents pH of 5.6 (rain water).

2.8. Tables

Table 2-1 - Comparison of carbon and sulfur analyses from particle size fractions collected from unweathered (n = 5) and weathered (n = 22) waste rock. Statistical analysis was conducted using a two-tailed t-Test (normal data and normal log transformed data) and/or rank sum analysis (non-normal data). a) Unweathered data from Smith et al. (2013a)

Particle size fraction	Element (wt. %)	Unweathered[a]		Weathered		t-Test	Rank sum	t-Test on log(data)	Reject null?
		μ	σ	μ	σ				
Pan	C	0.092	0.010	0.049	0.004	--	0.075	--	No
	S	0.046	0.007	0.048	0.011	0.706	--	--	No
0.15-0.30	C	0.034	0.005	0.024	0.001	--	0.016	0.011	Yes
	S	0.015	0.003	0.030	0.012	0.279	--	--	No
0.30-0.60	C	0.028	0.008	0.020	0.002	0.016	--	--	Yes
	S	0.010	0.004	0.019	0.006	0.406	--	--	No
0.60-1.18	C	0.028	0.007	0.019	0.005	--	0.009	0.006	Yes
	S	0.007	0.002	0.013	0.013	0.315	--	--	No
1.18-2.36	C	0.025	0.009	0.016	0.004	<0.001	--	--	Yes
	S	0.003	0.007	0.012	0.004	--	0.298	--	No
2.36-4.00	C	0.028	0.004	0.017	0.003	0.006	--	--	Yes
	S	0.006	0.003	0.006	0.006	--	0.351	0.710	No
Bulk	C	0.033	0.070	0.015	0.011	--	0.005	<0.001	Yes
	S	0.020	0.017	0.022	0.030	--	0.425	0.493	No

CHAPTER 3. THE IMPACT OF HETEROGENEITY ON THE GENERATION OF ACIDIC REGIONS AND BULK EFFLUENT IN A LOW SULFIDE WASTE ROCK TEST PILE

Summary

A 40,000 m^3 low sulfide waste-rock test pile was constructed at the Diavik Diamond Mine and subjected to natural weathering conditions for eight years. The test pile was deconstructed in 2014 to obtain samples for characterization of the pore-water composition, mineralogical evolution, and microbial distribution with high density and rigorous spatial control. The geochemical, mineralogical, and microbiological observations, combined with *in situ* data collected from the test pile, were used to examine the effect of geochemical and mineralogical heterogeneity within the test pile and the effect on drainage composition.

Pore-water chemistry data collected from approximately 350 locations within the test pile showed that the pore water throughout most of the test pile is characterized by near-neutral pH conditions, with low concentrations of dissolved metals. Isolated regions with elevated original S content were associated with low-pH pore water containing elevated concentrations of SO_4 and dissolved metals. The low-pH zones were typically in the upper elevations of the test pile where temperatures remain above 0 °C late into the active season.

The pore-water data set was utilized to assess the influence of ferrihydrite on attenuating Ni, Co, Zn, and Cu, and drainage quality. The heterogeneous distribution of sulfide minerals and thermal conditions in the deconstructed test pile resulted in geochemical zoning conducive to metal adsorption. Water from low-pH zones in the upper portions of the test pile infiltrated down into regions with circumneutral pH prior to discharge from the test pile. In the circumneutral regions, pore water was at saturation with respect to ferrihydrite and conditions were conducive to adsorption of dissolved metals. These conditions coincided with substantially reduced concentrations of dissolved metals in the test-pile effluent compared to other higher sulfide waste-rock systems (Sinclair *et al.*, 2015, Stockwell *et al.*, 2006).

3.1. Introduction

On a daily basis, approximately one million tonnes of mine waste is generated in Canada (Government of Canada, 1991). Waste rock includes country rock excavated to access ore bodies and sub-economic grades of ore minerals. Waste rock often contains reactive sulfide minerals such as pyrite [FeS_2] and pyrrhotite [$Fe_{(1-x)}S$] (Blowes *et al.*, 2014). Weathering of waste rock may result in the generation of low quality drainage through the oxidation of sulfide minerals and precipitation of secondary phases. Collectively, these processes can result in the generation of low-pH water containing high concentrations of dissolved metals and sulfate, referred to as acid mine drainage (AMD), or sulfate- and metal-laden drainage at neutral pH referred to as neutral mine drainage (NMD). Effluent affected by mine drainage has the potential to impact surface-water and groundwater quality for centuries (Blowes & Jambor, 1990).

The quality of mine drainage is dependent on numerous factors including the transport of water, oxygen, and heat; particle-size distribution; microbial community development; and the abundance of acid-generating and acid-consuming minerals (Amos *et al.*, 2015). The rate of sulfide oxidation is based on a number of factors including surface area, type, and concentration of oxidant; microbial catalysis; pH; and temperature. Microbial communities capable of catalyzing sulfide-oxidation reactions are ubiquitous (Nordstrom & Southam, 1997). Temperature has been identified as a strong control on the oxidation of sulfide minerals due to both the temperature dependence of abiotic oxidation and the optimum growth temperatures for bacteria implicated in sulfide oxidation (Belzile *et al.*, 2004).

Several studies have investigated the temperature dependent rates of pyrite and pyrrhotite oxidation (Ahonen & Tuovinen, 1992, Elberling *et al.*, 2000, Meldrum *et al.*, 2001, Elberling, 2005). Pyrite oxidation has been observed at temperatures as low as -11 °C. Elberling (2005) observed a 10 fold increase in pyrite oxidation rates for a 10 °C increase in temperature from -11 °C to -2 °C at which temperature the rate of oxidation increased by a factor of two for each 10 °C

increase in temperature. Meldrum *et al*. (2001) observed decreasing rates of pyrrhotite oxidation in intact tailings with decreasing temperature. The decrease in oxidation rate was strongest between 30 °C and 0 °C and no apparent oxidation was observed at -10 °C. Although pyrrhotite is more rapidly oxidized than pyrite, due to the lower activation energies required to initiate oxidation in pyrrhotite, the temperature dependence of oxidation is similar for pyrite and pyrrhotite (Ahonen & Tuovinen, 1992).

When the rate of sulfide oxidation is depressed, the rate of acid neutralization may be sufficiently rapid for the acid consuming capacity of rock to offset the acid generation capacity. Ahonen and Tuovinen (1992) observed that acid addition was not required to maintain pH below the target of 2.2 after the onset of sulfide oxidation in columns loaded with sulfide rich ore incubated at 37 °C. The acid-consuming capacity of the ore incubated at 4 °C required the addition of acid to maintain pH below 2.2 for the duration of the experiment.

When sulfide oxidation occurs, liberated metals may be sequestered through adsorption onto secondary minerals. Secondary Fe (oxy)hydroxide minerals can adsorb or co-precipitate metals and commonly form in mine wastes as finely dispersed coatings on other particles. The pH dependence of cation adsorption on Fe (oxy)hydroxides has been the focus of extensive studies (Davis & Leckie, 1978a, Davis & Leckie, 1978b, Benjamin & Leckie, 1981, Dzombak & Morel, 1990, Zhang *et al.*, 1992, Robertson & Leckie, 1998).

Iron (oxy)hydroxide surfaces are amphoteric due to the association of water molecules with the mineral surfaces. At low pH, water molecules associated with Fe (oxy)hydroxides surfaces are protonated resulting in a positive charge. As pH increases, H^+ dissociates from the mineral surface, the surface charge becomes more negative, and cations are attracted to the negatively charged Fe (oxy)hydroxide surfaces. The quantity of a given cation adsorbed to the Fe (oxy)hydroxide may change from 0-100% over one to two pH units (Dzombak & Morel, 1990).

Adsorption density increases with pH and with increasing concentration up to a maximum value of roughly 0.2 mol per mol of Fe (Dzombak & Morel, 1990).

Adsorption sites can be either strong or weak. The density of weak adsorption sites exceeds the density of strong adsorption sites at 0.2 and 0.005 mol per mol Fe, respectively (Dzombak & Morel, 1990). Cations initially adsorb more rapidly to weak sites and gradually move to strong adsorption sites where desorption is less likely (Dzombak & Morel, 1990).

Various Fe (oxy)hydroxides form under different geochemical conditions including schwertmannite at pH <4 and ferrihydrite at pH >4 (Lee *et al.*, 2002). Amorphous Fe (oxy)hydroxides transform to goethite at surficial temperatures and pressures as they age (Stipp *et al.*, 2002). Tonkin *et al.* (2002) determined that adsorption parameters for ferrihydrite can be used to model sorption on schwertmannite, and weak site adsorption constants for ferrihydrite are similar to constants for goethite. Therefore, parameters determined for hydrous ferric oxide by Dzombak and Morel (1990) can be used to model adsorption on the Fe (oxy)hydroxides expected to form under the conditions present in waste rock.

Studies focused on the pH-dependence of adsorption have shown that the transition metals tend to adsorb in the order Cu>Zn>Ni>Co for a variety of solids, including illite, Fe oxide, Mn oxide, Al oxide, and various soil types (Cama *et al.*, 2005, Welp & Brümmer, 1999, Lee *et al.*, 2002, Dzombak & Morel, 1990). The exception to this adsorption order was a slightly alkaline soil with a pH of 7.2 that adsorbed Co preferentially over Ni (Welp & Brümmer, 1999).

A series of laboratory and field experiments, conducted using waste rock from the Diavik Diamond Mine, NT, focus on AMD generation across a range of scales. Waste rock at Diavik is segregated according to sulfur content. Type I rock contains <0.04 wt.% S, Type II rock contains 0.04-0.08 wt.% S, and Type III rock contains >0.08 wt.% S. Experimental studies include investigations of humidity cells (1 kg), active-zone lysimeters (8 tonnes), test piles (70,000 tonnes), and instrumentation in the full-scale waste-rock dump (120 MMt). Previous publications have addressed the characterization of microbial, geochemical, temperature, particle-size, and

gas-transport regimes within these systems (Amos *et al.*, 2009, Bailey *et al.*, 2015, Smith *et al.*, 2013a, Smith *et al.*, 2013b, Neuner *et al.*, 2013, Chi *et al.*, 2013, Pham *et al.*, 2013, Bailey *et al.*, 2016, Bailey *et al.*, 2013, Langman *et al.*, 2014, Langman *et al.*, 2015b, Langman *et al.*, 2015a) and the interpretation of processes that contribute to the observed conditions (Pham, 2013, Bailey, 2013, Sinclair, 2014, Sinclair *et al.*, 2015, Krentz, 2014).

The focus of this chapter is the geochemical evolution of the Type I waste-rock test pile and the factors that affect the composition of the test-pile drainage. The Type I test pile, which was constructed in 2006, was deconstructed in 2014 to obtain undisturbed samples for characterization of the microbiology, mineralogy, geochemistry, ice distribution, volumetric moisture content, and particle-size distribution of the test pile (Chapter 2). This chapter presents the results of pore-water geochemistry, mineralogical, and microbiological measurements of samples collected from the deconstructed test pile, and compares these results to pre-deconstruction measurements and data collected from soil-water solution samplers (SWSS), basal collection lysimeters (BCLs), thermistors, and the basal drain (Figure 3-1).

3.1.1. Site description

The Diavik Diamond Mine is located on a 20 km^2 island in Lac de Gras approximately 300 km NE of Yellowknife, NT (Figure 3-2A). The mean annual air temperature at Diavik is -9.0 °C (1998-2007) with a maximum recorded temperature in July of 27 °C and minimum recorded temperature in January/February of -44 °C for this period. The site receives 280 mm of precipitation on average, of which approximately 35% falls as rain (Environment Canada, 2010).

Waste rock at the site is composed of granite and granite pegmatite containing biotite schist xenoliths. The granite and granite pegmatite are composed of 30-70% K-feldspar [$KAlSi_3O_8$], 15-46% quartz [SiO_2], 0-35% albite [$NaAlSi_3O_8$], 0-5% biotite [$KMg_3AlSi_3O_{10}(OH)_2$], 1-4% muscovite [$KAl_2(Si_3AlO_{10})(OH)_2$], and 2% other minerals including trace pyrite [FeS_2], chalcopyrite [$CuFeS_2$], sphalerite [(Zn,Fe)S], and galena [PbS]. The biotite schist contains 20-

50% quartz, 10-25% biotite, 35-55% albite, and an average of 0.14 wt. % sulfide (range: 0.02-0.42 wt.%). The dominant sulfide contained within the biotite schist is pyrrhotite [$Fe_{0.85}S$], with lesser amounts of pyrite, and trace chalcopyrite and sphalerite (Jambor, 1997, Diavik Diamond Mines Inc., 1998).

The Diavik Waste Rock Research Facility (DWRRF) was constructed to investigate the geochemical evolution of the waste rock with time under natural field conditions (Smith *et al.*, 2013c). The DWRRF includes three test piles composed of (1) low sulfide Type I run of mine (ROM) waste rock (0.035 wt. % S) with basal dimensions of 50 m by 60 m and a height of 15 m, (2) higher sulfide Type III ROM waste rock (0.053 wt. % S) with the same dimensions as the Type I pile, and (3) a covered pile with a Type III core (o.o82 wt. % S), a low permeability till layer, and a Type I thermal insulation layer with basal dimensions of 80 m by 125 m and a height of 15 m. All piles were constructed using standard push and end-dump methods with instrument faces constructed every 5 m. The Type I and Type III pile slopes are at the angle of repose of 38° (1.3H:1V) whereas the covered pile was re-contoured to 18° (3H:1V).

3.2. Methodology

3.2.1. Deconstruction and sample collection

The Type I test pile was deconstructed by excavating two parallel trenches oriented along the long axis of the pile as described in Chapter 2 and by Barsi *et al.* (2016). The first set of trenches were excavated to a depth of 1.2 m with all subsequent trenches excavated to a depth of 2.5-3 m. The trenches were sloped to 18° (3H:1V).

Samples were collected on each side of the trench at 5 m intervals with one sample for each vertical metre of wall. Vertical alignment was maintained between trenches to facilitate the generation of cross sections from each 5 m interval. As described in Chapter 2, the <1 cm particle-size fraction was preferentially selected for microbiology, pore water, and mineralogy studies.

Microbiology samples for most probable number enumeration (MPN) were collected using manufacturer-sterilized Falcon™ Tubes, 70% (v/v) ethanol sterilized nitrile gloves, and autoclave sterilized scoopulas. Samples were stored at 4 °C and shipped to the University of Waterloo for enumeration. Pore-water samples were collected using clean stainless steel trowels and manufacturer sterilized 69 oz Whirlpak® bags. Pore-water samples were extracted immediately or frozen until processing to prevent further reaction. Samples for mineralogical characterization were immediately frozen until processing.

Four cross sections are the focus of this study: three cross sections parallel to the short axis of the test pile at the 15 m, 25 m, and 35 m intervals, and one cross section parallel to the long axis of the test pile located 5 m west of the center line, referred to as the transverse cross section. Figure 3-2B indicates the locations of the cross sections.

3.2.2. Temperature data

The installation and distribution of thermistor strings for the collection of temperature data within the Type I pile was described by Smith *et al.* (2013c) and Pham *et al.* (2013).

Thermistor strings were installed on Face 1, 2, and 4 of the test pile with four strings on each of Face 1 and 4 and two strings on Face 2. The thermistor strings located along the tipping face 5 m west of the centre line were selected to generate the transverse temperature profile.

Temperature data was analyzed and integrated to provide monthly average temperatures. The average ambient air temperature for each month was used to generate surface nodes for the test pile. Inferred points were included along Face 3 of the transverse cross section to mitigate the influence of surface temperatures between Face 2 and Face 4 during data interpolation.

3.2.3. Water sample collection

3.2.3.1 In situ samples

In situ samples include soil water solution samplers (SWSS), basal collection lysimeters (BCL), and basal drain samples. The sampling procedure for *in situ* samples is described by Smith *et al.* (2013a). SWSS points were installed on Faces 1 and 2 at depths between 1 and 9 m. SWSS collect water from the matrix adjacent to the porous cup. Matrix material was placed around the SWSS during construction to provide adequate water retention for sample collection. BCL collection points were located beneath Faces 1 and 2 at a depth of 12 m, covered areas of 4 m^2 or 16 m^2, and collected both matrix and macropore flow. The basal drain collected effluent water from the 3000 m^2 basal liner.

The basal drain and drain lines running from the BCLs to the instrument trailer were fitted with heat trace to prevent ice blockage. Drain lines and sample-collection cells were open to the atmosphere as it was determined that atmospheric O_2 and CO_2 conditions were present throughout the test pile (Amos *et al.*, 2009).

3.2.3.2 Pore-water extraction samples

Pore-water samples were extracted from samples of the waste rock in the field and laboratory (Chapter 2). Samples were processed immediately following excavation or stored

frozen and thawed immediately prior to processing. Sample aliquots were placed in modified 200 mL Falcon™ tubes and centrifuged for 30 minutes at 8500 rpm. Additional aliquots were centrifuged as necessary to obtain a sufficient sample volume for measurement of pH, redox potential, alkalinity, and for analysis of dissolved cations and anions.

The 15 m cross section transects Faces 1 and 2 and intersects 1BWBlys4S, 1BWClys4S, and 1BCElys4S, the southern 16 m^2 BCLs (Figure 3-2B). The 25 m cross section transects Faces 2, 3, and 4. The 35 m cross section transects Faces 4 and 5. A cross section transverse to the 15 m cross section was constructed using pore-water samples from locations 5 m west of the center line of the test pile. Values were inferred out to the crest and batters of the test pile using the nearest pore-water values for all cross sections.

3.2.4. Water sample analysis

The pH, redox potential, electrical conductivity (EC), alkalinity, and NH_3-N measurements were conducted on *in situ* samples in the field, whereas measurements on pore-water samples were conducted in the field or laboratory depending on the location of sample extraction. Measurements of pH, redox potential, and electrical conductivity (EC) were conducted on unfiltered aliquots of *in situ* samples. A separate aliquot of *in situ* sample was filtered and used for determination of alkalinity. Due to limited volumes of pore-water samples available, alkalinity determinations were conducted on filtered aliquots of pore-water, which were previously used for measurements of pH and redox potential. Measurements of NH_3-N were conducted on filtered aliquots for both pore water and *in situ* sample types.

Samples for analysis of dissolved-metal content were filtered using 0.45 µm cellulose acetate filters, acidified to pH <2 with concentrated nitric acid, and analyzed via Inductively Coupled Plasma Mass Spectrometry (ICP-MS; Thermo XSeries) and Inductively Coupled Plasma Optical Emission Spectrometry (ICP-OES; Thermo iCAP 6500 Duo). Samples for analysis of

anions were filtered using 0.45 µm cellulose acetate filters and concentrations were determined via Ion Chromatography (IC; Dionex ICS-3000).

3.2.5. Geochemical modeling

PHREEQCi (Parkhurst & Appelo, 1999) was used to calculate geochemical speciation for SWSS, BCL, and a selection of pore-water samples. Modeling of adsorption isotherms using PHREEQCi was conducted on pore-water samples. Several phases were added to the WATEQ4F database for these calculations including solid and aqueous Co species, and mineral phases lepidocrocite, schwertmannite, and siderite (Langman *et al.*, 2015b).

To better compare the saturation index of mineral phases of varying complexity, results were normalized according to the following equation from Jurjovec *et al.* (2002):

$$SI_N = \frac{\left(\log \frac{IAP}{K}\right)}{N}$$

where IAP is the ion activity product, K is the equilibrium constant, and N is the number of ions in the solid phase. Water samples were considered saturated with respect to a given phase if SI_N was between -0.5 and 0.5.

3.2.6. Mineralogy samples

Samples of the waste-rock matrix material (<1 cm) were collected for mineralogical and geochemical characterization. These samples were freeze dried and subsampled for determination of C and S content and thin section preparation as described in Chapter 2. Polished thin sections were prepared using quartz glass slides, non-aqueous epoxy, polished to 60-µm thickness, and carbon coated for examination under an SEM.

Grains of pyrrhotite were identified and analyzed to determine the oxidation features and their characteristics, and the distribution and relative concentrations of Fe, S, Ni, and Cu using synchrotron micro X-ray fluorescence (µXRF) at beamline 13 ID-E (microprobe), GESCARS,

Advanced Photon Source (APS) at Argonne National Laboratory in Argonne, Illinois, USA. Beamline 13 ID-E delivers an incident beam energy of 2.4-28 keV using a Si(111) monochromator. Micro XRF maps were generated using a 2 x 2 µm beam and a Hitachi Vortex silicon-drift detector. Select grains were analyzed using a Hitachi S-3200N variable-pressure scanning electron microscope equipped with an energy-dispersive spectrometer (SEM-EDX) located at Canada Center for Mineral and Energy Technology (CANMET) in Ottawa, Canada. Spectra produced by the EDX analysis were used to identify alteration of pyrrhotite grains.

3.2.7. Most probable number enumeration

Most probable number enumeration was conducted using the technique described by Cochran (1950) and culture media for acidophilic Fe oxidizing bacteria (aIOB) and acidophilic S oxidizing bacteria (aSOB) described by Benner *et al.* (2000). In addition, neutrophilic S oxidizing bacteria (nSOB) were enumerated using the culture media for aSOB with the pH adjusted to 7.0 using HCl or NaOH as necessary (Chapter 2).

3.3. Results

3.3.1. *In situ* samples

A limited number of SWSS samples were available in 2007, one year after construction was complete. Samples were available from all depths in 2008. Circumneutral pH was initially observed at all depths, but by 2010 isolated regions of lower pH developed at 1 m and 7-9 m (Figure 3-3, data represent an average of all SWSS and BCL samples from each depth). These regions of lower pH persisted until deconstruction in 2014. Decreasing pH values (to pH <5.2) were recorded in BCL samples in 2013 after several years of circumneutral pH values.

Alkalinity, Ca, and SO_4 concentrations were stable from 2010-2013, with low concentrations near the top and base of the test pile and elevated concentrations in the central elevations. Average Fe concentrations for each depth were constant throughout the study period and were less than 1.5 mg L^{-1}. Average Al concentrations for each depth remained below 2 mg L^{-1} with the exception of the 2 m depth (4.5 mg L^{-1}) in 2011 and the 12 m depth (2.7 mg L^{-1}) in 2013. In general, the dissolved Al concentrations increased at lower elevations of the test pile in 2013.

Average Ni concentrations of up to 5 mg L^{-1} were observed in 2007 and 2008 with concentrations <2 mg L^{-1} in the following two years. From 2011-2013 increasing concentrations of dissolved Ni were observed, particularly at depths greater than 7 m. The distribution of Co, Zn, and Cu were similar to Ni but concentrations were typically lower.

In 2013, the final year of sampling prior to test-pile deconstruction, the maximum *in situ* concentrations of Cu, Zn, Ni, and Co were 2.4, 14.3, 8.9, and 2.0 mg L^{-1}, whereas maximum concentrations for all years were 14.2, 18.2, 15.0, and 3.6 mg L^{-1}, respectively.

The dissolution of calcite [$CaCO_3$] consumes acid produced during sulfide oxidation. Dissolution of calcite can maintain pH of 6.5-7.5 (Blowes & Ptacek, 1994). In general, *in situ* samples from locations with pH ≥7 were at equilibrium with respect to calcite throughout the study period (Figure 3-4). In regions with low pH, *in situ* pore-water samples were commonly

undersaturated with respect to calcite. With the exception of the 2 m and 5 m locations, *in situ* SWSS samples were commonly undersaturated with respect to dolomite. Although an exhaustive mineralogical investigation at the feasibility stage of the development of the Diavik mine did not locate dolomite in the waste rock, any dolomite present is likely to be providing acid-consuming capacity in this system (Jambor, 1997).

Following the exhaustion of carbonate minerals, $Al(OH)_3$ may dissolve to maintain pH between 4.0-4.3 (Blowes & Ptacek, 1994). *In situ* pore-water samples were initially at saturation with respect to amorphous $Al(OH)_3$ and the dissolved Al concentrations were correspondingly low. Elevated concentrations of dissolved Al, corresponding with under saturation with respect to amorphous $Al(OH)_3$, were first observed in the BCLs in 2009 and later at additional elevations. *In situ* pore-water samples were generally at equilibrium or slightly oversaturated with respect to alunite [$KAl_3(SO_4)_2(OH)_6$].

Jarosite [$KFe_3(SO_4)_2(OH)_6$], barite [$BaSO_4$], and gypsum [$CaSO_4$] are minerals with the potential to sequester SO_4. *In situ* pore-water samples were frequently at equilibrium with respect to jarosite and barite (Figure 3-5). The relationship between Ca and SO_4 concentrations and saturation with respect to gypsum was apparent in 2008. In 2008, *in situ* samples at saturation with respect to gypsum had elevated concentrations of Ca and SO_4 (>300 mg L^{-1}; >800 mg L^{-1}, respectively) and samples under saturated with respect to gypsum had lower Ca and SO_4 concentrations (<100 mg L^{-1}; <400 mg L^{-1}, respectively). As the SO_4 concentration increased with continued sulfide oxidation during subsequent years, the portion of the pile at equilibrium with respect to gypsum increased. Due to the relatively large reservoir of Ca available from calcite dissolution, gypsum precipitation likely exerts the strongest control on the concentration of SO_4.

The pH of water in waste rock systems has a strong influence on the pore water composition of Fe. At pH >4, concentrations of dissolved Fe are low due to the precipitation of ferrihydrite [$Fe(OH)_{3\,am}$] or schwertmannite [$Fe_{16}O_{16}(OH)_{12}(SO_4)_2$] (Lee *et al.*, 2002). At lower pH, dissolution of ferric (oxy)hydroxides maintains pore-water solutions at pH 2.5-3.5 and results in

elevated concentrations of dissolved Fe (Blowes & Ptacek, 1994). The pH of *in situ* samples was >4, with one exception, resulting in low concentrations of dissolved Fe. *In situ* samples were at equilibrium or slightly over saturated with respect to amorphous $Fe(OH)_3$ for the entire monitoring period which correlates with low concentrations of dissolved Fe observed in the aqueous samples.

3.3.2. Pore-water samples

3.3.2.1 pH

The low pH regions were the most developed in the 15 m cross section (Figure 3-6). The pH in the cross section ranged from 4.2 to 8.7 with an average of 6.6 (σ = 1.2). Well-developed regions with pH <6 were observed in the upper west (top left), upper east (top right), and basal portions of the cross section. Measurements of pH in the 25 m cross section indicate the presence of a diffuse low-pH region in the central portion of this section consisting of 12 samples (Figure 3-7). These samples were distributed across a 6 x 25 m area. The pH in the 25 m cross section ranged from 4.1 to 8.1 with an average of 6.9 (σ = 1.1). The low pH regions in the 35 m cross section were located close to the batter portions of the test pile and pH ranged from 4.5-8.5 with an average of 7.0 (σ = 1.0, Figure 3-8).

The results from the transverse cross section indicate that the regions with low pH were three dimensional in extent and were associated with the location of the original tip faces (Figure 3-9). The highest pore-water pH corresponded to a tip face with a low S content in the waste rock (0.018 wt. % S, Face 1) near the test-pile ramp. The lowest pore-water pH was associated with relatively high-S waste rock (0.033 wt. % S, Face 3). This relationship was not observed on Face 5, where the highest S waste rock (0.041 wt. % S) was present, but where pore-water pH was circumneutral.

3.3.2.2 Sulfate

In all four cross sections, elevated concentrations of SO_4 were associated with low pH regions. At the outer boundary of the test pile, where infiltration of rain and snowmelt occurred shortly before the initiation of the test-pile deconstruction, concentrations of SO_4 were lower. Sulfate concentrations in the range of 1,000-2,000 mg L^{-1} were observed throughout the majority of the test-pile. Sulfate concentrations up to 4,300 mg L^{-1} were associated with the low pH regions of the 15 m cross section. The low pH regions of the 25 and 35 m cross sections were associated with SO_4 concentrations up to 3,800 and 3,500 mg L^{-1}, respectively.

3.3.2.3 Alkalinity

Alkalinity was depleted in regions associated with low pH in all four cross sections. Alkalinity in the regions with pH <7 was typically less than 40 mg L^{-1} as $CaCO_3$, but in regions with elevated pH alkalinity concentrations were up to 165 mg L^{-1}.

3.3.2.4 Dissolved metals

Regions of elevated concentrations of dissolved metals in the test pile corresponded with regions of low pH. Iron concentrations in pore water were generally <1.5 mg L^{-1} and concentrations of Al were generally <0.2 mg L^{-1} with the exception of the low pH regions. The 15 m cross section contained the highest concentrations of dissolved Al and Fe. In the low pH region in the upper west portion of the 15 m cross section, dissolved Fe concentrations up to 6.4 mg L^{-1} and dissolved Al concentrations up to 65 mg L^{-1} were observed.

Where pH was greater than 6, Cu, Zn, Ni, and Co concentrations were commonly less than 0.02, 0.5, 0.5, and 0.2 mg L^{-1}, respectively. Concentrations of dissolved Cu, Zn, Ni, and Co were elevated in low pH regions with maximum concentrations observed in the 15 m cross section of 9.3, 36.4, 44.0, and 9.4 mg L^{-1}, respectively. Elevated concentrations of Cu, Zn, Ni, and Co were observed in the low pH regions of the other cross sections, but the highest concentrations of

dissolved metals were observed in the 15 m cross section. Sharp decreases in the concentration of all metals were observed where pH transitioned from <6 to circumneutral.

The primary source of Ni and Co in the unweathered waste rock is pyrrhotite where they are present at a ratio of 4:1 (Jambor, 1997). Congruent dissolution occurs when elements dissolve from a source in the same ratios they are present at in solid solution. In the effluent of the Type III test pile, which typically had a lower pH than the Type I test pile, the Ni:Co ratio was generally close to the ratio of 4:1 expected for congruent dissolution of pyrrhotite (Bailey *et al.*, 2016, Sinclair, 2014).

With the exception of five locations in the 15 m and 11 locations in the 35 m cross sections, the Ni:Co in the two cross sections was >4 indicating that that either Ni was released preferentially from pyrrhotite or that Co was retained within the test pile through dissolution of pyrrhotite or adsorption reactions. The average Ni:Co ratios in the 15 m and 35 m cross sections were 6.3 and 5.9, respectively. Regions of elevated Ni:Co ratios were particularly prominent at elevations where pore water with pH <6 was displaced downward into regions with higher pH. In low pH regions, the Ni:Co ratio was close to the expected value of four, indicating that preferential adsorption of Co is more likely a cause for the change in the Ni:Co ratio than preferential release of Ni.

3.3.3. Geochemical modeling

3.3.3.1 Carbonate minerals

In the 15 m cross section, pore-water samples were at saturation with respect to calcite where pH and alkalinity were elevated, above 7.5 and 50 mg L^{-1} respectively, and under saturated with respect to calcite elsewhere in the section, suggesting that calcite dissolution is neutralizing the pore-water pH (Figure 3-10). A similar pattern was observed with saturation with respect to dolomite.

Although the average pH and alkalinity of the 35 m cross section (7.0 and 25.7 mg L^{-1} as $CaCO_3$, respectively) was higher than the 15 m cross section (6.6 and 22.2 mg L^{-1} as $CaCO_3$,

respectively), the pore-water samples collected from 35 m cross section were largely undersaturated with respect to calcite and dolomite (Figure 3-11). Analysis indicates that the average pH of the 15 m cross section was statistically different from the 35 m cross section; however, the average alkalinity of the 15 m cross section was not statistically different from the 35 m cross section. Neither the pH or alkalinity data were normally distributed. A Mann-Whitney rank sum analysis produced P-values of 0.04 and 0.11 for the pH and alkalinity data sets, respectively.

Because the majority of the 35 m cross section had circumneutral pH and measurable alkalinity, it is unlikely that the acid-neutralization capacity due to calcite content of the waste rock in this region was exhausted. It is likely that less heterogeneous conditions in the 35 m cross section and/or greater flushing due to infiltration of snowmelt from the adjacent batter resulted in less geochemical zonation.

3.3.3.2 Aluminium hydroxide minerals

The behaviour of aluminium hydroxide minerals varied between the two modeled cross sections. The low pH regions in the 15 m cross section were associated with saturation with respect to alunite, whereas the low pH regions in the 35 m cross section were associated with under saturation with respect to amorphous $Al(OH)_3$. The pore water was at equilibrium or undersaturated with respect to amorphous $Al(OH)_3$ throughout the 15 m cross section with no clear relationship to the low pH regions.

Although saturation of pore water with respect to alunite was observed in regions where pH was low in the 15 m cross section, alunite is generally observed to form due to evaporative concentration (Lapakko, 2015). Due to the depth of the samples where saturation with respect to alunite was indicated, it is unlikely that evaporation was sufficient to form this mineral within the test pile. These observations suggest that if the aluminium hydroxide mineral content of the test

pile was evolving, dissolution of $Al(OH)_3$, if present, is favoured, contributing to acid neutralization.

3.3.3.3 Iron and sulfate containing minerals

Saturation index values for gypsum ranged between -0.5 and 0.5 for all but the top boundary of the 15 and 35 m cross sections. Pore water was at saturation with respect to barite throughout both cross sections. Gypsum is a stronger candidate for sequestration of SO_4 in the waste rock because Ca (μ = 6099 ppm, σ = 1303) is more abundant in the waste rock than Ba (μ = 385 ppm, σ = 145).

Saturation index calculations indicated that pore water was saturated with respect to jarosite in regions of the 15 m profile where pH was low and pore water was at saturation with respect to jarosite throughout the 35 m cross section. These results indicate the potential for jarosite to form within the test pile; however, jarosite has not yet been observed through mineralogical studies. Saturation with respect to ferrihydrite was indicated in regions of the cross sections where pH>6, particularly below low pH, elevated Fe concentration regions.

3.3.4. Temperature distribution

As described by others (Pham *et al.*, 2013, Sinclair *et al.*, 2015), average monthly internal temperatures throughout the Type I and III test piles were below 0°C during the winter. Beginning in June, the outer boundary of the test pile began to warm and a thawing front migrated down toward the base of the test pile with the thawed zone reaching its maximum extent in August or September (Figure 3-12). As ambient air temperatures decreased in the autumn, a freezing front migrated inward from the top, sides, and bottom of the test piles with average monthly internal temperatures falling below 0°C in December. This process resulted in a hydrologically isolated region in the central portion of the test pile with temperatures that remained above freezing late in the season.

3.3.5. Basal drain

Minimal flow reported to the basal drain of the Type I pile in the first year following construction and flow effectively ceased following the winter of 2012-2013 when flooding of the instrumentation trailer interfered with the operation of heat trace installed to prevent the basal drain from freezing. When the basal drain was excavated during the deconstruction activities in 2014, large sections were filled with ice, preventing the transmission of water to sampling and recording devices. Consequently, only data from 2007-2012 was included in analysis of basal-drain loading.

Investigation of the Type III pile by Sinclair *et al.* (2015) indicated that circumneutral pH water, containing low concentrations of sulfate and dissolved metals, reported to the basal-drain system early in each year. Spring flow was primarily derived from snowmelt traveling through relatively short flow paths through the batters of the test pile. Lower pH water, containing higher concentrations of sulfate and dissolved metals, arrived at the basal drain late in the season. Autumn flow was primarily derived from rain infiltration through the core of the test pile.

Fluctuating pH values were initially recorded from the Type I basal drain with pH values from 4.6 to 8.2 observed over the 2008 season. In following years, pH at the Type I basal drain stabilized with values from 6.1 to 7.5 recorded in 2012 (Figure 3-13). During 2008 and 2009, when the strongest declines in pH were observed, the average concentrations of Ca and SO_4 were <500 mg L^{-1}. As pH began to stabilize in 2010, the maximum Ca and SO_4 concentrations increased to 2,100 mg L^{-1} and 1,400 mg L^{-1}, respectively, before declining for the remainder of the experiment.

The masses of dissolved constituents observed in the basal-drain effluent were related to both rainfall and outflow volume (Table 3-1). The test pile received the largest volumes of rainfall in 2007, 2008, and 2011 with 153, 154, and 146 mm of rain, respectively. A total volume of 221.8 m^3 water reported to the Type I basal drain during the 2007-2012 period. No water samples were obtained from the basal drain in 2007, as the 'wetting up' of the test pile resulted in a minimal

volume of water reporting to the basal drain that year. The largest volume of effluent reporting to the basal drain occurred in 2011. This cumulative basal-drainage water from 2008-2012 contained 67.1 g Ni, 10.3 g Co, 17.1 g Cu, 13.6 g Zn, 12.1 g Al, 19.8 g Fe, and 87.1 kg SO_4. The largest masses of Cu and Al were recorded in 2008, while the largest masses of SO_4, Ca, Ni, Co, Zn, and Fe were recorded in 2011.

The volume of effluent from the Type I test pile was dependent on natural precipitation. No infiltration experiments or applied rainfall events were conducted on this test pile. A series of artificial rainfall events were applied to the Type III test pile (Neuner *et al.*, 2013), and over four times more water reported to the Type III basal drain than was observed in the Type I basal drain. Although the Type I test pile produced only 24% of the effluent produced by the Type III test pile up to 2012, the Type I test pile produced 62% of the mass of NO_3 and 187% of the Cl. Nitrate and Cl are derived from blasting residuals and behave as conservative tracers in waste rock at Diavik (Bailey *et al.*, 2013). Nitrate and Cl masses in effluent from the Type 1 pile peaked in 2010 and 2011 with maximum concentrations in 2010 of 9.1 g L^{-1} and 2.8 g L^{-1} and masses of 112.2 kg and 35.6 kg respectively. Lower maximum concentrations of both tracers were recorded in 2011, but similar mass loads (131.4 kg NO_3 and 29.3 kg Cl) were calculated for 2011 due to a much larger flow volume reporting to the basal drain in 2011. The volume of flow recorded in 2012 was comparable to 2010, but the maximum concentration and annual load of NO_3 and Cl were much lower. This observation indicates that the much of the explosive residue mass has been flushed from the test pile.

The average sulfide content of the <5 mm fraction of the Type I test pile was 0.035 wt.% S, whereas the average sulfide content of the <5 mm fraction of the Type III text pile was 0.053 wt. % S (Smith *et al.*, 2013b). Mass loadings of sulfide-oxidation products were lower in the Type I test-pile effluent with only 13% of Fe, 9% of SO_4, 2% of Ni, 1% of Co, 4% of Cu, and 1% of Zn in the Type III test-pile effluent. These disproportionately lower loadings are due to the lower

volumes of water and lesser concentrations of dissolved constituents released from the Type I rock than from the Type III rock.

3.3.6. Adsorption isotherms

Distinct variations in dissolved metal concentrations are associated with sharp changes in the pore-water pH as shown in Figures 3-6, 3-8, and 3-9. Geochemical modelling incorporating sorption calculations was conducted utilizing all pore-water samples. Dzombak and Morel (1990) determined coefficients for sorption of Cu, Zn, Ni, and Co on hydrous ferric oxide (HFO) through modeling the results of numerous sorption experiments. Balistrieri *et al.* (2003) experimentally determined coefficients in solutions that are appropriate for AMD systems where there are higher concentrations of dissolved metals relative to surface sites. Sorption calculations for the Type I test-pile system were conducted using the surface complexation coefficients presented by Balistrieri *et al.* (2003) and the sorption site density for HFO determined by Dzombak and Morel (1990).

A pore-water sample with a pH near 4 and elevated metal concentration was selected as the initial solution for modeling adsorption isotherms. The parameters used from the pore-water sample included temperature, pH, pe, alkalinity as $CaCO_3$, and the concentration of the metal of interest. Competing cations and anions were excluded from the initial solution; however, the ionic strength of the solution was fixed using 0.1 M $NaNO_3$ to maintain consistent geochemical conditions with the pore-water sample. A different pore-water sample was used for each metal of interest (Cu, Zn, Co, and Ni) to avoid using anomalously high metal concentrations as the initial solution condition. The solution was equilibrated with a given concentration of HFO at pH 4. The pH of the equilibrated solution was then increased in pH steps of 0.1 units up to pH 8.6. The concentration of total Fe provided to the initial solution was adjusted until a good fit with pore-water metal concentrations was observed. The surface complexation constants used in this model are presented in Table 3-2.

Several pore-water samples were excluded from adsorption isotherm curve fitting due to anomalous results and the excluded samples are presented in Table 3-3. The pH of the excluded samples span a range of 4.1-7.7 and metal concentrations of 4.5-22.8 mg L^{-1} Zn, 0.2-9.3 mg L^{-1} Cu, 5.6-59.9 mg L^{-1} Ni, and 1.5-13.4 mg L^{-1} Co.

Through a sensitivity analysis, it was determined that the adsorption isotherm generated using a total HFO concentration of 0.2 g L^{-1} Fe produced a fit consistent with the observed Zn, Cu, Co, and Ni measurements (Figure 3-14). This HFO concentration is consistent with observations from the pore-water data which indicated that the Ni:Co ratio in solution is typically close to that observed in the unaltered pyrrhotite when the pH is <6. The aqueous Ni:Co ratio is consistently equal to or greater than the ratio in pyrrhotite at pH >6.

A modeled HFO concentration of 0.2 g L^{-1} predicted a decrease in metal concentrations at pH >4. The aqueous concentrations of Cu and Zn decrease sharply as pH increases from 4 to 6, with the concentrations of Zn <6.5 mg L^{-1} and Cu <0.8 mg L^{-1} at pH >6. Cobalt and Ni concentrations in pore water do not decrease until the pH increases to 6. Concentrations of Ni and Co are elevated until pH >8. At pH >8, concentrations of Ni and Co are generally <0.1 and <0.08 mg L^{-1}, respectively.

The volumetric moisture content of Diavik waste rock ranges from 15-25% in the matrix material. The matrix material, defined as the size fraction <5mm, is the size fraction that holds water through capillarity and represents approximately 18% of the bulk waste-rock volume (Krentz, 2014). Based on these parameters, an Fe concentration of 0.2 g L^{-1}, or 5.4-9.0 g total Fe as HFO per m^3 of Type I waste rock, results in concentration trends for Cu, Co, Ni, and Zn that are similar to the observed attenuation of metal concentration with increasing pH. The Fe content of 5.4-9.0 g m^{-3}, distributed homogeneously throughout the 40,648 m^3 test pile (Smith, 2006), is equivalent to 219.5-365.8 kg of Fe.

Based on a cumulative mass of 87.1 kg of SO_4 recorded in effluent at the basal drain, 907 mol of S has been released from pyrrhotite in the test pile from sulfide oxidation. Oxidizing this mass of pyrrhotite would release 771 mol or 43.0 kg Fe based on the pyrrhotite composition of $Fe_{0.85}S$. Only 19.8 g or 0.4 mol of Fe was released through the basal drain. Comparing the mass of Fe and SO_4 released in the test pile drainage indicates that the majority of the Fe has been retained in secondary reaction products within the test pile.

The mass of Fe released through sulfide oxidation is only 12-20% of the mass of Fe predicted by adsorption isotherm modeling to be present in the test pile as secondary Fe minerals. A mass of 43.0 kg Fe results in a concentration of 1.1 g m^{-3} of Fe retained in the test pile.

3.3.7. Mineralogy investigation

To investigate cation retention at the grain scale, synchrotron µ-XRF mapping of pyrrhotite grains was conducted on samples from a vertical transect from the 15 m cross section. The selected transect passed through the lowest and highest pH regions of the test pile. Three pyrrhotite grains from the transect are presented in Figure 3-15.

The pyrrhotite grain in (A) was collected near the top of the test pile from a depth of 2.4 m and was associated with a pore-water pH of 4.4. This grain shows minimal secondary Fe, Ni, or Cu accumulation at the outside edges of the grain. This is indicated by the majority of the µ-XRF response occurring within the grain and the limited indication of an alteration rim around the grain in the photomicrograph.

The pyrrhotite grain in (C) was collected from the base of the test pile from a depth of 11.7 m and was associated with a pore-water pH of 5.0. There is indication of more Fe retention at the boundaries of the grain in (C) than in (A), with a grey reaction rim surrounding the grain visible in the photomicrograph in (C). The intensity of the fluorescence response is generally consistent across the grain indicating minimal accumulation or depletion of any of the elements of interest. A region at the upper right portion of the grain indicates accumulation of secondary Fe minerals

where the Fe spectra is associated with depleted S spectra (circled). There no indication of sorption of Ni or Cu associated with the secondary Fe accumulation. The elevated Cu signature in the upper right region is associated with a 2.5 µm residual sulfide grain indicated by an arrow on the photomicrograph.

The pyrrhotite grain in (B) was collected near the middle of the test pile from a depth of 5.6 m and was associated with a pore-water pH of 8.3. This grain has the most extensively developed reaction rim with each fragment of the grain surrounded by a grey reaction rim in the photomicrograph. A region of secondary Fe accumulation is visible in the fluorescence response where it extends beyond the grain boundary on the right side of the grain (circled). This Fe accumulation is associated with a weaker S response than is observed within the boundary of the sulfide grain, indicating the Fe is associated with secondary Fe (oxy)hydroxide rather than primary Fe sulfide. The region of secondary Fe accumulation on the right side of the grain is also associated with enriched Ni content. The accumulation of Ni associated with Fe (oxy)hydroxides indicates that Ni released through sulfide oxidation is retained in close proximity to the sulfide mineral under the geochemical conditions present in the central region of the test pile.

Spectra collected from grain (B) via SEM-EDX indicate decreasing S content from the core of the grain to the right margin. Spectra from point (a) (Figure 3-16) produced a strong S and Fe response indicating a dominantly Fe sulfide source. Spectra from point (b), collected in the reaction rim region of the grain, produced a weaker S response and a stronger O response indicating the presence of a partially oxidized, mixed Fe sulfide and Fe (oxy)hydroxide source.

Spectra from point (c) indicates that the grain located adjacent to the sulfide grain is an aluminosilicate mineral due to the strong Al, Si, and O response. Spectra from the secondary coating surrounding the aluminosilicate grain, point (d), indicates it has a dominantly Mn oxide composition due to the strong Mn and O peaks. Solubility of Mn is low under elevated pH conditions and Mn oxides have the capacity to adsorb Cu under circumneutral conditions (Lee *et al.*, 2002). The presence of an elevated Cu signal (Figure 3-15) associated with the Mn oxide rim

cannot be conclusively associated with sorption due to the strong S signal produced in the same region. Micro XRF penetrates below the surface of the thin section where a Cu sulfide mineral may be concealed.

3.3.8. Most probable number analysis

Most probable number analysis was conducted on approximately 50% of the samples from the 15 m and 35 m cross sections. Both cross sections typically had low counts of aSOB, moderate counts of aIOB, and elevated counts of nSOB.

Acidophilic SOB were observed at 40 of 45 enumerated locations in the 15 m cross section and 43 of 47 locations in the 35 m cross section. Median aSOB values of 17 counts g^{-1} and 13 counts g^{-1} were recorded for the 15 m and 35 m cross sections, respectively. An aSOB count of 350 g^{-1} was recorded at one location in the 15 m cross section, but counts of <30 g^{-1} were recorded at all other locations in the 15 m and 35 m cross sections (Figure 3-17). All of these counts are very low relative to aSOB populations observed in waste rock dumps (Schippers *et al.*, 2010) and are consistent with the predominance of neutral pH conditions in the test pile.

Acidophilic IOB were present at 44 of 45 locations in the 15 m cross section and 42 of 47 locations in the 35 m cross section. Counts of aIOB were typically <4 x 10^3 g^{-1} in each of the cross sections with median values of 170 counts g^{-1} in the 15 m cross section and 33 counts g^{-1} in the 35 m cross section. The maximum count in the 15 m cross section was 5 x 10^5 g^{-1} whereas the maximum count in the 35 m cross section was 2 x 10^4 g^{-1}. Maximum populations of aIOB up to 3x10^8 g^{-1} were observed in waste rock at other sites (Schippers *et al.*, 2010), more than three orders of magnitude greater microbial counts observed in the test pile.

The greatest microbial counts in both cross sections were nSOB and counts were observed at all enumerated locations. Counts of nSOB were typically >2 x 10^3 g^{-1} with median values of 5 x 10^3 counts g^{-1} in the 15 m cross section and 4 x 10^3 counts g^{-1} in the 35 m cross section. The maximum counts recorded were 4 x 10^6 g^{-1} in the 15 m cross section and 2 x 10^6 g^{-1} in the 35 m

cross section. The maximum counts of nSOB observed in the test pile are comparable to those observed in waste rock dumps elsewhere (Schippers *et al.*, 2010). The dominance of neutrophilic microbial species is consistent with the circumneutral conditions present in much of the test pile.

3.4. Discussion

3.4.1. Effect of heterogeneity on geochemical evolution

Waste rock was segregated during test-pile construction based on S analysis of drill cuttings from production blast holes or from visual classification of the cuttings when analytical equipment was not functioning. The blast holes were 12 m deep with 7 m spacing and the results were used to identify mineable blocks with volumes typically greater than 1000 m^3 (Smith *et al.*, 2013b). This segregation strategy led to variations in the S content, with individual samples from the Type I test pile containing 0.0028-0.26 wt. % S and face averages of 0.018, 0.022, 0.033, 0.021, 0.041 wt. % S for Faces 1 through 5, respectively (Smith *et al.*, 2013b).

The highest pH region of the transverse cross section corresponds with the face with the lowest original S content, and the lowest pH region corresponds with the face with the second highest S content. The relationship between S content and pH breaks down in Face 5, which is the batter portion of the cross section. The highest S content was observed in this batter, but pore-water pH was circumneutral. This observation is consistent with analysis of the Type III test pile conducted by Sinclair (2014). Sinclair determined that the batter region receives significantly more flushing due to the infiltration of snowmelt, resulting in a more mature geochemical regime.

NPR calculations conducted on samples from the 15 m cross section are consistent with the distribution of low pH regions and provide an indication of the remaining acid generation potential of the waste rock (Chapter 2). The region in the upper west portion of the 15 m cross section with a pH <6 occurs within a zone of potentially acid generating (PAG) waste rock. Another region of low pH water occurs in a zone of PAG waste rock along the base of the cross section. The low pH region in the upper east portion of the cross section does not correspond with PAG waste rock. The discrepancy may be due to (1) the use of total S rather than S^{2-} in the acid-base accounting, resulting in an overestimation of the remaining acid generating capacity

(Chapter 2), or (2) the sample density was insufficient to capture the potential acid generating capacity in this smaller region.

The heterogeneous distribution of sulfides within the waste rock at the time of test-pile construction resulted in discrete regions with net acid generation capacity. The seasonal temperature effects of the Arctic environment may have further restricted the regions where the rate of acid generation was sufficient to overwhelm the rate of acid consumption of the waste rock. Although the low pH regions were well predicted by the NPR results, there was a circumneutral region spanning the middle elevations of the 15 m cross section that intersected a region where the NPR measurements indicated the potential for acid generation.

Figure 2-9 and Figure 3-12F show that although the PAG region extends through the entire depth of the 15 m cross section, only the portion of the PAG region that remained above 0 °C late into the year generated a large well-defined region of pore water with low pH. The low pH region in the upper west portion of the 15 m cross section had a higher average NPR (3.6, σ = 3.2, n = 7) and a lower average pH (4.8, σ = 0.6, n = 11) than the low pH region at the base of the test pile (average NPR = 1.5, σ = 0.6, n = 7; average pH = 5.2, σ = 0.4, n = 10) where temperatures were below 0°C for most of the year. Low temperatures may have suppressed S oxidation in the lower half of the test pile throughout most of the year limiting the release of acidity; consequently, the acid-neutralization capacity of the waste rock was sufficient to maintain pH above 6 in most of the region.

3.4.2. Comparison of *in situ* and pore-water samples

The deconstruction of the Type I test pile was conducted to investigate the geochemical evolution of the waste rock with rigorous spatial control and on a finer scale than was possible using *in situ* investigation techniques. The *in situ* SWSS samples were located on Face 1 and 2 and were in closest proximity to the 15 m cross section. In general, the SWSS samples from 2013 display the trends observed in the 2014 pore-water samples from the 15 m cross section. The low

pH regions near the top and bottom of the 15 m cross section and the region of elevated SO_4 concentration in the central elevations were captured by the SWSS data. The variation in metal concentrations near the top of the 15 m cross section also was indicated in the SWSS samples by large error bars at the 2 m depth (Figure 3-3).

One area of discrepancy was at the base of the test pile. The SO_4 concentration was <1,000 mg L^{-1} in the 2013 BCLs but up to 4,300 mg L^{-1} at base of 15 m cross section. This difference is due to sample density, because 12 of 13 BCL samples collected in 2013 came from eastern BCL set which correspond with pore-water SO_4 concentration of 600-1,600 mg L^{-1}.

A comparison of the SWSS and pore-water sample mean concentrations was conducted using the two-sided t-Test. BCL samples were excluded from this analysis because there were indications that snowmelt had a significant contribution to BCL water composition (J. Zak, personal communication, 2016). Snowmelt produces a large volume of low concentration drainage with short residence time early in the active season, whereas samples derived from rain infiltration produce drainage with longer residence time and higher concentrations (Sinclair *et al.*, 2015). The influence of snowmelt on the BCL samples renders them inappropriate to compare to pore-water measurements which are primarily derived from rain water infiltration.

The null hypothesis that the mean concentration or pH of the pore-water samples was not significantly different from the mean concentration or pH of the SWSS samples (2007-2013) was evaluated. The pH, alkalinity, Fe, Ni, Co, Cu, Zn, SO_4 were the parameters investigated. The null hypothesis was rejected for Fe, SO_4, and alkalinity (P values of 0.01, $2x10^{-5}$, and $4x10^{-9}$, respectively). Conversely, there was no indication that the SWSS data were statistically different from the pore-water samples for pH, Ni, Co, Cu, or Zn (P values of 0.09, 0.07, 0.19, 0.38 and 0.78, respectively). A summary of the results for the two-sided t-test is included in Table 3-4.

The 2013 SWSS data was then compared to the full deconstruction data set to remove temporal influence. Finally, the 2013 SWSS data was compared to samples from the 15 m cross section to remove temporal and spatial influence. Removing temporal influence resulted in a null

hypothesis that could not be rejected for Fe (P value of 0.06). Removing both temporal and spatial influence resulted in a null hypothesis that could not be rejected for alkalinity (P value of 0.66). No data set restrictions resulted in a null hypothesis that could not be rejected for SO_4.

Mechanisms that likely contributed to temporal variability of Fe concentrations include: (1) decrease in the sulfide oxidation rate over time due to passivation of particle surfaces (Mayer *et al.*, 2002, Davis & Ritchie, 1986), or (2) the development of conditions conducive to secondary precipitation of Fe in later years. Temporal and spatial variability in alkalinity is likely due to depletion of calcite content in the waste rock through acid neutralization reactions. The lower mean pH in the 15 m cross section was likely the result of accelerated depletion of calcite in this region. Several factors may have impacted the correlation of SO_4 in SWSS and pore-water samples. Mineralogical controls on SO_4 concentrations, impacts from the sample collection methods, or the density of SWSS samples may have contributed to the discrepancy between pore-water and SWSS sample groups.

As indicated by the SWSS samples, a greater proportion of the samples were at saturation with respect to gypsum in the later years of the experiment. As saturation with respect to gypsum increased over time, the concentration of SO_4 in the SWSS samples increased and became more variable as indicated by the large error bars on SO_4 data points in Figure 3-3. The result is that the concentration of SO_4 in SWSS samples collected near the beginning of the experiment are not representative of pore-water samples extracted following deconstruction.

There was a much greater density of pore-water samples than of SWSS samples. Only 18 SWSS sample locations were available and 130 samples were collected from those locations between 2007 and 2013. SWSS samplers only provided water samples intermittently throughout the summer, and from year to year depending on precipitation. Pore water was extracted from approximately 350 locations spread throughout the test pile and every sample yielded enough water to conduct analyses.

With the exception of SO_4, measurements conducted on samples collected from the SWSS provided an indication of the progress of geochemical evolution of the pore water within the test pile, and the SWSS data set was representative of the pore-water data set. The extremes in pH and SO_4 and dissolved metal concentrations, and the geochemical zonation that developed within the test pile, were not as apparent from the SWSS data set as from the pore-water data due to the heterogeneous nature of the waste rock and the limited number of *in situ* sample points available.

3.4.3. Dissolved Metal Attenuation

3.4.3.1 Metal sorption

The pore water from the Type I test pile had an average pH of 7.0, which is higher than the average pH (pH 5.1) of *in situ* water samples collected from SWSS of the Type III test pile. A pronounced pH zonation developed in the Type I test pile with low pH regions often underlain by regions of circumneutral pH. As water moved through the test pile via matrix flow, sulfide oxidation generated low pH and metal- and sulfate-rich pore water in discrete zones of the test pile. This pore water was displaced down through regions of the test pile where the acid-neutralization capacity of the waste rock was sufficient to maintain circumneutral pH.

As the low-pH and metal- and sulfate-rich water encountered regions with residual calcite, the pH increased and the pore water became saturated with respect to Fe (oxy)hydroxides. As the pH increased, adsorption on Fe (oxy)hydroxides was increasingly favoured and dissolved metals were removed from solution in the sequence Cu>Zn>Co>Ni, resulting in Ni:Co ratios in the circumneutral regions of the test pile that were elevated relative to those found in pyrrhotite.

The observation that Co adsorbs at a lower pH than Ni is contrary to several studies of metal adsorption on clay, soil, and Fe (oxy)hydroxides (Cama *et al.*, 2005, Welp & Brümmer, 1999, Lee *et al.*, 2002, Dzombak & Morel, 1990) and on oxide precipitates from mine effluent (Balistrieri *et al.*, 2003, Lee *et al.*, 2002). An exception to this was observed in an adsorption

experiment by Welp and Brümmer (1999) that indicated that Co adsorbed preferentially over Ni on slightly alkaline soil.

Under the low pH present near the surface of the test pile, adsorption isotherm modeling indicated minimal adsorption of metals. Adsorption isotherm modeling indicated a greater tendency for Cu, Zn, Ni, and Co sorption at pH > 8. As a consequence, lower dissolved metal concentrations will be present in the high-pH regions of the test pile due to adsorption on Fe (oxy)hydroxides. As pore water percolated to the base of the test pile, cations liberated in the low pH region were adsorbed in the region of elevated pore-water pH in the middle elevations of the test pile. Thermal suppression of sulfide oxidation at the base of the test-pile resulted in a region with moderately low pH and generally low dissolved concentrations.

Adsorption modeling indicated that an Fe content of 5.4-9.0 g m^{-1} as Fe (oxy)hydroxide was required to generate the observed attenuation of Zn, Cu, Ni, and Co within the test pile. The Fe content determined through sulfate released from the basal drain indicated a much lower Fe content of 1.1 g m^{-1} was present within the test pile. The discrepancy between the calculated and modeled concentration of Fe suggests concentration of the HFO mass in discrete regions of the test pile. Given that pore water at saturation with respect to ferrihydrite occurred locally within the test pile where pore water with high concentrations of Fe percolated into regions of circumneutral pH, it is unlikely that Fe (oxy)hydroxides were distributed homogeneously throughout the test pile.

Whereas modeling of the HFO content in the test pile is useful to demonstrate that the mass of Fe in the system is capable of producing the observed metal attenuation, this model excludes competition between metal ions for adsorption sites. When competition is accounted for, the concentration of HFO required to produce the observed attenuation rate would be higher than 0.2 g L^{-1}.

In addition to the heterogeneous distribution of Fe in the test pile, the discrepancy between the modeled and calculated mass of Fe present in the test pile may be due to the retention

of SO_4 within the test pile in secondary sulfate-bearing minerals. Calculation of Fe content retained within the test pile through SO_4 release assumes that SO_4 acts as a conservative tracer in the test pile system. Saturation index calculations indicated that SO_4 may be retained within the test pile through the formation of gypsum or other sulfate minerals. Retention of SO_4 in the test pile system via formation of secondary minerals may have resulted in the calculation of a lower Fe content retained within the test pile than was present in reality. The mass of S released from the test pile as SO_4 represents a 0.1% loss of the original S content. Comparison of weathered and unweathered S content in the waste rock indicated that there was no statistically significant difference change in S content, indicating that S was retained within the test pile (Chapter 2).

3.4.3.2 Comparison to Type III test pile effluent

Because the temperature regimes and C content (0.033 wt. % and 0.027 wt. % in the Type I and Type III test piles, respectively) in both test piles were similar, the most likely cause for the formation of lower pH water in the Type III test pile is the higher S content of the Type III waste rock (0.053 wt. % in the Type III test pile, compared to 0.035 wt. % S in the Type I test pile). As a result of greater availability of sulfide minerals in the Type III pile, the acid neutralization potential of this rock is overwhelmed, and the mass of metals and SO_4 released from the Type III test pile is substantially higher. These results demonstrate that although the S content of the Type I and Type III waste rock are low and differ by only <0.02 wt. %, the difference in the AMD generation capacity of the two waste-rock categories is substantial.

3.4.3.3 Implications for AMD prevention

The low-pH conditions and high metal concentrations observed in samples collected from SWSS samplers in the Type III test pile indicate that thermal suppression of sulfide oxidation is not sufficient to maintain neutral pH conditions in the higher S Type III waste rock (Sinclair *et al.*, 2015). The greatest reduction in effluent affected by sulfide oxidation will therefore be

accomplished by limiting the mass of sulfide minerals available for oxidation. The proposed closure plan for the Diavik waste rock is to maintain permanently frozen conditions through the use of a thermal barrier cover. This cover is intended to minimize the movement of oxygen and water through core regions of the waste rock pile, thereby limiting the mass of sulfide minerals available for oxidation and the release of metal- and sulfate-rich effluent (Diavik Diamond Mines Inc., 2011).

The results of the Type I test pile deconstruction program indicate that a small decrease in the S content has a large effect on the geochemical evolution of the waste rock at Diavik. Face 3, with a S content of 0.033 wt. %, had a much lower pH (average pH 6.0) than Face 1, with a S content of 0.018 wt. % (average pH 7.6). The Type I test pile, with an average S content of 0.035 wt. % S and NPR of 12.2, produced circumneutral drainage five years after construction whereas the Type III test pile, with an average S content of 0.053 wt. %. And NPR of 2.2, produced drainage with a pH <5 for the majority of the active season in the same year (Sinclair *et al.*, 2015). The average acid-generating potential of the test piles accurately predicted which test pile would produce low-pH effluent.

In addition to generating circumneutral drainage, the mass of metals and sulfate released from the Type I test pile was reduced by 87-99% over the study period compared to the Type III test pile. Use of the Type I waste rock as a thermal insulation layer is supported by this research as it will generate lower concentrations of dissolved metals and SO_4 when subject to the conditions in the active zone of the waste dump.

3.4.4. Microbial communities

The microbial counts observed in the enumerated samples are comparable to counts observed in the Type I basal drain for the 2008-2010 period (Bailey, 2013). The counts of aIOB and aSOB in this study were lower than the maximum values reported in the literature for waste-rock dumps but the counts of nSOB were comparable (Schippers *et al.*, 2010).

The only sample with elevated aSOB counts in the 15 m cross section was collected from a location with a pH of 4.7. Elevated counts of nSOB and aIOB were associated with regions of the test pile that were circumneutral to slightly alkaline. The elevated counts of nSOB were also concentrated at the base of the test pile where temperatures remain below 0 °C for the majority of the year. The presence of a large community of microorganisms associated with low temperatures suggests that psychrotolerant species (tolerant of temperatures below 5 °C) are dominant in the waste rock at Diavik. Molecular analysis of DNA isolates from the test pile will assist in the determination of whether the microbial community present in the waste rock at the site is similar to those identified previously at other sites, or if a novel community is present.

3.5. Conclusions

As a result of the heterogeneity inherent in the waste rock, low pH regions formed within the Type I test pile associated with regions of elevated S content. The regions of low pH generated pore water with elevated concentrations of SO_4, Fe, Al, Ni, Co, Cu, and Zn. In regions of the test pile where lower S content combined with the seasonal suppression of the sulfide oxidation rate, a sharp transition to regions of circumneutral pH occurred. As pore water with low pH in upper elevations of the test pile percolated down into regions of circumneutral pH, the elevated concentrations of Fe resulted in conditions conducive to precipitation of Fe (oxy)hydroxides.

Adsorption isotherm modeling predicted that sorption of metals would occur where pH transitioned from acidic to circumneutral in the presence of 0.2 g L^{-1} Fe as HFO. The observed patterns of metal attenuation using approximately 350 pore water samples spanning a pH range from 4.1-8.7 was consistent with adsorption modeling results. An Fe concentration of 0.2 g L^{-1} as HFO would result in a total mass of Fe (oxy)hydroxide that was 4.1-8.5 times greater than the mass of Fe predicted to be present in the test pile based on release of SO_4 through the basal drain. The discrepancy between the mass of Fe predicted in the test pile through adsorption isotherm modeling and the calculated mass of Fe retained within the test pile based on SO_4 released through the basal drain indicates that Fe is not homogenously distributed throughout the test pile. The results of saturation index calculations predict saturation of pore water with respect to ferrihydrite at pH transition zones, indicating that HFOs were thermodynamically stable in discrete regions of the test pile.

The Type I test pile had a circumneutral effluent at the end of year five whereas the more extensively studied Type III test pile had an effluent pH <5. The higher average pH and the geochemical heterogeneity of the Type I test pile resulted in an 87-99% reduction in the mass loading of Fe, Al, Ni, Co, Cu, and Zn from the Type I test pile compared to the Type III test pile.

SWSS and BCL sample collection points provided data representative of conditions within the Type I test pile but failed to capture the heterogeneity of conditions within the pile. The range of concentrations for the constituents of interest observed in the higher density deconstruction samples was up to five times greater than observed in the SWSS samples. This difference is likely the result of the limited number of SWSS and BCL sample points available and the inconsistent capacity for the SWSS to produce water samples. An adequate water sample volume was produced from all 350 deconstruction samples analyzed, but water samples were retrieved from only 18 SWSS sample locations.

Microbial populations in the test pile reflected the dominantly circumneutral pH conditions present. Analysis of microbial populations from the waste rock indicated that populations of aSOB and aIOB are low relative to previous studies of waste-rock dumps. Maximum populations of nSOB observed in the test pile were comparable to populations observed in other mining environments.

3.6. Figures

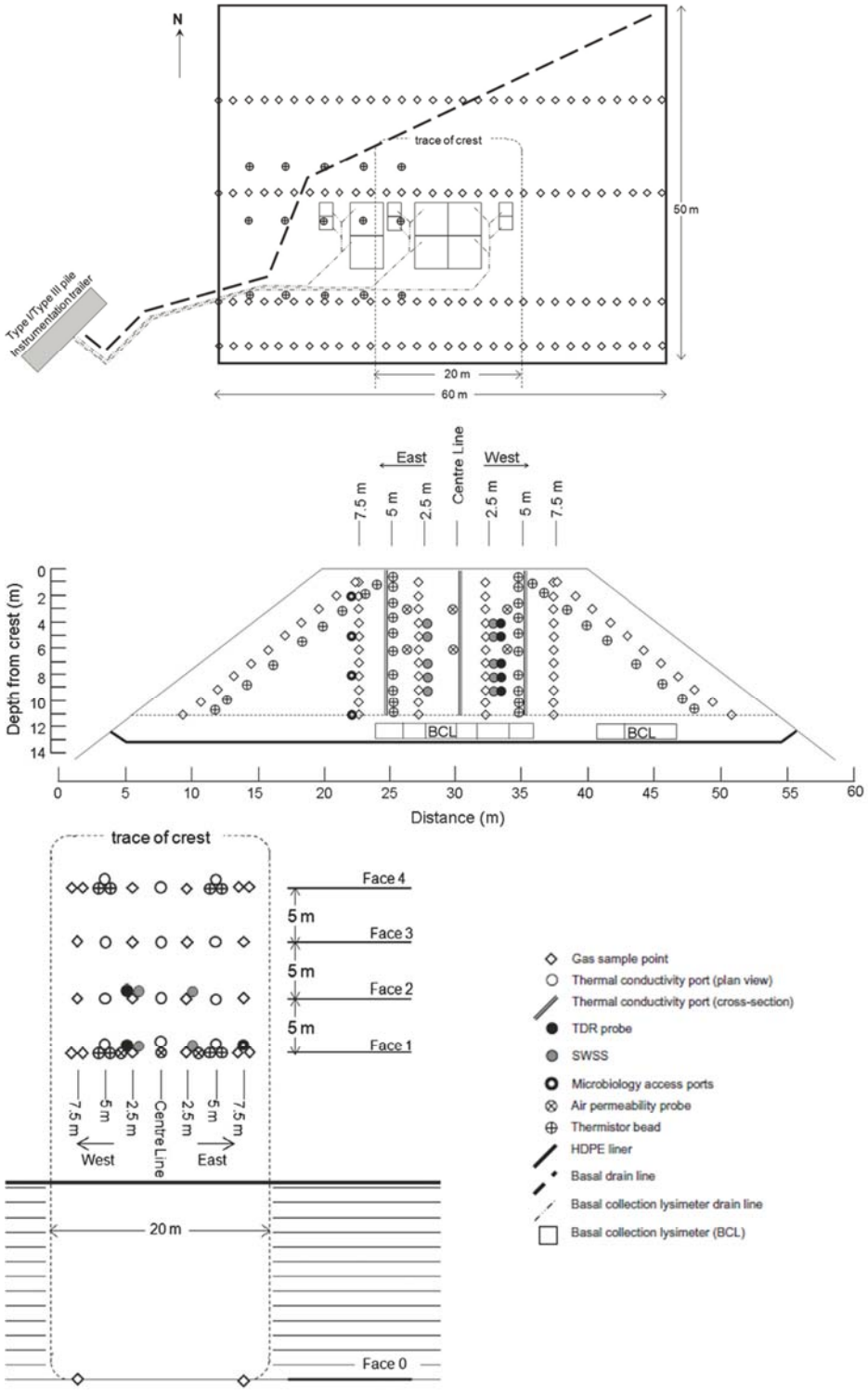

Figure 3-1: Instrumentation distribution for the Type I test pile adapted from Smith et al. (2013c).

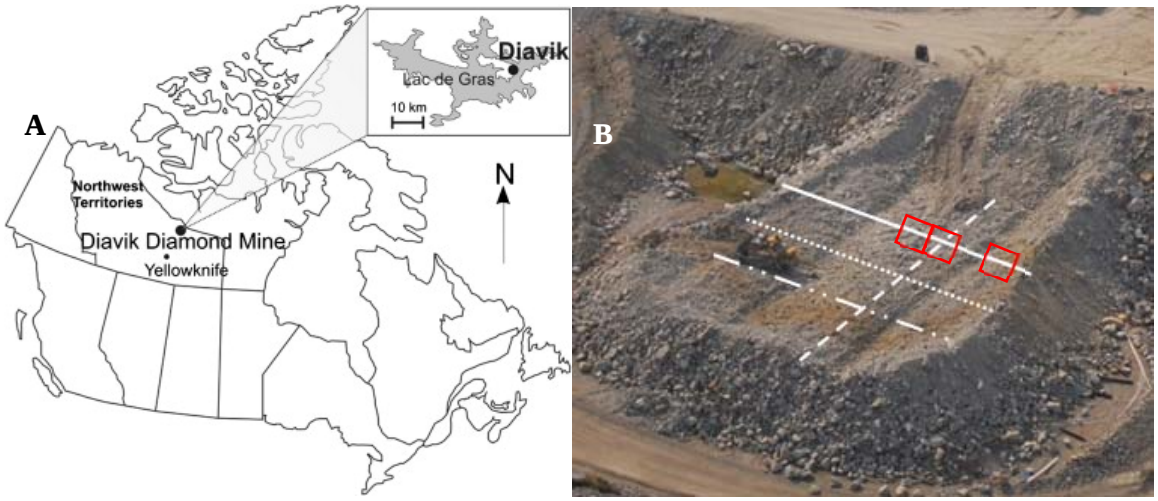

Figure 3-2: A) Location of Diavik Diamond Mine, Northwest Territories, Canada (Smith et al., 2013c) and B) approximate location of the 15 m (solid), 25 m (dotted), 35 m (dash-dot), and transverse (dashed) cross sections. Red boxes indicate approximate location of 1BWBlys4S, 1BWClys4S, and 1BCElys4S. Image shows the Type I test pile following excavation of the third level of sampling trenches.

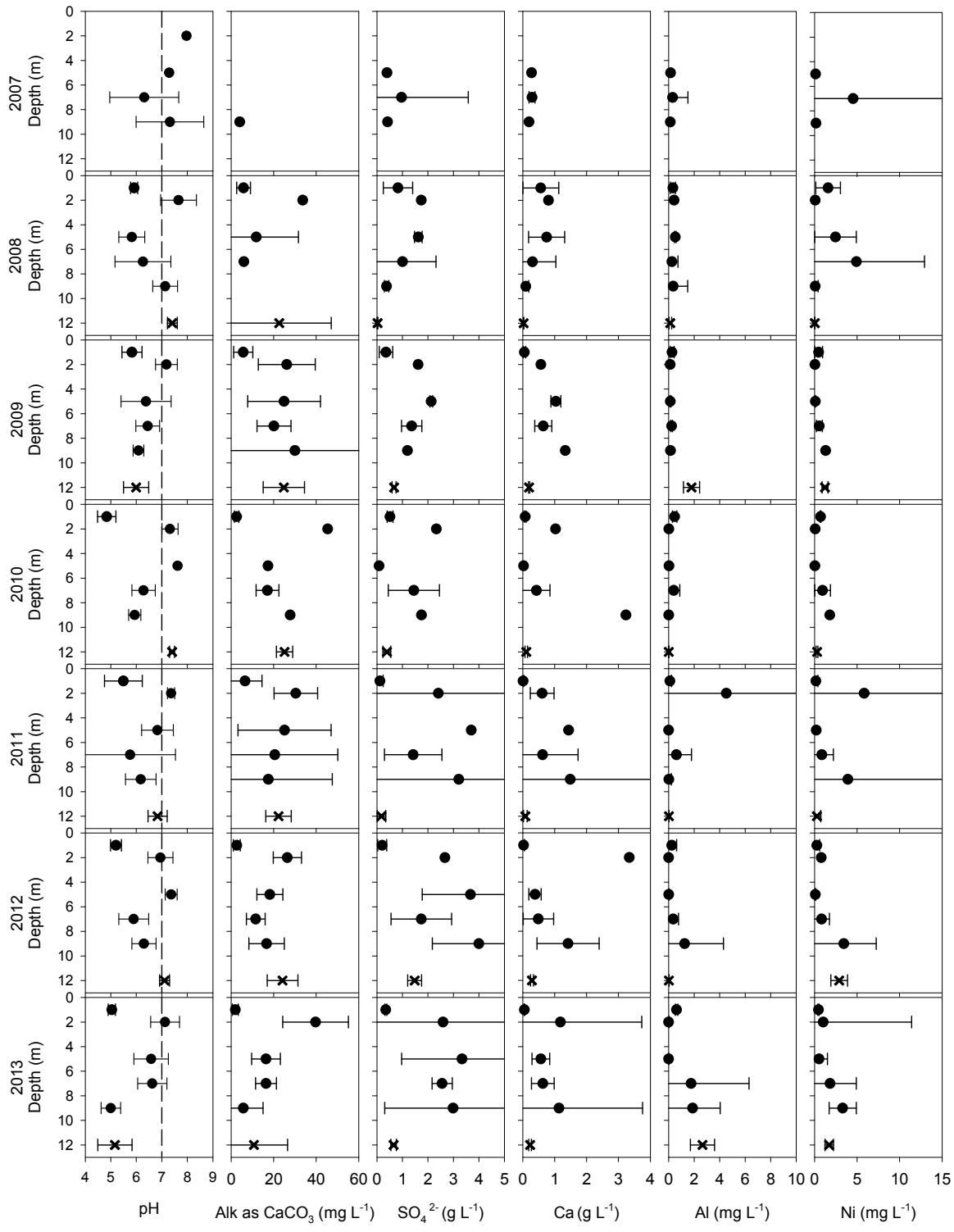

Figure 3-3: SWSS and BCL data. Each point represents the average concentration of sample collection points at the depth specified and error bars represent the 95% confidence interval. The average Fe concentration was >1.5 mg L^{-1} and Co, Cu, and Zn distribution was similar to Ni.

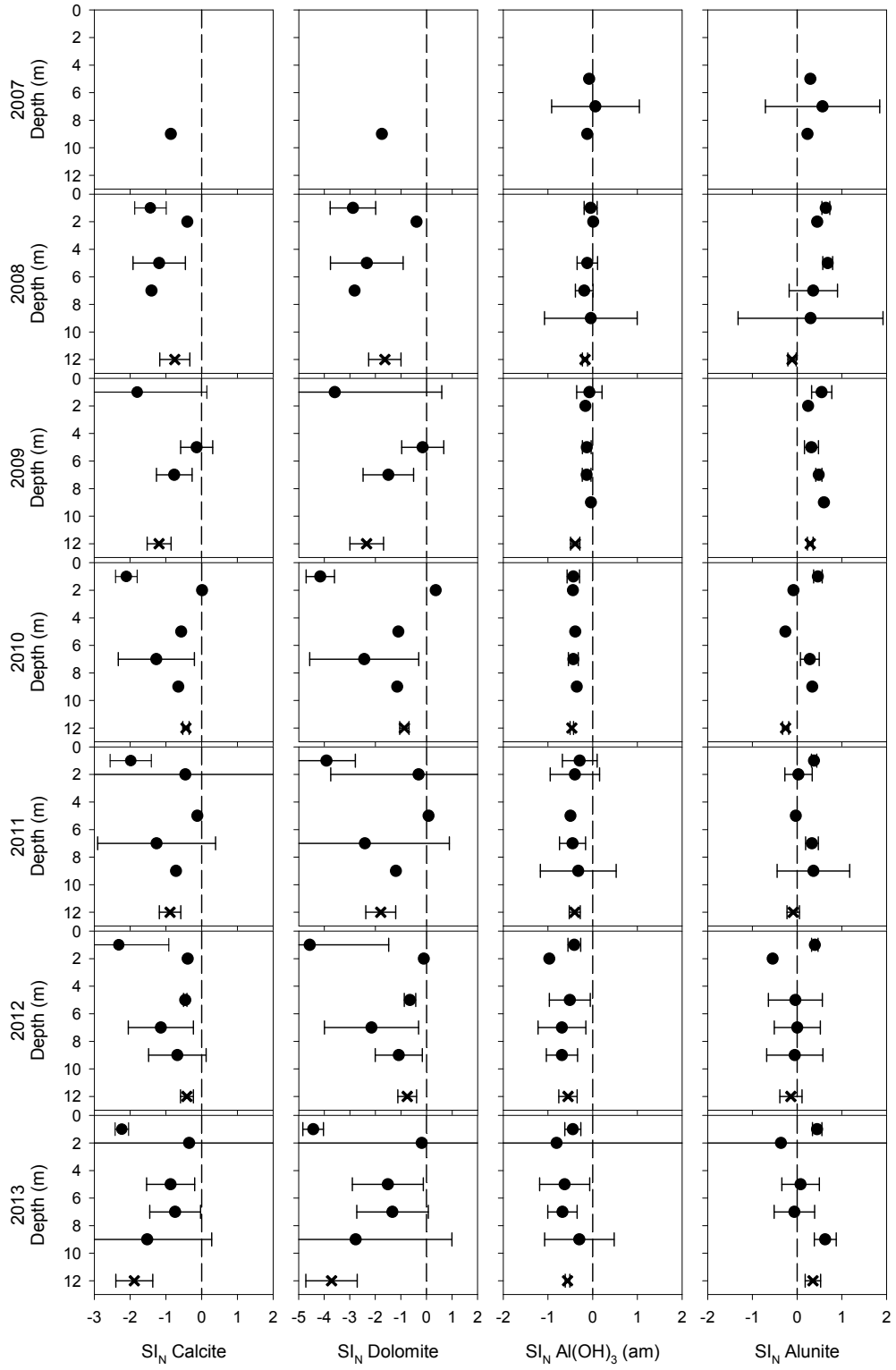

Figure 3-4: Carbonate and aluminium mineral saturation index calculations for SWSS and BCL samples. Each point represents the average concentration of several sample collection points at the depth specified and error bars are the 95% confidence interval.

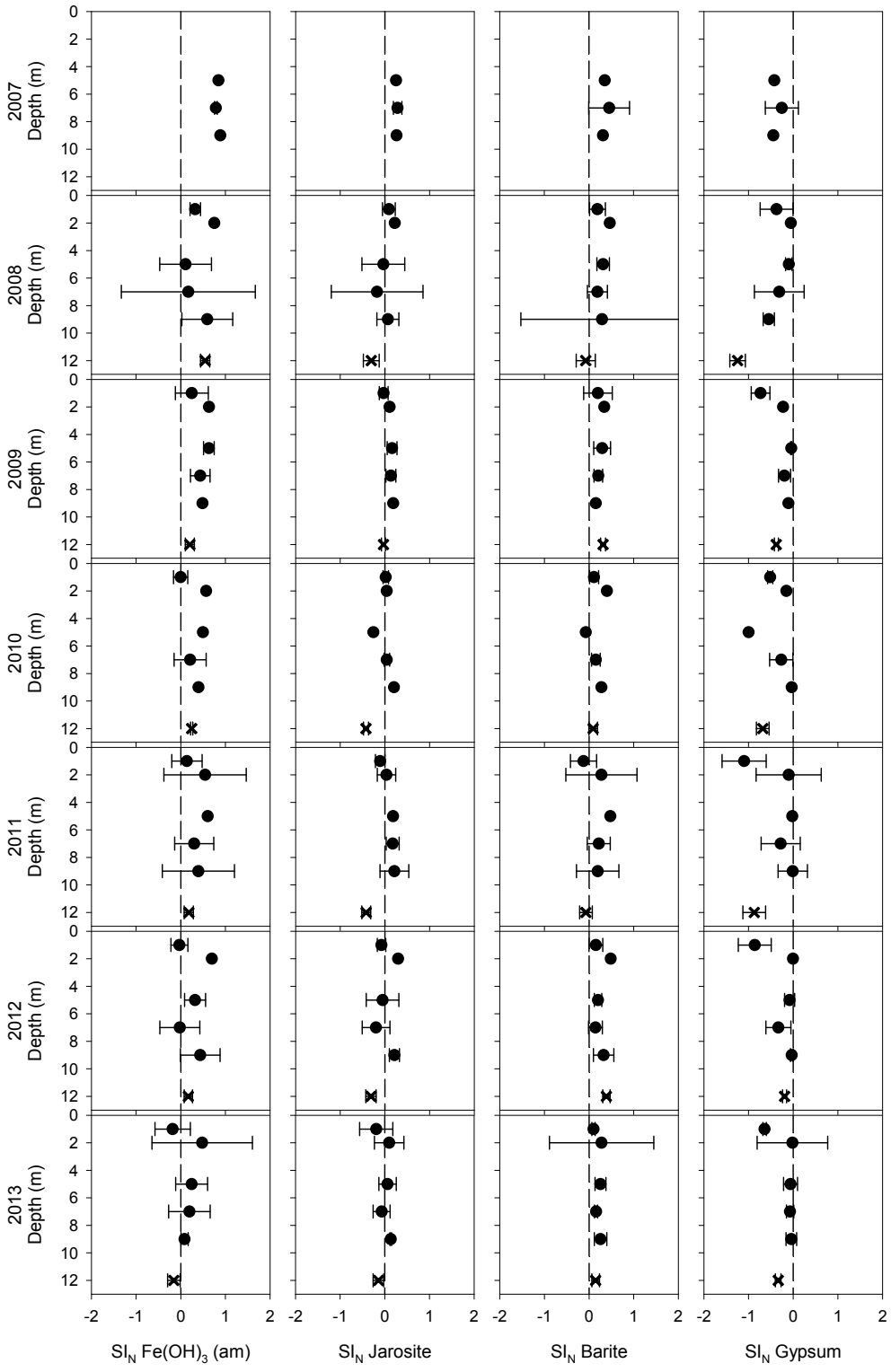

Figure 3-5: Iron and sulfate saturation index calculations for SWSS and BCL samples. Each point represents the average concentration of several sample collection points at the depth specified and error bars are the 95% confidence interval.

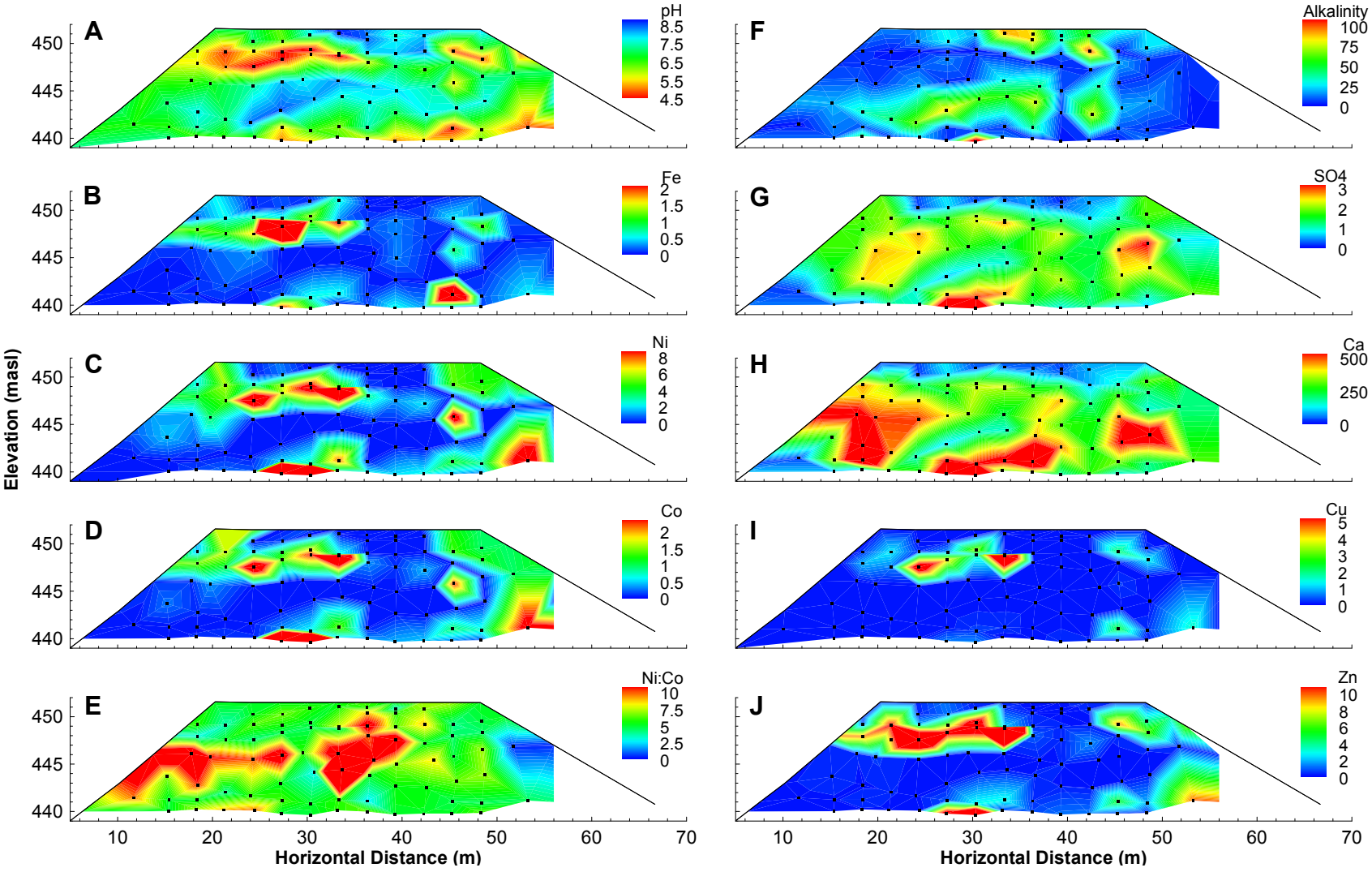

Figure 3-6: Distribution of pore-water concentrations in the 15 m cross section. (▪) indicates sample location and black outline indicates test pile boundary. A) pH, B) Fe (mg L^{-1}), C) Ni (mg L^{-1}), D) Co (mg L^{-1}), E) Ni:Co ratio, F) alkalinity (as mg L^{-1} $CaCO_3$), G) SO_4 (g L^{-1}), H) Ca (mg L^{-1}), I) Cu (mg L^{-1}), J) Zn (mg L^{-1}).

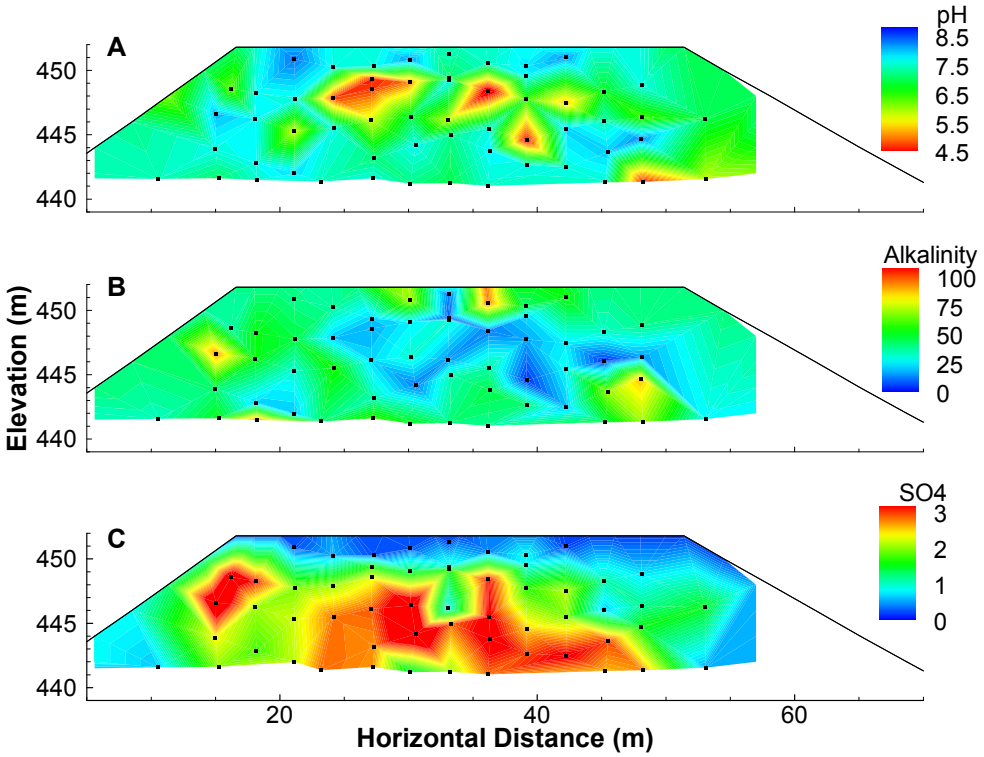

Figure 3-7: Distribution of pore-water concentrations in the 25 m cross section. (▪) indicates sample location and black outline indicates test pile boundary. A) pH, B) alkalinity (as mg L^{-1} $CaCO_3$), C) SO_4 (g L^{-1}).

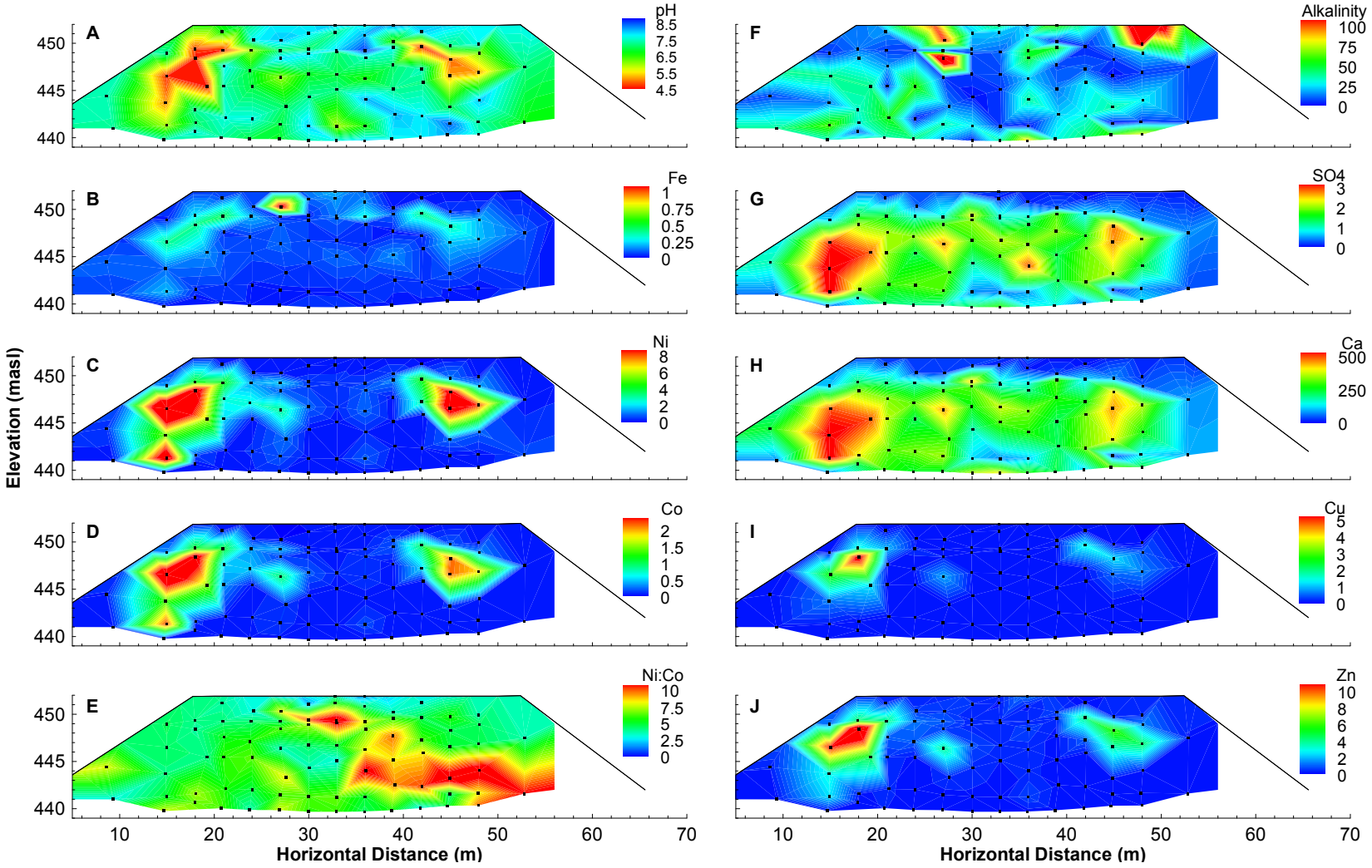

Figure 3-8: Distribution of pore-water concentrations in the 35 m cross section. (•) indicates sample location and black outline indicates test pile boundary. A) pH, B) Fe (mg L^{-1}), C) Ni (mg L^{-1}), D) Co (mg L^{-1}), E) Ni:Co ratio, F) alkalinity (as mg L^{-1} $CaCO_3$), G) SO_4 (g L^{-1}), H) Ca (mg L^{-1}), I) Cu (mg L^{-1}), J) Zn (mg L^{-1}). Note similarity of the Ni, Co, Cu, and Zn distributions. In addition, Ca and SO_4 distributions are remarkably similar.

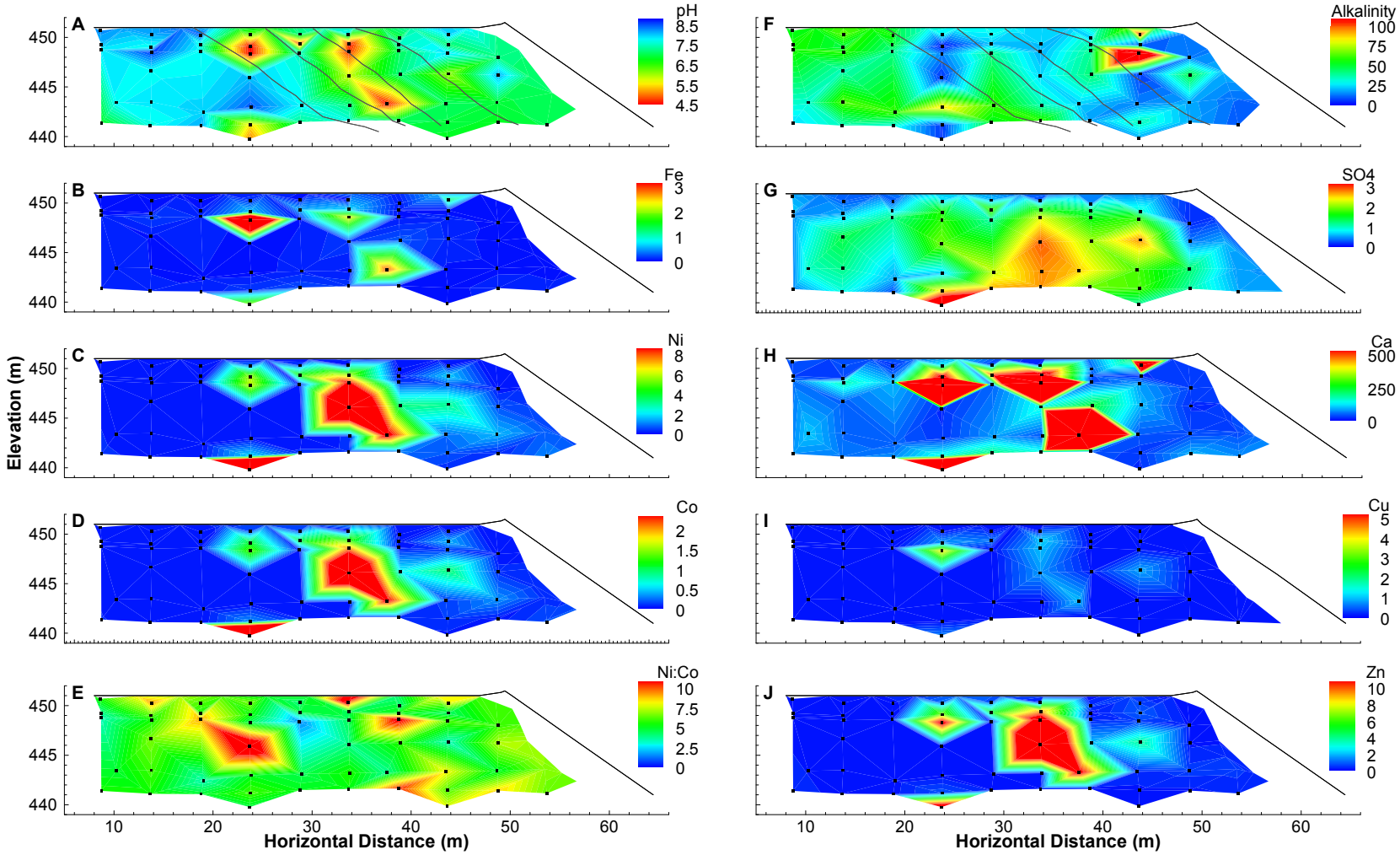

Figure 3-9: Distribution of pore-water concentrations in the transverse cross section. (▪) indicates sample location, black outline indicates test pile boundary, and grey lines indicate position of construction faces. Sulfur content (in wt. %) of construction faces was Face 1: 0.018, Face 2: 0.022, Face 3: 0.033, Face 4: 0.021, Face 5: 0.041 (from left to right). A) pH, B) Fe (mg L^{-1}), C) Ni (mg L^{-1}), D) Co (mg L^{-1}), E) Ni:Co ratio, F) alkalinity (as mg L^{-1} $CaCO_3$), G) SO_4 (g L^{-1}), H) Ca (mg L^{-1}), I) Cu (mg L^{-1}), J) Zn (mg L^{-1}).

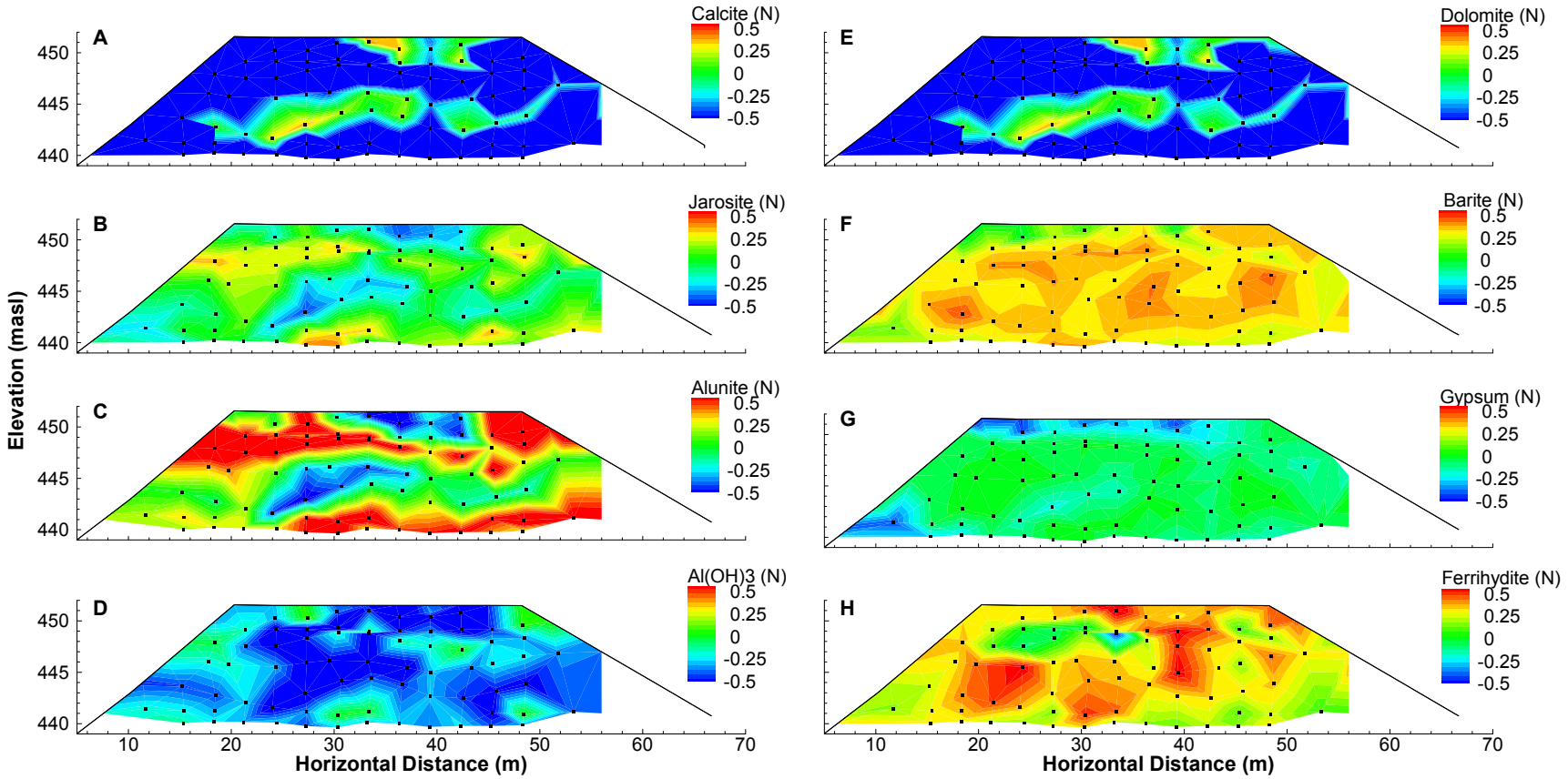

Figure 3-10: Normalized pore-water saturation index calculations for the 15 m cross section. (▪) indicates sample location.

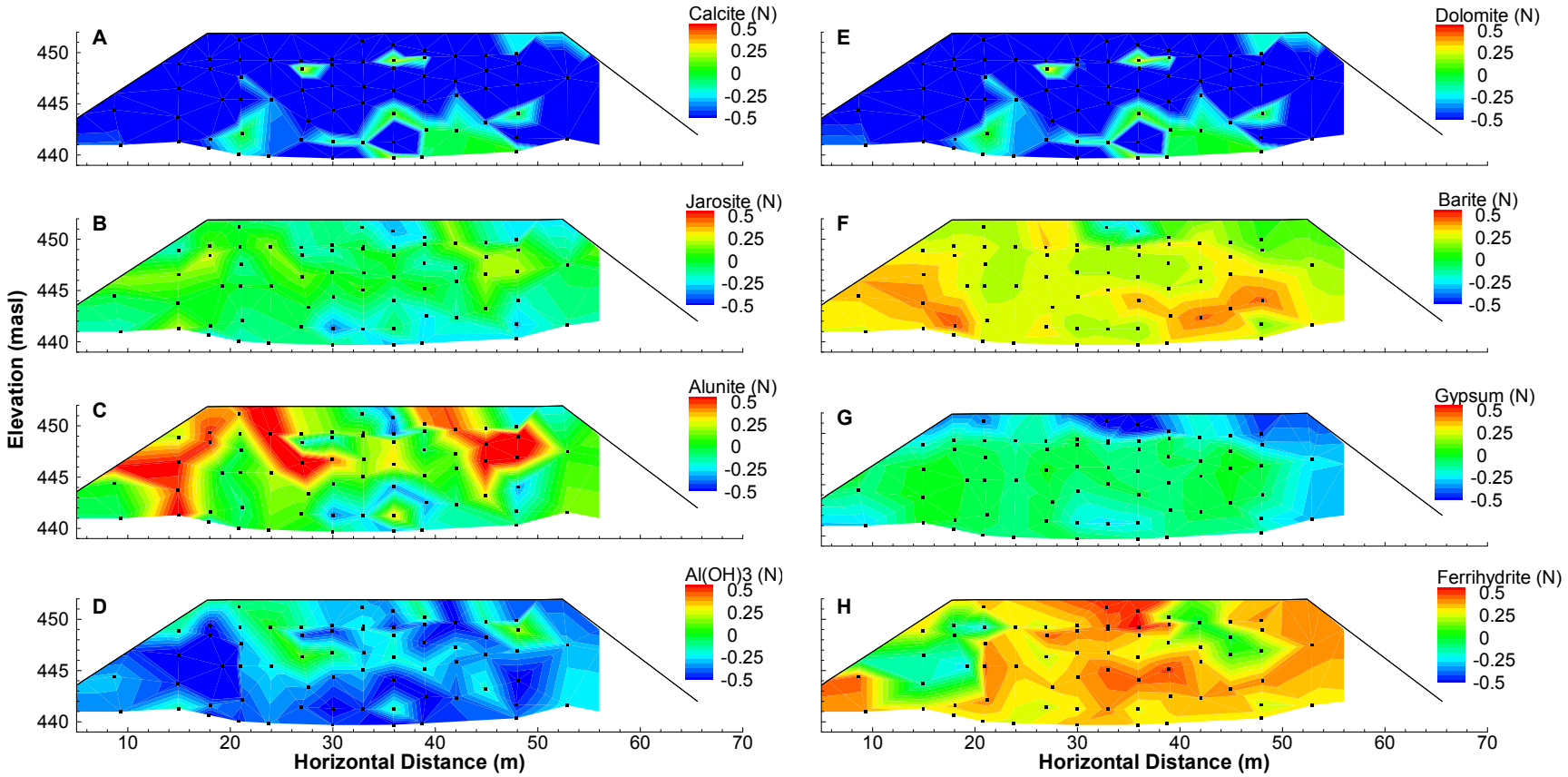

Figure 3-11: Normalized pore-water saturation index calculations for the 35 m cross section. (▪) indicates sample location

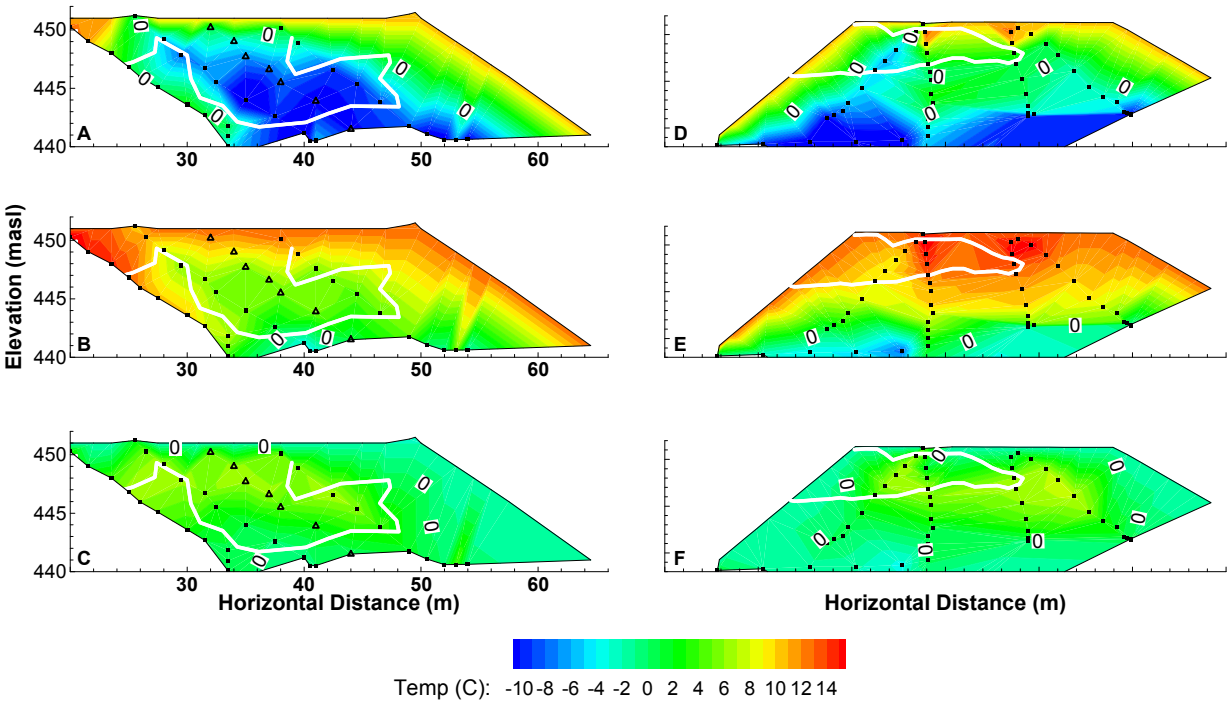

Figure 3-12: Temperature distribution for the transverse (A, B, and C) and 15 m (D, E, and F) cross sections for June (A and D), August (B and E), and October (C and F). (•) indicates in situ measurement location, (Δ) indicates inferred temperature based on average of adjacent samples, and the white line indicates region where pH≤7.

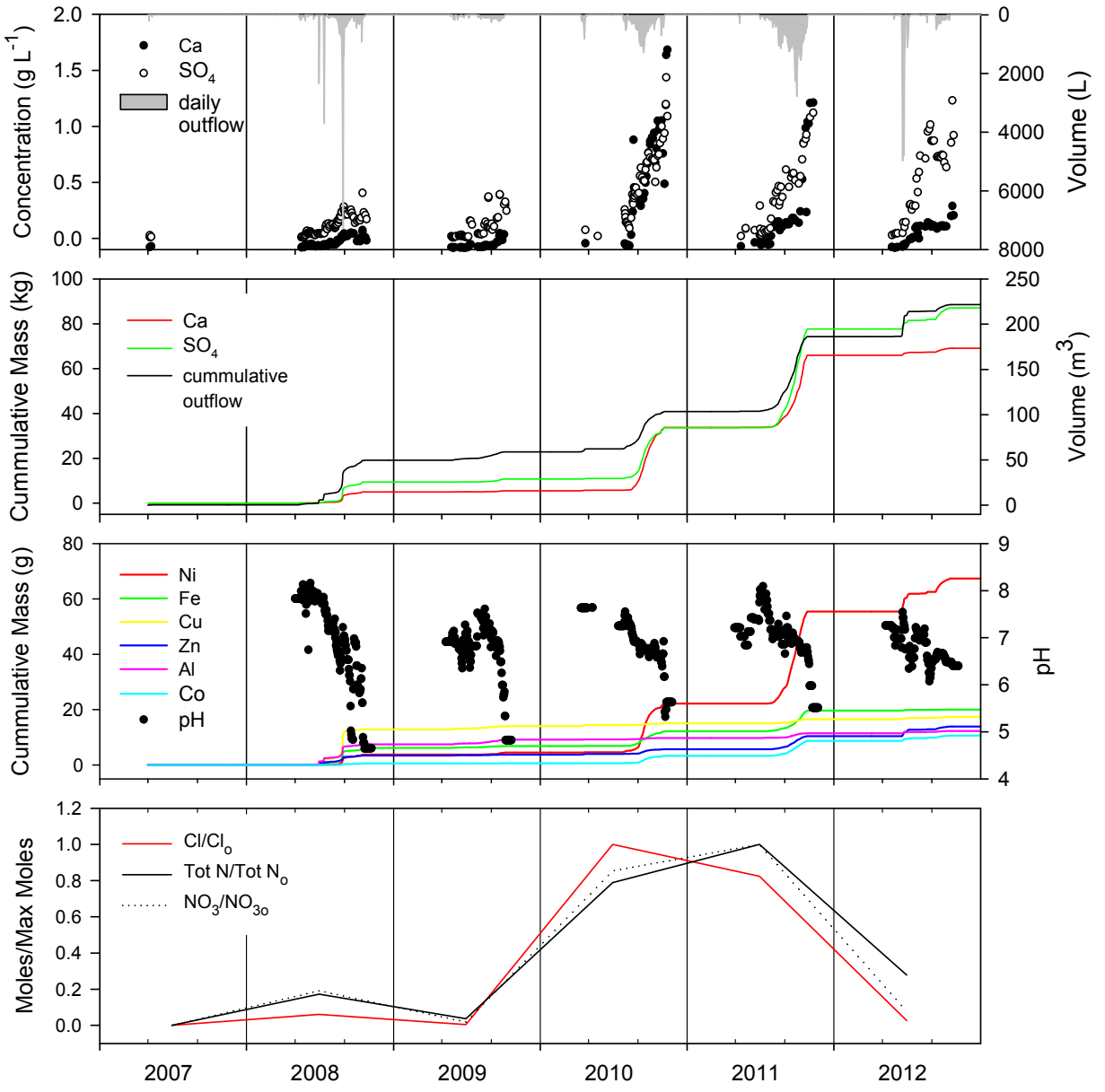

Figure 3-13: Mass loading of selected constituents at the basal drain by year including daily outflow volume (grey bars), cumulative outflow volume (black line) and individual pH measurements (black circle). Cl and NO_3 concentration peaked in 2010 and 2011 respectively.

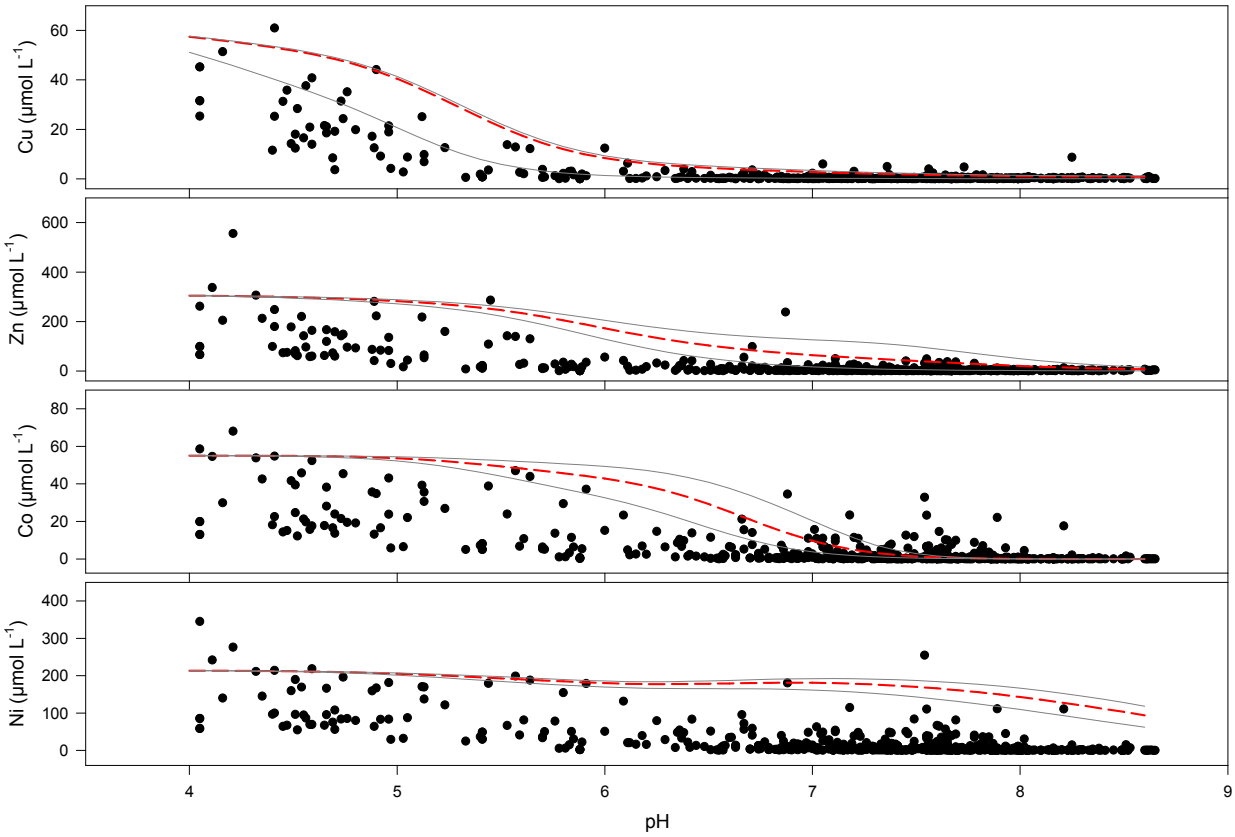

Figure 3-14: Adsorption isotherms. (•) represents pore-water sample, solid lines represent model results at 0.09 (upper) and 0.4 (lower) g L⁻¹ total Fe, red dashed line represents 0.2 g L⁻¹ total Fe.

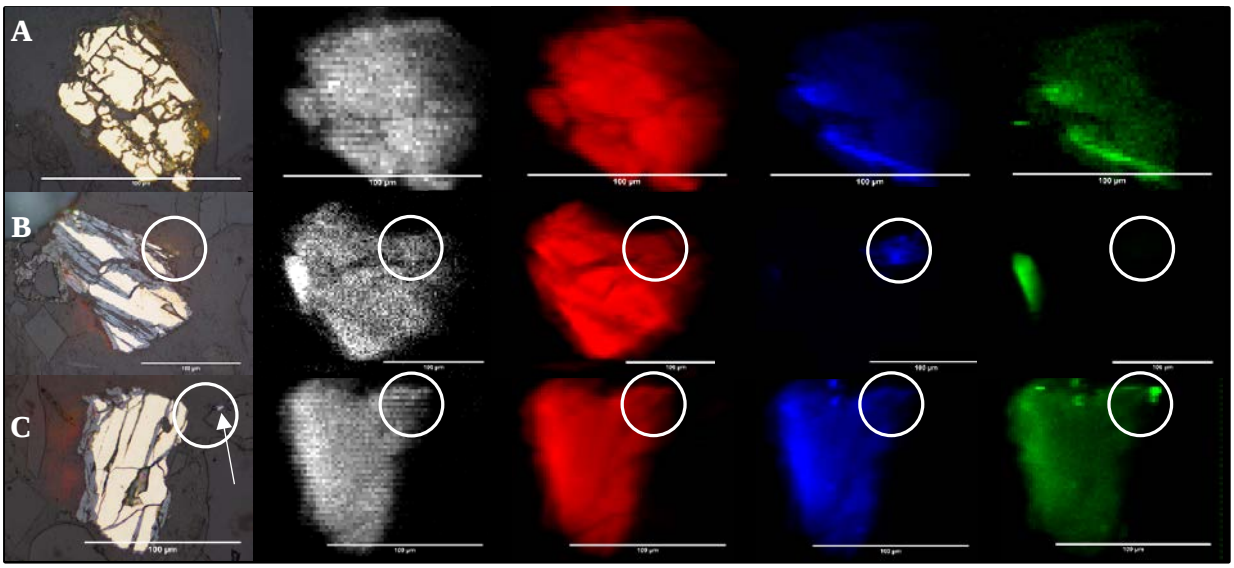

Figure 3-15: Photomicrographs and µ-XRF maps of individual pyrrhotite grains from a vertically aligned profile from the core of the test pile. From left to right: reflected light photomicrograph, S distribution (grey), Fe distribution (red), Ni distribution (blue), and Cu distribution (green). From a depth of A) 2.4 m and pH 4.4, B) 5.6 m and pH 8.3, and C) 11.7 m and pH 5.0. Scale bar on each image represents 100 µm. The sample from the top of the profile (A) indicates limited metal accumulation. The sample from the middle elevation (B) indicates secondary accumulation of Fe and Ni adjacent to the pyrrhotite grain, identified by circle. The sample from the bottom of the profile (C) indicates limited accumulation of secondary Fe but not Ni, identified by circle; arrow indicates residual sulfide grain responsible for strong Cu signal.

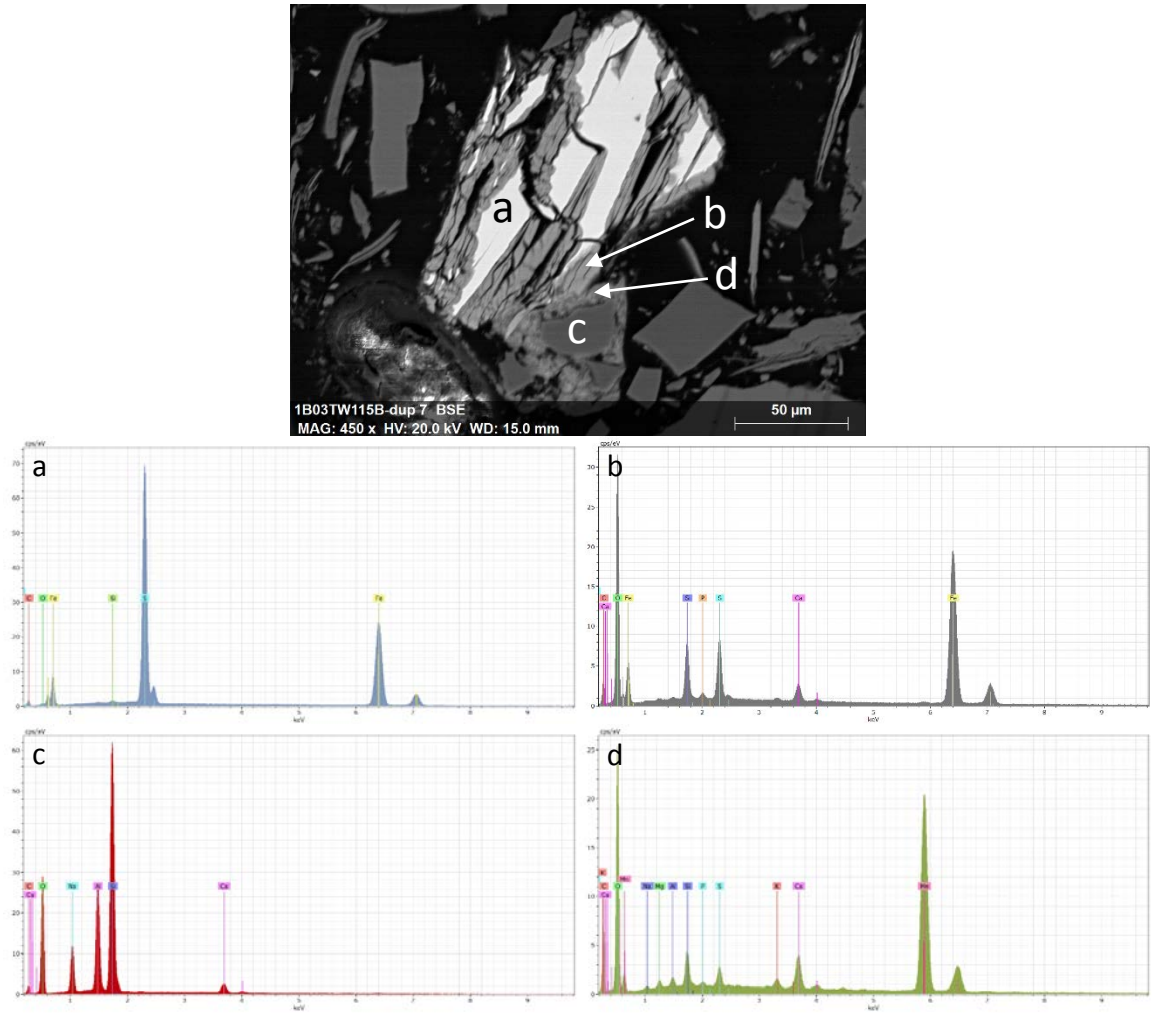

Figure 3-16: SEM and EDX image of grain (B) in Figure 3-15 with EDX spectra. Top - SEM image showing bright, unaltered sulfide core and grey reaction rim. Letters indicate location of EDX analysis. a) EDX within the unaltered sulfide core indicating a dominantly Fe sulfide mineralogy. b) EDX from the reaction rim indicating a mixed Fe oxide and Fe sulfide composition. c) EDX from a grain located adjacent to the sulfide grain having a Na-Ca aluminosilicate composition (plagioclase). d) EDX from the secondary coating on grain (c) indicating a Mn oxide composition.

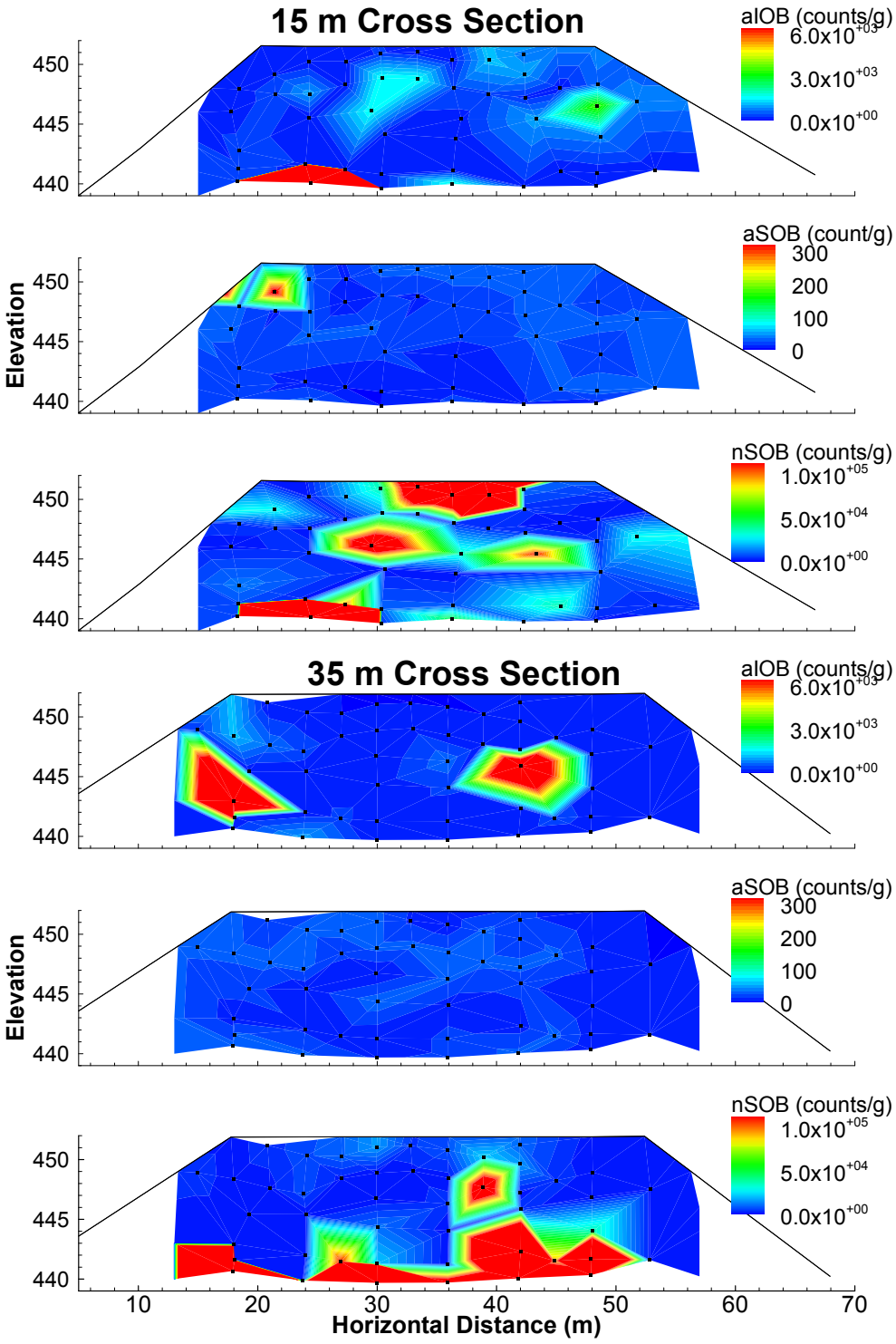

Figure 3-17: MPN enumeration from the 15 m and 35 m cross sections.

3.7. Tables

Table 3-1 - Annual Type I basal drain mass loading (a) Type III data from Sinclair (2014) with exception of Zn and Cu which are from personal communication (2016) (b) data from Krentz (2014)

Year	Rainfall (mm)[b]	Flow (m^3)	SO_4 (kg)	Cl (kg)	NO_3 (kg)	Ca (kg)	Ni (g)	Co (g)	Cu (g)	Zn (g)	Al (g)	Fe (g)
2007	153	0.3	--	--	--	--	--	--	--	--	--	--
2008	154	49.3	0.0	2.1	25.1	5.0	3.7	0.5	12.8	3.4	7.4	6.1
2009	74	9.4	27.5	0.2	2.4	0.6	0.6	0.0	1.1	0.3	1.7	0.6
2010	98	44.5	6.1	35.6	112.2	28.1	17.7	2.6	1.0	1.9	0.6	5.3
2011	146	82.9	44.1	29.3	131.4	31.9	33.2	5.3	1.4	4.6	1.6	7.4
2012	68	35.4	9.4	1.0	10.3	3.1	11.9	1.9	0.8	3.4	0.8	0.4
Type I Total	540	221.8	87.1	68.2	281.3	68.7	67.1	10.3	17.1	13.6	12.1	19.8
Type III Total[a]		937.4	1020.0	36.5	455.0	139.0	4390.0	885.0	456.5[a]	1269.8	2680.0	150.0
TI:TIII (%)		24%	9%	187%	62%	49%	2%	1%	4%	1%	0%	13%

Table 3-2 - Adsorption constants, (a) inferred based on linear free energy relationships (Balistrieri et al., 2003)

Element	K_1	K_2
Cu	3.74	0.89
Zn	1.92	-0.64
Ni	1.32	-1.08
Co[a]	1.32	-1.54

Table 3-3 - Anomalous pore-water samples excluded from adsorption isotherm fitting. N/A - values not considered anomalous and therefore included in the analysis.

Sample ID	pH	Cu (mg L^{-1})	Zn (mg L^{-1})	Ni (mg L^{-1})	Co (mg L^{-1})
1B02TE115F	4.2	9.348	N/A	N/A	N/A
1B02TW115C	4.3	6.613	N/A	N/A	N/A
1B02TW115C-DUP	4.1	8.093	N/A	N/A	N/A
1B02TW125F	6.2	1.374	7.909	24.31	5.441
1B02TW135E	4.5	5.641	14.42	9.928	2.701
1B03TW125B	5.7	N/A	21.58	15.31	3.922
1B03TW125E	7.7	4.139	N/A	N/A	N/A
1B03TW135E	4.5	1.146	4.536	5.649	1.453
1B06TW115A	5.4	N/A	22.18	43.95	9.408
1B06TW115B	5.0	N/A	13.35	37.83	8.14
1B06TW115B-BV1	6.0	N/A	19.6	58.59	12.5
1B06TW115B-BV2	5.4	N/A	22.83	59.93	13.3
1B06TW115B-BV3	5.9	N/A	20.9	59.91	13.41
1B06TW115B-BV4	4.6	N/A	18.65	53.71	11.67
1B06TW115B-BV5	5.5	N/A	18.73	53.32	11.95
1B06TW115B-BV6	4.9	N/A	18.4	51.73	11.44
1B06TW115B-BV7	6.9	0.1871	15.58	49.58	10.34

Table 3-4 - Summary of two-sided t-test results (A) All SWSS and all pore-water data included in analysis, (B) 2013 SWSS and all pore-water data, and (C) 2013 SWSS and pore-water data from the 15 m cross section.

Parameter		**μ_{PW}**	**σ^2_{PW}**	**μ_{SWSS}**	**σ^2_{SWSS}**	**P value**	**Hypothesis: $\mu_{PW} = \mu_{SWSS}$**
pH	A	7.03	1.10	6.90	0.41	0.09	Accepted
Alkalinity	A	32.01	731.31	23.57	107.68	$4x10^{-9}$	Rejected
	B	32.01	731.31	20.35	132.50	$2x10^{-4}$	Rejected
	C	22.15	821.54	20.35	132.50	0.66	Accepted
Fe	A	0.21	0.33	0.36	0.19	0.01	Rejected
	B	0.21	0.33	0.13	0.021	0.06	Accepted
Ni	A	1.89	18.75	1.22	7.66	0.07	Accepted
Co	A	0.39	0.90	0.28	0.42	0.19	Accepted
Cu	A	0.22	0.66	0.30	0.57	0.38	Accepted
Zn	A	1.50	14.20	1.37	11.16	0.78	Accepted
SO_4	A	1324.40	$8.55x10^5$	2085.35	$2.25x10^6$	$2x10^{-5}$	Rejected
	B	1324.40	$8.55x10^5$	3275.72	$4.19x10^6$	$3x10^{-4}$	Rejected
	C	1572.76	$8.39x10^4$	3275.72	$4.19x10^6$	0.001	Rejected

CHAPTER 4. CONCLUSIONS

4.1. Summary of findings

Acid neutralization reactions in the Type I test pile resulted in the depletion of 29-55% of the C content of particle-size fractions <4.00 mm over an eight-year weathering period. This corresponded with a total S content that was not significantly different from samples of unweathered waste rock. A similar result was observed in the bulk matrix samples with a 40% decrease in C content but no significant change in total S content.

The consistency in S content may be the result of retention in secondary S-bearing minerals. The C and S results were used to calculate NPRs. NPRs indicated that regions identified as PAG or uncertain PAG typically had low pore-water pH. If substantial retention of S as secondary minerals occurred in the test pile, NPRs likely represent an overestimation of the acid generating potential remaining at the time of deconstruction.

Pore-water pH results compared well with paste pH determined using both distilled water or $CaCl_2$ saturated solution. Pore-water pH measurements were on average 0.2 pH units lower than $CaCl_2$ saturated paste pH and 0.6 pH units lower than distilled water paste pH. All three of the pH measurement methods used were appropriate for identifying acidic environments within the test pile.

Elevated concentrations of dissolved metals and SO_4 were observed in the regions with low pH. Faces with low original S content were circumneutral to slightly alkaline, whereas faces with high original S content typically had low pH. Face 5, which had the highest original S content at 0.041 wt. %, had circumneutral pH. This was likely the result of high volumes of snowmelt infiltrating the batter region (Sinclair, 2014).

Temperature dependent suppression of sulfide oxidation rates was indicated in regions of the test pile that were subject to freezing temperatures for a greater portion of the year. The most prominent example of this is a region in the middle elevations of the 15 m cross section where NPR indicated PAG material but pH was circumneutral. Sharp decreases in metal concentration were observed where regions of low pH were located above regions of circumneutral pH. These

regions of circumneutral pH were associated with saturation with respect to ferrihydrite and elevated Ni:Co ratios.

Adsorption isotherm modeling indicated that a concentration of 0.2 g L^{-1} of Fe as ferrihydrite would decrease Cu, Zn, Co, and Ni concentrations with increasing pH similar to the trends observed in the Type I test pile. Modeling indicated that Co would be preferentially adsorbed over Ni. Preferential sorption of Co was indicated by the elevated Ni:Co ratios observed in pore water in the circumneutral pH regions.

As a result of (1) the lower availability of sulfides and greater NP:AP ratios in the Type I waste rock, (2) the effect of temperature on sulfide oxidation rates, and (3) sorption of metals in circumneutral regions, the mass loading of SO_4 and dissolved metals was much lower in the Type I test pile than in the Type III test pile.

4.2. Recommendations

The results of this study demonstrate that although the S concentration in the Diavik waste rock is low relative to that commonly found in at mine sites, some of the waste rock is potentially acid generating due to the low neutralization capacity. The overall S content of the Type I test pile was low, but heterogeneity resulted in regions with elevated S content. Sulfide oxidation in these regions can result in the generation of low pore-water pH and elevated metal and SO_4 concentrations.

Segregation of the waste rock based on S content is a worthwhile endeavour to mitigate AMD. The Type I test pile contained only 0.018 wt. % less S than the Type III waste rock, but this change resulted in a significant decrease in the mass loading of dissolved metals and SO_4 to the basal drain. Due to the lower S concentration in the Type I waste rock, the acid neutralization capacity and the suppression of oxidation rates due to low temperatures was sufficient to maintain circumneutral pH in large regions of the test pile.

References

Ahonen, L., Tuovinen, O.H., 1992. Bacterial oxidation of sulfide minerals in column leaching experiments at suboptimal temperatures. Appl. Environ. Microbiol. 58, 600-606.

Amos, R.T., Blowes, D.W., Bailey, B.L., Sego, D.C., Smith, L., Ritchie, A.I.M., 2015. Waste-rock hydrogeology and geochemistry. Appl. Geochem. 57, 140-156.

Amos, R.T., Blowes, D.W., Smith, L., Sego, D.C., 2009. Measurement of wind-induced pressure gradients in a waste rock pile. Vadose Zone J. 8, 953-962.

ASTM C136/C136M-14 Standard Test Method, 2014. Standard Test Method for Sieve Analysis of Fine and Coarse Aggregates. In: Anonymous Annual Book of ASTM Standards, American Society for Testing and Materials.

ASTM C702/C702M-11 Standard Practice, 2011. Standard Practice for Reducing Samples of Aggregate to Testing Size. In: Anonymous Annual Book of ASTM Standards, American Society for Testing and Materials.

ASTM D6913-04 Standard Test Method, 2009. Standard Test Methods for Particle-Size Distribution (Gradation) of Soils Using Sieve Analysis. In: Anonymous Annual Book of ASTM Standards, American Society for Testing and Materials.

Azam, S., Wilson, W.G., Herasymuik, G., Nichol, C., Barbour, L.S., 2007. Hydrogeological behaviour of an unsaturated waste rock pile: A case study at the Golden Sunlight Mine, Montana, USA. Bull. Eng. Geol. Environ. 66, 259-268.

Bailey, B.L., 2013. Geochemical and microbiological characterization of effluent and pore water from low-sulfide content waste rock.

Bailey, B.L., Blowes, D.W., Smith, L., Sego, D.C., 2016. The Diavik Waste Rock Project: Geochemical and microbiological characterization of low sulfide content large-scale waste rock test piles. Appl. Geochem. 65, 54-72.

Bailey, B.L., Blowes, D.W., Smith, L., Sego, D.C., 2015. The Diavik Waste Rock Project: Geochemical and microbiological characterization of drainage from low-sulfide waste rock: Active zone field experiments. Appl. Geochem.

Bailey, B.L., Smith, L.J.D., Blowes, D.W., Ptacek, C.J., Smith, L., Sego, D.C., 2013. The Diavik Waste Rock Project: Persistence of contaminants from blasting agents in waste rock effluent. Appl. Geochem. 36, 256-270.

Balistrieri, L.S., Box, S.E., Tonkin, J.W., 2003. Modeling precipitation and sorption of elements during mixing of river water and porewater in the Coeur d'Alene River basin. Environ. Sci. Technol. 37, 4694-4701.

Barsi, D., 2017. Spatial Variability of Particles in Waste Rock Piles.

Barsi, D., Atherton, C., Zak, J., Beier, N., Sego, D.C., Amos, R., Smith, L., Blowes, D., 2016. Characterizing Particle Size Distribution of Waste Rock.

Belzile, N., Chen, Y.-., Cai, M.-., Li, Y., 2004. A review on pyrrhotite oxidation. J. Geochem. Explor. 84, 65-76.

Benjamin, M.M., Leckie, J.O., 1981. Competitive adsorption of cd, cu, zn, and pb on amorphous iron oxyhydroxide. J. Colloid Interface Sci. 83, 410-419.

Benner, S.G., Gould, W.D., Blowes, D.W., 2000. Microbial populations associated with the generation and treatment of acid mine drainage. Chem. Geol. 169, 435-448.

Blowes, D.W., Ptacek, C.J., 1994. Acid-neutralization Mechanisms in Inactive Mine Tailings. In: Blowes, D.W. and Jambor, J.L. (Eds.), The Environmental Geochemistry of Sulfide MIne-WastesMineralogical Association of Canada, pp. 271-292.

Blowes, D.W., Ptacek, C.J., Jambor, J.L., Weisener, C.G., Paktunc, D., Gould, W.D., Johnson, D.B., 2014. 11.5 - The Geochemistry of Acid Mine Drainage. In: Turekian, H.D.H.K. (Ed.), Treatise on Geochemistry (Second Edition)Elsevier, Oxford, pp. 131-190.

Blowes, D.W., Jambor, J.L., 1990. The pore-water geochemistry and the mineralogy of the vadose zone of sulfide tailings, Waite Amulet, Quebec, Canada. Appl. Geochem. 5, 327-346.

Cama, J., Ayora, C., Querol, X., Moreno, N., 2005. Metal adsorption on clays from pyrite contaminated soil. J. Environ. Eng. 131, 1052-1056.

Chi, X., Amos, R.T., Stastna, M., Blowes, D.W., Sego, D.C., Smith, L., 2013. The diavik waste rock project: Implications of wind-induced gas transport. Appl. Geochem. 36, 246-255.

Cochran, W.G., 1950. Estimation of bacterial densities by means of the “most probable number”. Biometrics 6, 105-116.

Davis, G.B., Ritchie, A.I.M., 1986. A model of oxidation in pyritic mine wastes: part 1 equations and approximate solution. Appl. Math. Model. 10, 314-322.

Davis, J.A., Leckie, J.O., 1978a. Effect of adsorbed complexing ligands on trace metal uptake by hydrous oxides. Environ. Sci. Technol. 12, 1309-1315.

Davis, J.A., Leckie, J.O., 1978b. Surface ionization and complexation at the oxide/water interface II. Surface properties of amorphous iron oxyhydroxide and adsorption of metal ions. J. Colloid Interface Sci. 67, 90-107.

Diavik Diamond Mines Inc., 2011. Interim Closure and Reclamation Plan - Version 3.2.

Diavik Diamond Mines Inc., 1998. Diavik Geochemistry Baseline Report.

Dockrey, J.W., Lindsay, M.B.J., Mayer, K.U., Beckie, R.D., Norlund, K.L.I., Warren, L.A., Southam, G., 2014. Acidic microenvironments in waste rock characterized by neutral drainage: Bacteria–mineral interactions at sulfide surfaces. Minerals 4, 170-190.

Dzombak, D.A., Morel, F.M.M., 1990. Surface Complexation Modeling Hydrous Ferric OxideWiley.

Elberling, B., 2005. Temperature and oxygen control on pyrite oxidation in frozen mine tailings. Cold Reg. Sci. Technol. 41, 121-133.

Elberling, B., 1993. Field Evaluation of Sulphide Oxidation Rates. Nordic Hydrology 24, 323-338.

Elberling, B., Schippers, A., Sand, W., 2000. Bacterial and chemical oxidation of pyritic mine tailings at low temperatures. J. Contam. Hydrol. 41, 225-238.

Environment Canada, 2010. Monthly Data Report for Ekati A, Northwest Territories, Bulk Data 1998–2010.

Government of Canada, 1991. State of Canada's EnvironmentMinistry of Supply and Services, Ottawa.

Hageman, P.L., Seal, R.R., Diehl, S.F., Piatak, N.M., Lowers, H.A., 2015. Evaluation of selected static methods used to estimate element mobility, acid-generating and acid-neutralizing potentials associated with geologically diverse mining wastes. Appl. Geochem. 57, 125-139.

Jambor, J.L., 1997. Mineralogy of the Diavik Lac de Gras Kimberlites and Host Rocks. Report to Diavik Diamond Mines Inc.

Johnson, D.B., Hallberg, K.B., 2003. The microbiology of acidic mine waters. Res. Microbiol. 154, 466-473.

Jurjovec, J., Ptacek, C.J., Blowes, D.W., 2002. Acid neutralization mechanisms and metal release in mine tailings: A laboratory column experiment. Geochim. Cosmochim. Acta 66, 1511-1523.

Krentz, A., 2014. The hydrologic behaviour of waste rock piles in the Canadian arctic: snowmelt infiltration and the onset of long term freezing in test piles.

Langman, J.B., Blowes, D.W., Veeramani, H., Wilson, D., Smith, L., Sego, D.C., Paktunc, D., 2015a. The mineral and aqueous phase evolution of sulfur and nickel with weathering of pyrrhotite in a low sulfide, granitic waste rock. Chem. Geol. 401, 169-179.

Langman, J.B., Moore, M.L., Ptacek, C.J., Smith, L., Sego, D., Blowes, D.W., 2014. Diavik waste rock project: Evolution of mineral weathering, element release, and acid generation and neutralization during a five-year humidity cell experiment. Minerals 4, 257-278.

Langman, J.B., Blowes, D.W., Sinclair, S.A., Krentz, A., Amos, R.T., Smith, L.J.D., Pham, H.N., Sego, D.C., Smith, L., 2015b. Early evolution of weathering and sulfide depletion of a low-sulfur, granitic, waste rock in an Arctic climate: A laboratory and field site comparison. J. Geochem. Explor. 156, 61-71.

Lapakko, K.A., 2015. Preoperational assessment of solute release from waste rock at proposed mining operations. Appl. Geochem. 57, 194-205.

Lee, G., Bigham, J.M., Faure, G., 2002. Removal of trace metals by coprecipitation with Fe, Al and Mn from natural waters contaminated with acid mine drainage in the Ducktown Mining District, Tennessee. Appl. Geochem. 17, 569-581.

Light, T.S., 1972. Standard solution for redox potential measurements. Anal. Chem. 44, 1038-1039.

Lindsay, M.B.J., Moncur, M.C., Bain, J.G., Jambor, J.L., Ptacek, C.J., Blowes, D.W., 2015. Geochemical and mineralogical aspects of sulfide mine tailings. Appl. Geochem. 57, 157-177.

Mayer, K.U., Frind, E.O., Blowes, D.W., 2002. Multicomponent reactive transport modeling in variably saturated porous media using a generalized formulation for kinetically controlled reactions. Water Resour. Res. 38, 131-1321.

Meldrum, J.L., Jamieson, H.E., Dyke, L.D., 2001. Oxidation of mine tailings from Rankin Inlet, Nunavut, at subzero temperatures. Can. Geotechn. J. 38, 957-966.

Moncur, M.C., Jambor, J.L., Ptacek, C.J., Blowes, D.W., 2009. Mine drainage from the weathering of sulfide minerals and magnetite. Appl. Geochem. 24, 2362-2373.

Neuner, M., Smith, L., Blowes, D.W., Sego, D.C., Smith, L.J.D., Fretz, N., Gupton, M., 2013. The Diavik waste rock project: Water flow through mine waste rock in a permafrost terrain. Appl. Geochem. 36, 222-233.

Nordstrom, D.K., 2011. Mine waters: Acidic to circumneutral. Elements 7, 393-398.

Nordstrom, D.K., 1977. Thermochemical redox equilibria of ZoBell's solution. Geochim. Cosmochim. Acta 41, 1835-1841.

Nordstrom, D.K., Southam, G., 1997. Geomicrobiology of sulfide mineral oxidation. Rev. Mineral. 35, 381-390.

Parkhurst, D.L., Appelo, C.A.J., 1999. User's Guide to PHREEQC (Version 2) – A Computer Program for Speciation, Batch-Reaction, One-Dimensional Transport, and Inverse Geochemical Calculations. U.S. Geological Survey Water-Resources Investigations Report 99-4259, 310 p.

Parviainen, A., Lindsay, M.B.J., Pérez-López, R., Gibson, B.D., Ptacek, C.J., Blowes, D.W., Loukola-Ruskeeniemi, K., 2012. Arsenic attenuation in tailings at a former Cu–W–As mine, SW Finland. Appl. Geochem. 27, 2289-2299.

Pham, H.N., 2013. Heat Transfer in Waste-Rock Piles Constructed in a Continuous Permafrost Region.

Pham, N.H., Sego, D.C., Arenson, L.U., Blowes, D.W., Amos, R.T., Smith, L., 2013. The diavik waste rock project: Measurement of the thermal regime of a waste-rock test pile in a permafrost environment. Appl. Geochem. 36, 234-245.

Price, W.A., 2009. Prediction Manual for Drainage Chemistry From Sulphidic Geologic Materials. 1.20.1.

Robertson, A.P., Leckie, J.O., 1998. Acid/base, copper binding, and Cu2+/H+ exchange properties of goethite, an experimental and modeling study. Environ. Sci. Technol. 32, 2519-2530.

Schippers, A., Breuker, A., Blazejak, A., Bosecker, K., Kock, D., Wright, T.L., 2010. The biogeochemistry and microbiology of sulfidic mine waste and bioleaching dumps and heaps, and novel Fe(II)-oxidizing bacteria. Hydrometallurgy 104, 342-350.

Sinclair, S., 2014. *Influence of freeze-thaw dynamics and spatial contributions on geochemical loading from a low sulfide waste-rock pile*.

Sinclair, S.A., Pham, N., Amos, R.T., Sego, D.C., Smith, L., Blowes, D.W., 2015. Influence of freeze–thaw dynamics on internal geochemical evolution of low sulfide waste rock. Appl. Geochem. 61, 160-174.

Smith, L., 2006. Test Piles Project 2006 Construction Summary.

Smith, L.J.D., Bailey, B.L., Blowes, D.W., Jambor, J.L., Smith, L., Sego, D.C., 2013a. The Diavik waste rock project: Initial geochemical response from a low sulfide waste rock pile. Appl. Geochem. 36, 210-221.

Smith, L.J.D., Blowes, D.W., Jambor, J.L., Smith, L., Sego, D.C., Neuner, M., 2013b. The diavik waste rock project: Particle size distribution and sulfur characteristics of low-sulfide waste rock. Appl. Geochem. 36, 200-209.

Smith, L.J.D., Moncur, M.C., Neuner, M., Gupton, M., Blowes, D.W., Smith, L., Sego, D.C., 2013c. The Diavik waste rock project: Design, construction, and instrumentation of field-scale experimental waste-rock piles. Appl. Geochem. 36, 187-199.

Stipp, S.L.S., Hansen, M., Kristensen, R., Hochella Jr., M.F., Bennedsen, L., Dideriksen, K., Balic-Zunic, T., Léonard, D., Mathieu, H.-., 2002. Behaviour of Fe-oxides relevant to contaminant uptake in the environment. Chem. Geol. 190, 321-337.

Stockwell, J., Smith, L., Jambor, J.L., Beckie, R., 2006. The relationship between fluid flow and mineral weathering in heterogeneous unsaturated porous media: A physical and geochemical characterization of a waste-rock pile. Appl. Geochem. 21, 1347-1361.

Tonkin, J.W., Balistrieri, L.S., Murray, J.W., 2002. Modeling metal removal onto natural particles formed during mixing of acid rock drainage with ambient surface water. Environ. Sci. Technol. 36, 484-492.

Welp, G., Brümmer, G.W., 1999. Adsorption and solubility of ten metals in soil samples of different composition. J. Plant Nutr. Soil Sci. 162, 155-161.

Zak, J., 2017. Hydrologic investigations of waste rock test piles in a permafrost environment.

Zhang, Y., Charlet, L., Schindler, P.W., 1992. Adsorption of protons, Fe(II) and Al(III) on lepidocrocite (γ-FeOOH). Colloids and Surfaces 63, 259-268.